COORDINATING THE TRANSPORT CYCLE OF THE MYOSIN-V MOTOR MYO2 WITH SECRETORY VESICLE DELIVERY AND EXOCYTOSIS

A Dissertation

Presented to the Faculty of the Graduate School

of Cornell University

In Partial Fulfillment of the Requirements for the Degree of

Doctor of Philosophy

by

Kirk William Donovan

August 2014

COORDINATING THE TRANSPORT CYCLE OF THE MYOSIN-V MOTOR MYO2 WITH SECRETORY VESICLE DELIVERY AND EXOCYTOSIS

Kirk William Donovan, Ph. D.

Cornell University 2014

The polarization of proteins, lipids, and organelles within a eukaryotic cell allows for the spatial regulation of numerous biological processes. *Saccharomyces cerevisiae* displays exaggerated polarized growth of its plasma membrane during budding through the directed transport of secretory vesicles. In addition, several organelles are actively transported into the growing bud. These processes are accomplished using formin-nucleated actin cables extending from the bud tip and neck and the myosin-V motor Myo2p. While many of the components linking Myo2p to its various cargoes are known, the dynamic behavior of the motor and how its dynamics is regulated at the molecular level remains unclear. Here I define the *in vivo* delivery cycle of a myosin-V in its essential function of secretory vesicle transport, and show how that transport is coordinated with other events in exocytosis.

I determined that Myo2p is activated from an inactive state by binding to competent secretory vesicles. This inactive state is caused by an autoinhibitory interaction between the head and tail of the motor. Mutations that disrupt this interaction render the motor constitutively active and compromise cargo transport functions. About 10 motors associate with each secretory vesicle during rapid transport to sites of cell growth. Motor release is temporally regulated by vesicle-bound Rab-GTP hydrolysis and requires vesicle tethering via the exocyst complex, but does not require vesicle fusion with the plasma membrane. Additionally, I developed a vesicle-tracking assay to study single-vesicle fusion dynamics at the cortex. This aided in the creation of

a timeline of events for exocytosis, allowing for the dynamics of single-vesicle populations of the Rab Sec4p, the exocyst complex, and Myo2p to be visualized. The components of this transport cycle are highly conserved in mammalian cells, so these results should be generally applicable to other myosin-V delivery cycles.

BIOGRAPHICAL SKETCH

Kirk was born in the middle of the White Mountains of New Hampshire to Kevin and Kathleen Donovan. Many childhood days were spent hiking, swimming and camping in the summer, and downhill skiing in the winter. Kirk attended primary school at Josiah Bartlett Elementary in Bartlett, N.H., where he credits his 7th grade life science class (taught by Joe Yahna) for sparking his interest in biology. At Kennett High School in Conway, N.H., Kirk was on the boy's soccer and downhill ski racing teams for all four years, captaining the ski team in his senior year. His interest in biology grew after taking the A.P. Biology class and being selected to take part in a summer molecular biology course at the St. Paul's School Advanced Studies Program in 2003.

Following his high school graduation in 2004, Kirk attended St. Lawrence University in Canton, NY. Kirk was active in student government and served as an admissions tour guide and writing center mentor for three years. Two summers were spent at the New York State Department of Health in Albany, NY profiling the genetics of Antarctic foraminifera under Dr. Sam Bowser. For his senior honors thesis, Kirk worked with Dr. Ana Estevez researching Apoptosis Inducing Factor (AIF) and Poly(ADP-ribose) polymers in mouse hippocampal neurons under ischemic conditions. By pure serendipity, Kirk met his future advisor Anthony Bretscher while working a college admissions event at St. Lawrence, and he encouraged Kirk to consider Cornell University for his post-graduate studies. He feels very fortunate to have selected Cornell and Tony's lab for his dissertation work.

To my family, friends, and mentors who have

motivated me along the way

ACKNOWLEDGMENTS

This dissertation would not be possible without the support and assistance of so many people. I'd first like to thank my research mentor, Dr. Tony Bretscher, for his constant encouragement and hours of fruitful discussion. His countless suggestions at all stages of the project have made this dissertation what it is. I don't think I could have asked for a better research advisor under whom to complete my Ph. D. His attitude and demeanor also created an amazing lab culture; many days and nights were spent with fellow lab-mates celebrating the successes, commiserating when things didn't go to plan, and learning techniques from one another. In particular, I'd like to thank Dr. Felipe Santiago and Dr. Irina Chernyakov for teaching me proper yeast genetics when starting out and being there for general experimental guidance. I'd also be remiss if I didn't mention the Weill Institute, our NIH R01 yeast grant (GM39066), and the NIH BMCB training grant for funding and support over the past six years.

I'd also like to thank a number of important people in my life that helped me get this far. Getting away from research and reuniting with my St. Lawrence friends has been a very welcome distraction at different points along the way. Closer to home in Ithaca, I'd like to thank Jess, Colin, Jon, Lexi, Tony, Leah, Bryan, Adam, Kelly, and dozens of others for sharing cheers, beers, laughs, and general good times. Tom, you're always there to hold me up when I'm down. Finally, I'd like to thank my parents, Kevin and Kathleen, and brother Chris. Your continuous support has driven me to excel both in the lab and out.

TABLE OF CONTENTS

Cont.

LIST OF FIGURES

LIST OF ABBREVIATIONS

AD	*GAL4* activation domain
AMPA	α-Amino-3-hydroxy-5-methyl-4-isoxazolepropionic acid
ADP	adenosine diphosphate
ATP	adenosine triphosphate
BD	*GAL4* DNA-binding domain
cctail	the coiled-coil and globular tail domain of Myo2p
CDK	cyclin dependent kinase
DAD	diaphanous autoregulatory domain
DID	diaphanous inhibitory domain
DRF	Diaphonous-related family (formin class)
EDTA	ethylenediaminetetraacetic acid
EM	electron microscopy
ER	endoplasmic reticulum
GAP	GTPase Activating protein
GDI	GDP dissociation inhibitors
GDP	guanosine-5'-diphosphate
GTD	globular tail domain (of a myosin-V)
GTP	guanosine-5'-triphosphate
GTPase	class of proteins that bind GTP
GEF	guanine-nucleotide exchange factor (protein class)
FLIP	fluorescence loss in photobleaching
FRAP	fluorescence recovery after photobleaching
lgl	lethal giant larvae (protein class)

mRNA	messenger ribonucleic acid
NMDA	N-methyl-D-aspartate
PI4P	phosphatidylinositol 4-phosphate
SNARE	SNAP (Soluble NSF Attachment Protein) Receptor
SM	Sec1/Munc18-class (protein family)
TGN	trans-Golgi network

CHAPTER 1

POLARIZED MEMBRANE TRAFFICKING IN YEAST

One of the fundamental properties of all life is the ability to separate cellular activities both spatially and temporally. Doing so enables a cell to confine different functions to distinct areas. This ability, termed "cell polarity," requires tight integration of signaling networks, membrane trafficking, and the cytoskeleton. For example, in Figure 1.1, the four eukaryotic cells presented have a highly ordered, polarized organization that enables each to perform a specific function. The epithelial cell of the small intestine (A) has a distinct apical domain for the uptake of nutrients that are then transported out of the cell towards the bloodstream through the basolateral domain. The pancreatic acinar cell (B) specializes in secreting digestive enzymes into ducts found on its apical side to allow for digestion in the gut. A neuron (C) must ensure that neurotransmitters are packaged, delivered, and released at synapses that can be several meters from the cell body in some mammals. Finally, a budding yeast (D) needs to specify a site on its plasma membrane from which to grow a bud, and then devote a great deal of energy directing membranes and organelles into it. All of these processes require a high degree of self-organization and feedback cycles to maintain polarity. One of the most important ways cells maintain polarity is through the trafficking of various components, such as proteins and lipids, to distinct places within the cell. Many times, this trafficking requires the coordination of molecular motors with the cargo it is tasked with delivering.

Budding yeast is one of two model systems used in the Bretscher Lab to study the creation and maintenance of polarized systems. Specifically, budding yeast is used to elucidate the molecular mechanisms behind how a polarized actin cytoskeleton contributes to asymmetric growth during the generation of a bud. One of the primary players in this system is the class-V

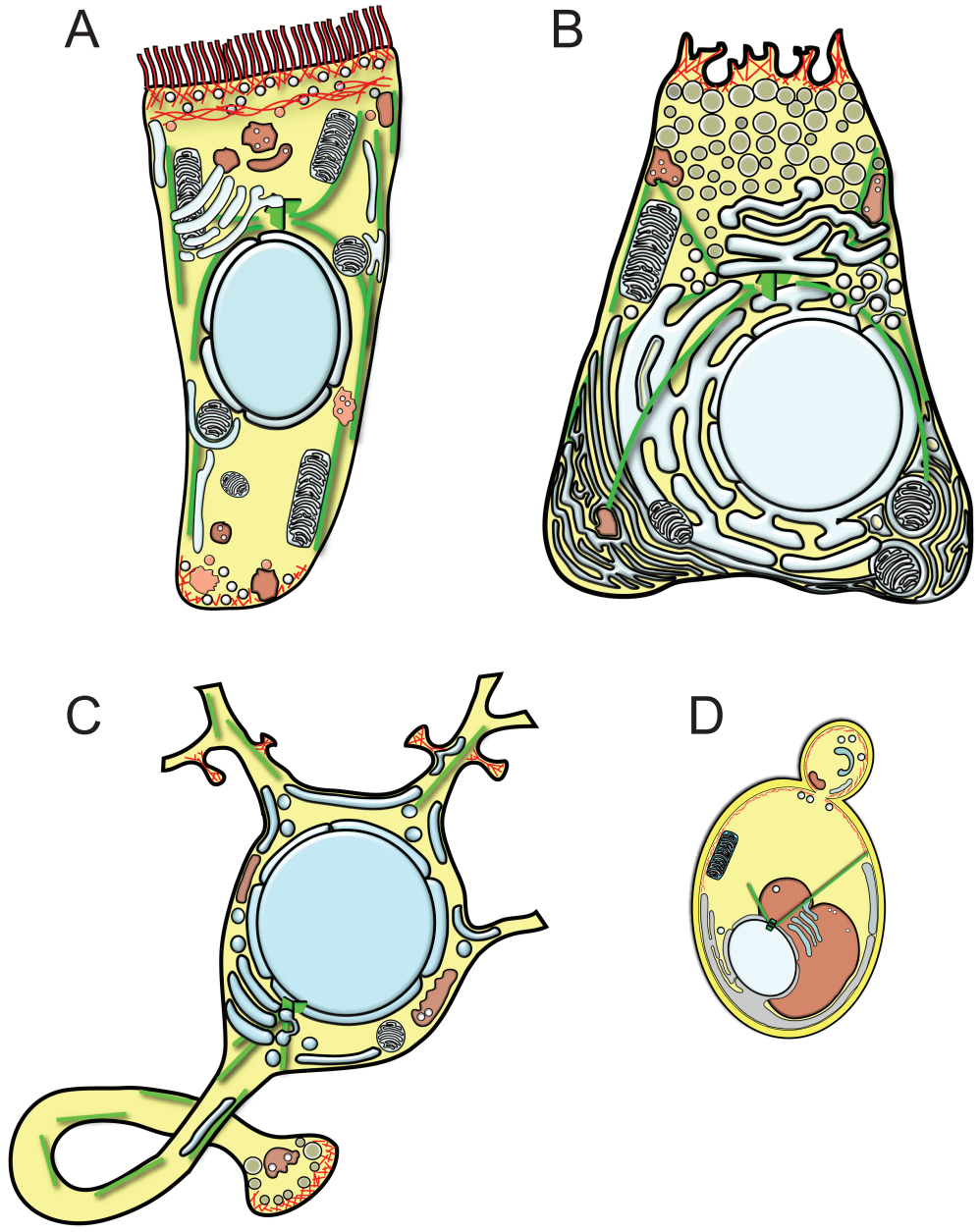

Figure 1.1. Polarized structures allow eukaryotic cells to perform specific functions.

A. An intestinal epithelial cell with apical and basolateral domains allows for the selected transport of nutrients into and out of the cell.
B. The apical domain of a pancreatic acinar cell allows for the secretion of digestive enzymes into the luminal space.
C. Axon and dendrite projections in a neuron enables electro-chemical signal fidelity over large distances.
D. A yeast cell grows a bud after choosing a specific site on its cortex from which to direct secretory membranes and organelles.

Red lines indicate actin cables while green lines indicate microtubules. Images adapted from F. Santiago.

family of myosin motors, which transport membrane-bound organelles, mRNA, and secretory vesicles into the growing bud. The importance of myosin-V motors is underscored by the findings that defects in MyoVa in humans cause Griscelli syndrome while defects in MyoVb result in microvillus inclusion disease (Pastural et al., 1997; Müller et al., 2008). In this dissertation, I will present work detailing how the activity of one canonical member of the myosin-V family, Myo2p, coordinates its activity with secretory vesicle delivery, tethering, and fusion.

Budding Yeast as a Model for Cell Polarity

Budding yeast has been one of the workhorses in eukaryotic cell biology for half a century, mostly due to its ease of genetic manipulation, ability to live in a haploid or diploid state, and short life cycle. Many of the early biochemical and metabolic pathways were first traced in budding yeast before being found, more or less conserved, in higher eukaryotes. However, their striking asymmetric growth has cemented budding yeast as a clear model for studying the establishment and maintenance of a polarized system.

Budding yeast in the wild has three clearly defined polarized states: budding, shmooing, and pseudohyphal growth (Figure 1.2). With sufficient nutrients, yeast chooses a specific location on its plasma membrane from which to bud and then direct secretory components toward that site for membrane growth. In the presence of mating factors, haploid yeast senses a chemo-attractive gradient and grows a “shmoo” projection toward the opposite mating type. Lastly, under conditions where nutrients are limiting, wild yeast will adopt an exploratory pseudohyphal growth pattern characterized by elongated, tethered cells with uni-polar budding to invade a substrate (Herskowitz, 1988).

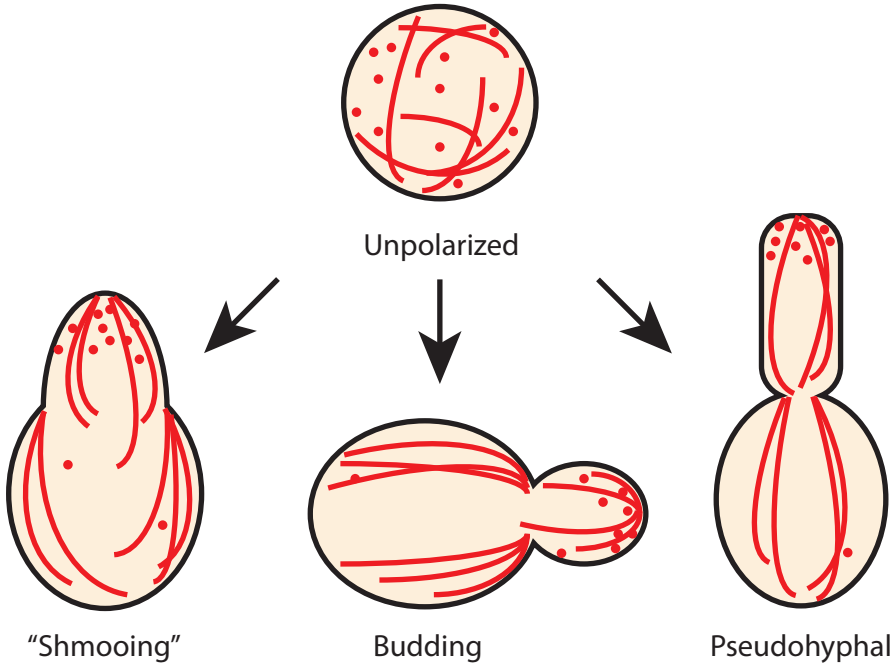

Figure 1.2. Three alternate growth strategies all require a polarized actin cytoskeleton. An unpolarized cell can develop differently depending on the presence or absence of certain chemicals and nutrients in the environment. All three strategies utilize a polarized actin cytoskeleton to enable growth. Actin cables are shown with red lines while actin patches are shown as red dots.

While these three different growth states are exploited for different conditions, they all utilize the same underlying cell polarity cues and machinery. These include selecting a site to grow the projection, establishing a polarized actin cytoskeleton and transport machinery, and then marshalling resources in the form of secretory cargo and organelles to enable growth. Research in many different model systems has shown that this framework for polarized growth is highly conserved through evolution. Indeed, many of the key players that establish and maintain this polarity (such as Cdc42, formin nucleators, filamentous actin, and class-V myosin motors) are seen in nearly all eukaryotes. Thus, the mechanisms first described in yeast are oftentimes directly applicable to systems found in higher organisms.

Saccharomyces cerevisiae serve as a much simpler model for actin-based transport because, unlike higher eukaryotes, budding yeast does not utilize microtubule-based transport for polarized growth. This is likely due to their small size of no more than about 8 μm in length. Budding yeast is also a good model for studying polarized growth because they have spatially-segregated areas of cargo capture in the mother cell and delivery to the growing projection; this makes phenotypic analysis far easier than in higher cells which usually do not show quite as high a degree of polarized growth. For these reasons, budding yeast remains an ideal model organism to study polarized, actin-based growth of a cell.

Laying the Tracks: Establishing a Polarized Actin Cytoskeleton

Yeast were firmly established as a tool for studying polarized growth thanks to a series of genetic screens in the l970s that created conditional mutants, coupled with an expanding toolkit of reagents to study the cytoskeleton (Hartwell et al., 1971; Hartwell et al., 1974; Novick and Schekman, 1979; Novick et al., 1980). The Pringle Lab was the first to stain cells with

rhodamine phalloidin and visualize actin puncta and long cables originating at sites of growth (Adams and Pringle, 1984). Further work with the microtubule poisoning drug nocodazole found no effect on the initiation and growth of a bud; this implied that actin alone was responsible for polarized growth and was consistent with the previous finding that the single *ACT1* gene is essential (Ng and Abelson, 1980). That microtubules were not required for bud site selection, emergence, and growth was rather surprising since it was at odds with a large body of work on secretion in mammalian cells.

Over the next decade, other actin binding proteins were discovered including fimbrin (Sac6p; Adams et al., 1989) , tropomyosin (Tpm1/2p; Drees et al., 1995; Liu and Bretscher, 1989), capping protein (Cap1/2p; Amatruda et al., 1990), profillin (Pfy1p; Haarer et al., 1990) and cofilin (Cof1p; Moon et al., 1993). Mutations affecting many of these genes lent further support for actin-centric growth and division. While there was mounting evidence that actin played some role in endocytosis, the functional differences between actin cables and actin patches was not fully appreciated until the creation of fast-acting conditional tropomyosin mutants in the Bretscher Lab that clearly showed actin cables direct polarized growth via the secretory pathway (Pruyne et al., 1998). Further work with mutants affecting endocytosis and the discovery of the Arp2/3 complex showed that actin patches are sites of endocytosis that are also polarized towards sites of growth. Since this dissertation concerns motor delivery of secretory cargo on actin filaments, an understanding of their creation and localization is required.

The basic scheme for establishing polarity in yeast is as follows: (1) specify the prospective bud site through previous polarity cues, (2) establish polarization machinery using positive feedback loops at the prospective bud site, and (3) recruit formin proteins to assemble the polarized actin cytoskeleton that drives bud growth. Note that bud site selection in yeast

differs depending on whether the yeast is haploid or diploid. Bud8p and Bud9p serve as landmarks for bipolar budding in diploid cells while Bud10p, using cues left over from the septin ring at the last budding event, is the landmark for axial budding in haploid cells (Pruyne et al., 2004).

Amplification of Polarity Cues Through Positive Feedback Loops

Extensive research over the past two decades has implicated the Rho GTPase Cdc42p as the master regulator of polarity initiation following bud site selection. In brief, Cdc42p activation (that is, a GTP-bound protein) is thought to arise stochastically with a positive feedback mechanism amplifying its effects. Cdc24p, the Guanine nucleotide Exchange Factor (GEF) for Cdc42p, binds to the ras-like GTPase Rsr1p already present at the prospective bud site due to its own activation from the upstream *BUD* gene products (Shimada et al., 2000). In the absence of upstream cues, a single bud site is still selected. This involves the stochastic activation of Cdc42p in one or several locations at the prospective bud site. Amplification of the Cdc42-GTP signal occurs through further local clustering of the scaffold Bem1p, the PAK kinase Ste20p, and the GEF Cdc24p. Cdc42-GTP recruits the scaffolding platform though an interaction with the PAK Ste20p CRIB-domain, which activates the kinase (Lamson et al., 2002; Leberer et al., 1997). Since the scaffold protein Bem1p binds to both PAK Ste20p and the GEF Cdc24p, further activation of additional Cdc42p molecules in the vicinity is ensured through the PAK-dependent activation of Cdc24p (Kozubowski et al., 2008). This allows the local clustering of active-Cdc42p at the prospective bud site. Additional work has shown that local cluster size is reinforced through passive GTP hydrolysis if Cdc42-GTP wanders away from this cap and also through Myo2p-dependent vesicle trafficking of Cdc42p at exquisitely tuned rates (Johnson et

al., 2011; Layton et al., 2011). Recent mathematical modeling studies suggest that vesicular trafficking of Cdc42 is not strictly necessary, but does create interesting effects related to polarity cap wandering and dilution (Savage et al., 2012). Further, multiple Cdc42p caps (which have been detected *in vivo*) can turn into one through either competition or merging models. Competition models usually show the slightly larger cap "winning out" due to it having more Cdc42-GTP to bind to the more limiting Bem1p complexes; clustering can occur when two patches wander towards one another, with the area between them slowly acquiring additional Cdc42p/Bem1p complexes and biasing activation toward the center of the two patches (Howell et al., 2009; Savage et al., 2012). The end result allows for concentration of Cdc42-GTP in one particular site, which can then be used to recruit downstream effectors to further drive cell polarity.

Establishing a Polarized Actin Cytoskeleton

The generation of a polarized actin cytoskeleton is accomplished by two formin isoforms of the Diaphanous-related family (DRF), Bni1p and Bnr1p. These two nucleators function at different locations depending on the growth stage of the bud, with Bnr1p consistently remaining at the bud neck while Bni1p moves from bud tip to bud neck towards the end of bud growth in late-G2 phase. The recruitment of Bni1p is mediated by the Rho GTPases (including Rho3p, Rho4p, and Cdc42p) and the polarisome complex (consisting of Spa2p, Pea2p, and Bud6p), which also has a role in modulating the formin's behavior (Moseley and Goode, 2005). Formin nucleators of the Diaphanous-related family contain a diaphanous inhibitory domain (DID) and diaphanous autoregulatory domain (DAD) at opposite termini; their interaction is believed to inhibit nucleation of actin filaments at the FH2 domain. Binding of Rho proteins to the N-

terminus relieves this inhibition and allows selective nucleation at the polarity site (Goode and Eck, 2007). A similar scheme recruits Bnr1p to the bud neck, but relies on septin proteins as a landmark for polarity (Buttery et al., 2007; Gao et al., 2010).

Following activation at the proper location, formin nucleators use their FH1 domain to capture profilin-bound actin monomers and incorporate them into an actin cable. Use of profilin (Pfy1p) dramatically speeds up the rate of actin assembly and allows the formin to quickly shuttle actin from the cytoplasm to the FH1 domain for incorporation into the growing filament (Kovar et al., 2005; Romero et al., 2004). FH2 domain-directed nucleation by formins proceeds from the barbed end of an actin filament; this has numerous advantages including protecting the barbed end from capping proteins and anchoring cables to the site of cell polarity so that plus-end directed myosin-V motors can move toward them. During nucleation, accessory factors such as fimbrin (Sac6p) and tropomyosin (Tpm1/2p) serve to bundle and stabilize a growing cable, respectively (Adams et al., 1991; Pruyne et al., 1998). Bni1p and Bnr1p *in vitro* can nucleate individual cables several microns in length, although in cells the individual cables are usually no longer than about 500 nm before the formin is displaced (Karpova et al., 1998). Length may be controlled by displacement factors, such as Bud14p, as puncta of Bni1-3xGFP have been seen riding down long actin filaments at the rate of treadmilling, 300 nm/sec (Buttery et al., 2007; Chesarone et al., 2009).

In total, these results show that polarized structures can arise through symmetry-breaking feedback cycles. The establishment of a single Cdc42p polarity cap allows for the recruitment and activation of specific nucleating factors known as formins. These nucleators can then in turn build highly polarized, extended actin filaments. It is on these cables that class-V myosin motors deliver components into the growing bud.

Myosin-V Motors: Transporting Cargo Along Polarized Actin Cables

Completion of a polarized cytoskeleton allows the cell to transport various components to the polarity site. The myosin superfamily of motors is an ancient lineage stretching back to near the beginning of eukaryotic life. The basic domain structure of all myosins consists of an N-terminal ATPase domain, or "head", where the catalytic activity occurs. This is followed by a light chain binding domain of variable length called the "neck", which can influence the behavior of the motor. Finally, a domain of variable function occupies the C-terminus (Sellers et al., 2008). This domain can serve as a dimerization domain between one or several monomers and/or act as a binding platform for additional proteins coupled to specific cargos.

Of the 17 classes of motors discovered, budding yeast have genes for five motors from three different classes; these three classes are highly conserved through evolution and are found in nearly all eukaryotes. Myo1p is the conventional class II myosin, which provides the force necessary for the constriction event at the bud neck (Bi et al., 1998). Myo3p and Myo5p are class I myosins; they interact with Arp2/3-nucleated branched actin filaments at endocytic sites and provide the force necessary to pull clathrin-coated pits into the cell against the force of turgor pressure (Geli and Riezman, 1996). Finally, Myo2p and Myo4p are the class-V myosins; in general, this class of motors has a high duty ratio, long neck domain and globular tail to allow them to move cargo along polarized actin cables. Most class-V motors, including the subject of this dissertation, are dimers. This means that two monomers strongly interact at the C-terminal coiled-coil domain, or "stalk." Before continuing on to the exact role class-V myosins play in the yeast cell, I will first touch upon the basic domain architecture and how they function (Figure 1.3). As a quick note on myosin-V nomenclature, the four domains (head/lever-arm/coiled-coil/tail) are usually referred to as separate entities in yeast, while mammalian work almost

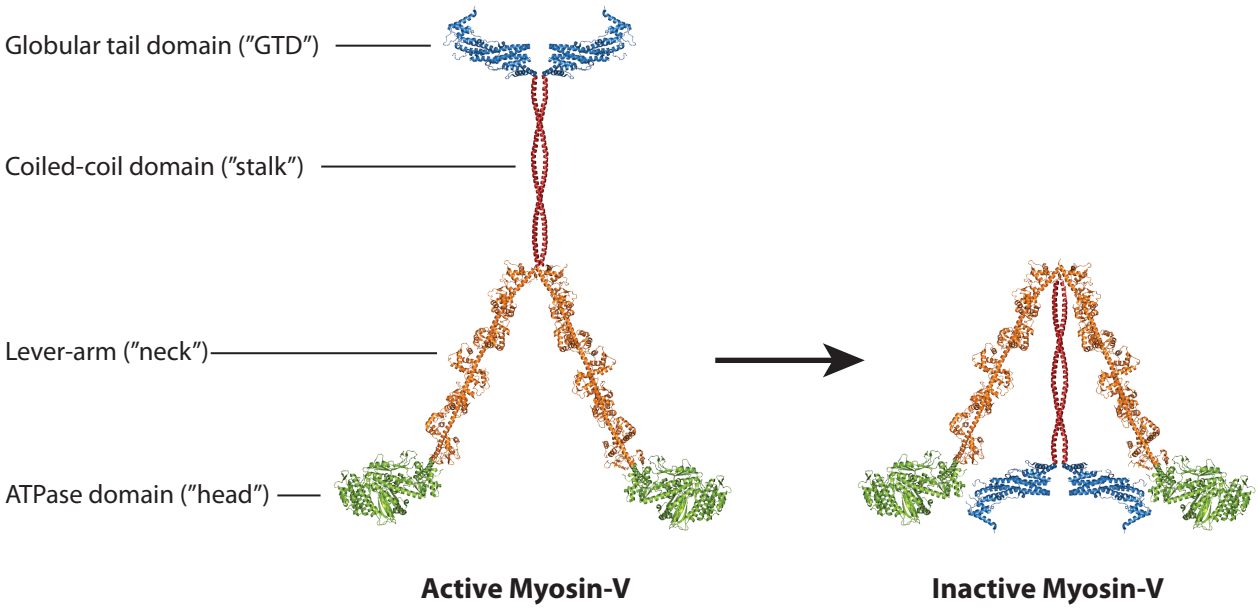

Figure 1.3. Domain architecture of the active and inactive forms of myosin-V. Structural model created using PDB accession numbers 2F6H and 2DFS.

always refers to the head/lever-arm fragment as the "head" and the coiled-coil/tail fragment as the "globular tail domain" or GTD.

The Head Domain

Crystal structures of the myosin-V motor domain were solved in both the pre- and post-stroke conformations (Coureux et al., 2004; 2003). These structures show features that are largely consistent with other classes of myosins but also show novel features that explain how it functions differently than conventional myosins. In all myosins, changes in motor conformation are associated with the specific nucleotide that is bound, with all myosins following a cycle of no nucleotide → ATP → ADP + P_i → ADP→ no nucleotide. Large structural changes occur during the hydrolysis step and myosin-V motors are no different. The major change to this cycle in class-V myosin motors is its slow release of ADP from the active site coupled to a high affinity for filamentous actin with ADP bound (La Cruz et al., 1999). This is due to the closure of a cleft separating the two sides of the actin-binding interface, causing it to resemble the structure of conventional class-II myosins in the strong-actin binding state (Coureux et al., 2003; 2004). The importance of this new interface can be seen in the *myo2-66* allele, the first temperature sensitive yeast mutant discovered, which lies near this cleft and completely abrogates all Myo2p function at the restrictive temperature (Lillie and Brown, 1994). While ADP release is slow in myosin-Vs, all other steps in the nucleotide cycle occur rapidly (La Cruz et al., 1999). Thus, myosin-V motors have adapted to spend much of their duty cycle in the strong actin binding, ADP-bound state. Most motors in this family have a high duty ratio, or the fraction of time the myosin motor is bound to filamentous actin. For MyoVa, this was calculated to be 0.7 (La Cruz et al., 1999). Having a high duty ratio is a critical feature of having processive movement, or the ability for a

motor to travel long distances without dissociation from the filament. Single molecule MyoV motors have been shown *in vitro* to take up to 60 'hand-over-hand' steps (4.2 μm, given its 74 nanometer step length) without falling off the filament (Shiroguchi and Kinosita, 2007; Warshaw et al., 2005; Yildiz et al., 2003).

The lack of processive movement of class-V myosins in yeast has been a longstanding controversy and at first glance seemed to separate them from higher myosin-V motors (Reck-Peterson et al., 2001). Myo4p, which functions in the transport of cortical ER and mRNA into the bud (Bobola et al., 1996; Estrada et al., 2003; Takizawa et al., 1997), is not a canonical myosin-V as it has not been shown to function as a true dimer. Thus, it is not processive by itself because there isn't an alternate head to hold it onto the actin filament once it dissociates. Instead, multiple Myo4p monomers can attach to a single receptor protein, as in the case of the mRNA receptor She3p; in this way, processive movement as a whole complex is ensured (Krementsova et al., 2011). Interestingly, the Myo4p motor domain appears to have all the features of a processive motor as a chimeria with the Myo4p head and MyoVa lever arm and tail domain was processive (Krementsova et al., 2006). This indicates that the motor domain alone is not the only factor in conferring processivity.

That other factors can confer processivity to myosin-V motors has recently solved the longest-running controversy related to Myo2p. Unlike MyoV motors from higher organisms, Myo2p does not co-sediment with actin in the presence of ATP (Reck-Peterson et al., 2001). Further, there was a decrease in the velocity of sliding actin cables with decreasing motor concentration during motility assays; for processive motors, there is no concentration dependence to the velocity. Note that in these assays, naked BODIPY-conjugated F-actin was used. From these experiments, the Mooseker Lab concluded that Myo2p is not a processive

motor *in vitro* (and calculated a duty ratio of 0.2) which appears to be inconsistent with its role in the cell. A year later, Daniel Schott in our lab published data showing GFP-Sec4 positive vesicles moving in a Myo2p-dependent processive manner (Schott et al., 2002), which contradicted the *in vitro* data. An answer to this puzzle was recently published by Kathy Trybus' lab. They found that while Myo2p is not processive on naked actin cables, it is highly processive on tropomyosin-decorated actin cables (Hodges et al., 2012). Both Tpm1p and Tpm2p greatly increased the number of steps Myo2p could take on actin filaments (averaging 34 steps with Tpm1p) by increasing the time the motor spends in the tight F-actin binding, ADP-bound state (Hodges et al., 2012). Additional regulators, such as the kinesin-like protein Smy1p functioning as an electrostatic tether between Myo2p and actin filaments, have been suggested to slightly increase Myo2p processivity *in vitro* as well (Hodges et al., 2009).

The Lever Arm

Following the head domain is the lever arm, or neck domain. While its secondary structure is one long alpha helix (predicted to be ~21 nm in yeast), it serves a variety of functions. The first is related to its length. When the trailing head domain of the motor hydrolyzes ATP, it creates a slight conformational change that is amplified by the lever arm. This moves the entire head/lever arm forward 13 actin monomers, or ~74 nm, in a hand-over-hand fashion to a new binding site (Yildiz et al., 2003). The 74 nm step size is characteristic of most myosin-V motors as this distance is twice the helical repeat of the actin filament; this allows the motor to proceed in one dimension and not spiral around the helix of the actin filament (Hammer and Sellers, 2011). Changing the length of the lever arm has been shown both

in vitro and *in vivo* to be important for both the step size of the myosin and the effective rate of speed that it travels (Purcell et al., 2002; Sakamoto et al., 2005; Schott et al., 2002).

While the secondary structure of the lever arm is important for its movement, the primary structure can affect its regulation. The lever arm largely consists of a series of IQ motifs (IQxxxRGxxxRxx[VLFY]) that serve as binding sites for regulatory and essential light chains. In yeast and mammalian cells, each monomer has six IQ motifs for a total of twelve per motor. Interestingly, MyoVa was discovered in part due to its function as a binding partner for one of the light chains, calmodulin (Espindola et al., 1992; Espreafico et al., 1992). Subsequent purification of chicken MyoVa revealed the existence of additional light chains of 10, 17, and 23 kDa (Espindola et al., 2000). Yeast calmodulin, Cmd1p, was later found to bind to Myo2p, but unlike its mammalian counterparts this occurs in a calcium-independent manner (Brockerhoff et al., 1994; Reck-Peterson et al., 2001). An additional light chain for Myo2p was found by BLAST searching for calmodulin homology sequences, which turned up Mlc1p (Stevens and Davis, 1998). While the overall IQ motif in the lever arm is conserved, their sequences do differ; this can have important effects on the stability and function of the motor. For instance, the IQ1-bound light chain has been shown in chicken MyoVa to modulate the kinetics of the motor domain *in vitro* (La Cruz et al., 2000). In higher myosin-V motors, calcium levels can regulate the binding of calmodulin to the motor in an IQ-motif-specific manner (Martin and Bayley, 2004). This can have important functional consequences both *in vitro* and possibly *in vivo*, as described in the next section. Lastly, Myo2p may transport the *lgl* homologs Sro7/77p to sites of exocytosis through its interaction with the lever arm (Rossi and Brennwald, 2011).

The Coiled-Coil Dimerization Domain

The coiled-coil domain, or stalk, is the interface where two myosin-V monomers come together to form a dimer in canonical motors. The length and structure of this domain varies widely across evolution, despite being predicted to be mostly alpha helical. In yeast, this domain is predicted to be about 24 nm in length with no interruptions to the alpha helix. Mammalian myosin-V motors, however, are much longer with 57 nm of coiled coil structure plus two interrupting loops (Hammer and Sellers, 2011). These loops are predicted to aid in the folding of the autoinhibited form, as discussed in the next section. Further, alternate splice variants exist in higher eukaryotes that can affect downstream binding partners. Specifically, Exon F in MyoVa introduces a 26 amino acid loop near the beginning of the C-terminal tail that is required for melanosome binding in mouse melanocytes (Au and Huang, 2002; Wu et al., 2002). While yeast do not have splice variants, the coiled-coil does serve as a GTPase binding effector. Importantly, the secretory vesicle Rab Sec4p can only bind to Myo2p in a coiled-coil dependent manner (Jin et al., 2011; Santiago-Tirado et al., 2011). Further, Rho3p was found to interact with the coiled-coil by yeast two-hybrid experiments. This interaction appears to be required for growth because a Rho3p point mutation that abolishes binding leads to the accumulation of post-Golgi secretory vesicles in the mother cell at low temperatures (Adamo et al., 1999; Robinson et al., 1999).

The Globular Tail Domain

The globular tail domain (GTD) at the C-terminal region of the motor is responsible for two actions: binding cargo and (at least in vertebrate myosin-Vs) autoinhibition. Numerous studies across many different model systems have shown that transport by the motor relies on receptor-mediated cargo binding; that is, protein intermediaries bridge the interaction between

the motor and cargo. A detailed description of both cargo binding and autoinhibition will follow, but an understanding of the basic structure of the tail is first needed. The tail domain was discovered during initial characterization of the motor through observation by rotary shadow electron microscopy (Cheney et al., 1993). It was predicted to be the cargo-binding domain due to its globular nature and was the least conserved portion of the motor. Experiments in yeast later showed that this was the case, as mutations to the tail abrogated vacuole movement and secretory vesicle movement without affecting the function of other cargos (Catlett and Weisman, 1998; Schott et al., 1999). Mild proteolysis of recombinant tail domain showed that the tail can be subdivided into two fragments termed subdomain I and subdomain II; an analysis of mutants showed that the vacuole-binding region inhabited subdomain I, while the vesicle binding region was present on the more highly conserved subdomain II (Pashkova and Weisman, 2005). Interestingly, both subdomains are required for the motor to function, which implies a high degree of communication between the two subdomains.

Detailed structures of the globular tail domain now exist for both mammalian motors and Myo2p and they all show the same overall structure even though they are quite divergent in sequence (Nascimento et al., 2013; Pashkova et al., 2006; Velvarska and Niessing, 2013; Wei et al., 2013). In yeast, the tail consists of two bundles of alpha helices connected by a single long terminal alpha helix that runs the length of the tail; this helix explains how the two subdomains cannot function on their own as it is probably involved in stabilization. The extensive contact between the two subdomains may help coordinate cargo binding. When the structure of the tail was solved, it was found that mutants defective in vacuole binding mapped to a cluster on the N-terminal helix bundle (in subdomain I). Certain mutants defective in secretory vesicle binding (specifically near the Y1415 site) were on subdomain II on the opposite face of the tail from

mutants affecting vacuole inheritance (Figure 1.4). Interestingly, a basic patch of residues is highly conserved in most myosin-V tails. In yeast Myo2p, these residues (specifically R1402/K1473) were shown to interact with the exocyst component Sec15p but in higher myosin-Vs were also shown to interact with the head domain to form an autoinhibited motor complex (Jin et al., 2011; Li et al., 2008). This will be discussed in a following section, but such an autoinhibited complex has not been shown to exist for yeast myosin-Vs.

Post-translational modifications to the GTD have been shown to have important implications for cargo binding and release in vertebrate myosin-V motors (Karcher et al., 2001). Mass-spectrometry mapping of *Xenopus* egg extract MyoVa showed that a single residue, S1650, could be phosphorylated by calcium/calmodulin-dependent protein kinase II (CaMKII). The removal of this phosphate in recombinant MyoVa tails caused the tail to dissociate from membranes. Thus, phosphorylation can control the binding of organelles. This residue is conserved in some fungal species, but not in budding yeast. Myo2p has, however, been shown to be phosphorylated *in vivo* in a cell-cycle dependent manner on a series of several residues just before subdomain I that are not well conserved (Legesse-Miller et al., 2006). Further analysis showed that mutating these residues did not affect cell growth or cargo binding. However, there is some incomplete evidence that that the phosphatase Ptc1p may regulate Myo2p association with the vacuole receptor Vac17p, the peroxisome receptor Inp2p, and the mitochondrial receptor Mmr1p. Deletion of Ptc1p caused mislocalization of the cargos and a slight mislocalization of Myo2p (Jin et al., 2009). Further work is needed though to explain how exactly this occurs.

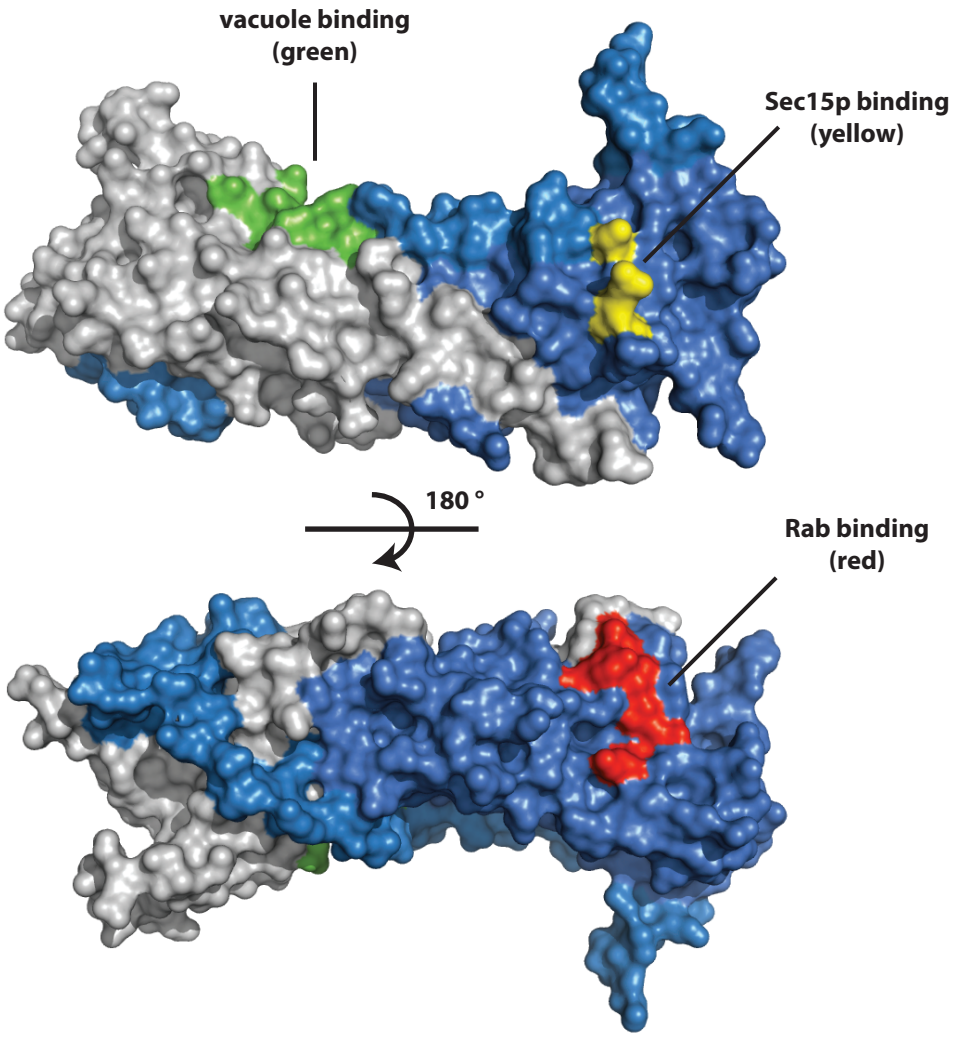

Figure 1.4. Cargo binding regions of the Myo2p tail. The overall subdomain I is shown in grey while the overall subdomain II is shown in blue. On subdomain I, the vacuole binding area is shown in green. On subdomain II, the Rab binding area is shown in red while the Sec15p binding area is shown in yellow.

Regulation of Myosin-V Motors

It should be clear by now that the overall function of class-V myosin motors can be distilled into two very simple actions: bind a cargo, and move it to a different place. As detailed above, these actions are accomplished at opposite ends of the motor, with cargo binding occurring in the C-terminal "tail" domain and movement being made possible by ATP hydrolysis in the head domain. How, then, does the head domain "know" that there is cargo bound at the tail domain? For an optimally efficient motor, some level of control is needed to prevent motors from traveling without cargo.

Autoinhibition Regulates Vertebrate Myosin-V Motor Activity

Clues to a regulatory element present in class-V myosins can be seen in some of the very first biochemical papers. The Mooseker lab was among the first to purify a class-V myosin, and reported that chicken brain myosin-V was a dimer with two head domains and a long stalk leading to a globular domain of unknown function (Cheney et al., 1993). They also were the first to notice an interesting motor regulation paradox. In the presence of EDTA and actin filaments, ATPase activity was about 25-fold over baseline activity without actin filaments. With 10 μM calcium and actin filaments, this activity increased to about 200-fold. This implied that calcium might have some role in stimulating motor activity. However, when excess calcium was used in standard motility assays, there was a drastic reduction in actin filament movement compared with experiments run with EDTA.

This paradox was closer to being resolved in 2004 when three groups independently published MyoV sedimentation data (Krementsov et al., 2004; Li et al., 2004; Wang et al., 2004). They found that under conditions of high ionic strength or high calcium motors sediment at 11S

while at low ionic strength or low calcium they sediment at 14S. When subjected to electron microscopy, it was revealed that the 14S motors were folded in a triangular shape while the 11S population adopted an elongated conformation. This folded conformation appeared to be an interaction between the head domains and the globular tail domain and was the first visual evidence of a conformational change. Supporting this, a "tail-less" heavy-meromyosin fragment does not sediment at 14S and its ATPase activity is not regulated by calcium, suggesting that the globular tail is required for regulation of ATPase activity (Li et al., 2004; Wang et al., 2004). Adding back the globular tail separately in *trans* can reduce ATPase activity and actually creates a triangular shaped motor when viewed by EM (Li et al., 2006; Thirumurugan et al., 2006). Thus, ATPase activity is attenuated when the motor domain is in close proximity to the tail domain. It should be noted that this calcium regulation is not usually physiologically relevant since a high calcium concentration leads to a dissociation of the calmodulin light chain from the lever arm. There has been one report of calcium regulation *in vivo*, which will be discussed later in this section.

Detailed cryo-electron microscopy projections of myosin-V in its autoinhibited state have been published by two separate groups that show the same broad mechanism of autoinhibition but with some important differences (Liu et al., 2006; Thirumurugan et al., 2006). Both groups found that the motor folds at the interface between the lever arm and coiled-coil, and that the unstructured loops present in the coiled-coil domain (which Myo2p lacks) have an important role in orienting the head and tail domains (Figure 1.3). They also both found that the motor binds the head at regions near the motor's active site and far away from the actin-binding site.

By analyzing two-dimensional myosin-V crystals on a lipid surface, Liu and colleagues (2006) found that the tail domain bound to loop 1 of the motor domain in a post-power stroke conformation. This position would leave the motor best able to bind the tail with ADP bound, where the motor normally binds F-actin. Loop 1 binding has been shown to modulate the ATP cycle in myosin-II studies, which might indicate a mechanism for slowing the hydrolysis rate seen in biochemical studies (Sweeney et al., 1998). Further, they showed that at low concentrations myosin-V can decorate actin filaments, consistent with their model.

Thirumurugan and colleagues (2006) used single molecule negative staining to reveal a different tail binding area, at nearby negatively charged lobe on the surface that is highly conserved among myosin-V homologs but not among other myosins. This cryo-electron structure instead showed a post-rigor conformation, which would be predicted to bind weakly to filamentous actin. Since this interaction region is far away from the ATPase domain or loop 1 that modulates it, the authors propose an allosteric mechanism that controls ATPase activity. They also performed biochemical studies and were unable to decorate actin filaments with motors, which supports their model.

The duty cycle state myosin-V is left in when inactive is not a trivial question and would have physiological implications on how the motor recycles after delivering its cargo. Three models exist for recycling myosin motors from sites of exocytosis. First, after unloading its cargo, the motor could fold up and recycle by binding to a minus-end directed myosin-VI motor. This seems unlikely as there is little colocalization between the two myosin species. Alternatively, if the motor is present in a post-rigor conformation as Thirumurugan and colleagues support, one could imagine that the autoinhibited motor could recycle back via diffusion. However, actin treadmilling (or retrograde actin flow) also provides an interesting

means of recycling and would be favorable if the motor is locked in an ADP state as Liu and colleagues suggest.

The concentration of F-actin in certain places, while variable and difficult to measure, has been estimated to be as high as 435 μM (Taylor, 2007). By comparison, striated fly muscle is 770 μM. This F-actin density might make it difficult for a 30 nm long folded myosin to recycle back for another round of transport. Other constriction points, such as the bud neck or dendritic spine opening, also might make it unfavorable for diffusion-based recycling. By holding on to actin cables in an inactive state as actin treadmills at 100-300 μm/s (Lin and Forscher, 1995; Yang and Pon, 2002), a myosin-V could be recycled out of such actin rich areas. The biophysics of myosin-V motors in actin rich areas also suggests this is possible, and it has been calculated that myosin-V could travel 3.1 μm before falling off (Taylor, 2007). Such retrograde travel along actin cables has been reported for class-X myosin motors in filopodia (Berg and Cheney, 2002), though the structure these myosins adopt may not be similar to myosin-V motors.

Several recent studies suggest that the tail of myosin-V binds to the head in the orientation favored by Thirumurugan and colleagues, which would argue for weak F-actin binding in the inhibited state. Biochemical work identified one highly conserved acidic residue in the head and two basic residues in the tail that mediate this interaction (Li et al., 2008). Addition of the tail domain to wildtype motor domains follows a concentration-dependent decrease in ATPase activity. However, alanine point mutations at position D136 in the head, or at K1706/K1779 in the tail abrogates this effect (Li et al., 2008). Finally, when these mutants were subjected to electron microscopy, an open conformation motor was observed. In the simplest model, these residues would form an ionic bond between the head and tail domains when in close proximity, forming the closed 14S conformation of the motor. This data was supported last

year, when the human MyoVa tail structure was solved (Velvarska and Niessing, 2013); the best fit for molecular docking of the tail to the head was the site supported by Thirumurugan and colleagues.

Regulation of Activity Through Cargo Binding

Thus, it is clear that mammalian myosin-V motors exist in two states: an elongated 11S conformation with high ATPase activity, and a folded 14S conformation with low ATPase activity. Calcium has been shown to stimulate conformational change, but the levels needed to perform this conformational change are not usually physiological. What else could trigger the conformational change? An attractive model is that cargo binding to a motor in the inhibited state would activate the motor. This would allow the motor to be active only when cargo is attached to the tail.

A clue that some type of motor regulation occurs *in vivo* was found by the Hammer group, with their initial identification of Rab27a and melanophilin as receptors for MyoVa (Wu et al., 2002). Briefly, Rab27a on melanosomes binds to melanophilin, which then binds to MyoVa via Exon F (which is located just before the globular tail domain and required for binding). They found that mutations to melanophilin caused the MyoVa motor to be diffusely localized in cells, and not on actin structures. Further, when they overexpressed a minimal portion of melanophilin that binds to MyoVa, the motor was relocated to the periphery of the cell on actin structures. These results together suggest that motor activation requires cargo binding.

The Ikebe group was first to publish biochemical evidence that cargo binding regulates conformation changes in the motor (Li et al., 2005). Their biochemical system featured a MyoVa motor lacking the globular tail domain, but including exon F. Adding the globular tail domain

alone reduced ATPase activity as expected, since the motor was adopting the closed conformation even though it was acting in *trans*. However, adding melanophilin to this system stimulated ATPase activity four-fold. They further showed that the myosin-binding region on melanophillin is sufficient to activate the motor activity, and that Rab27a (which is also a part of the receptor complex) did *not* stimulate activity. This was the first biochemical evidence of a cargo stimulating motor activity.

A combination of calcium stimulation and cargo binding has also been shown to activate MyoVb in dendritic spines. MyoVb traffics AMPA and NMDA receptors on recycling endosomes to the dendritic spine surface during long-term potentiation. Dendritic spines usually have low calcium levels, where MyoVb would be inactive in the absence of cargo. An action potential can increase the local concentration of calcium as high as 30 μM, which *in vitro* will elongate the motor (Sabatini et al., 2002). Wang and colleagues (2008) found that increasing calcium concentration (to as high as 1 mM) in an immunoprecipitation experiment stimulates the interaction between MyoVb and the receptors present on the recycling endosome, Rab11 and FIP2. Using truncation and known mutants that inhibit this interaction, they showed that the head-tail mechanism is relieved under these conditions (Wang et al., 2008). Thus, they appear to show a link between the calcium influx to a dendritic spine during long-term potentiation and cargo recruitment. How the motor is able to move processively under high calcium levels, which it cannot do *in vitro*, was not discussed.

Does Myo2p undergo autoinhibitory regulation?

An interaction between the head and tail of yeast Myo2p has not been described. However, there are several lines of evidence that point to the motor adopting an inhibited

conformation. First, the basic residues in the tail that are predicted to interact with the head are conserved (R1402 and K1473) and are presented on the surface in the same orientation as in mammalian MyoV tails (Nascimento et al., 2013; Pashkova et al., 2006; Velvarska and Niessing, 2013; Wei et al., 2013). Crucially, these residues are not conserved in the other yeast myosin-V, Myo4p, which is predicted to be a monomer and not adopt the same conformation when moving cargo (Heuck et al., 2010). This line of reasoning is complicated, however, with the recent finding that this basic patch on Myo2p also binds to Sec15p, which likely does not bind to Myo4p (Jin et al., 2011). Conserved acidic residues in the head of Myo2p also exist (specially E137, but also D123 and E135) but little is known about their placement because a crystal structure of the Myo2p head does not exist. Threading the yeast Myo2p primary structure around a mammalian MyoVa head does place them pointing out from the surface in a clustered arrangement (this thesis) but it cannot be confirmed without a detailed crystallographic structure.

Other pieces of evidence do not quite fit with a head-tail autoinhibition model in yeast. Yeast two-hybrid experiments between head and tail fragments have not detected an interaction on at least two occasions in the Bretscher lab, including work done by myself; work done in the Weisman lab by Pashkova and colleagues (2006) also failed to detect an interaction. This could be explained by a particularly transient interaction, a lack of an accessory protein, or lack of a post-translational modification. Secondly, the coiled-coil domain of Myo2p is predicted to be about 24 nanometers in length given its alpha-helical nature; this would be far short of the 57 nanometers of coiled-coil in its mammalian counterparts and whose length seems to be important for myosin autoinhibition. Further, the coiled-coil of Myo2p does not have the two unstructured loops dividing the domain as MyoV motors have. These unstructured loops are predicted to help the molecule fold into the right conformation (Hammer and Sellers, 2011). Despite these

potentially damning pieces of evidence, secondary structure prediction algorithms suggest that Myo2p has ~60 unstructured residues after the coiled-coil domain and before the globular tail domain that could aid in folding. Further, the lever arm domain of Myo2p is nearly the same length as the coiled-coil, which could allow it to adopt the proper conformation if the "hinge" is between them as in vertebrate motors (Figure 1.3).

The Secretory Pathway

Because this thesis concerns how myosin-V motor proteins coordinate their activities with the secretory pathway, I will first present an overview of the relevant steps and transitions before discussing secretory cargo binding. George Palade in the 1960s first used an autoradiographic technique to follow pulsed radiolabeled proteins in guinea pig pancreas cells (Jamieson and Palade, 1966; 1967). This showed that proteins flow first from the endoplasmic reticulum to the Golgi complex in vesicular carriers, and then from the Golgi complex into zymogen granules to be exocytosed. However, unbiased mutagenic screens performed in the late 1970s in yeast allowed for the genetic dissection of the steps involved in secretion; subsequent experiments allowed for a very complete picture of the underlying machinery (Novick and Schekman, 1979; Novick et al., 1980).

The Early Secretory Pathway

As I use certain mutants from the early secretory pathway, I will briefly summarize the ER-Golgi transition and COPII vesicles. The process of forming COPII vesicles at ER exit sites begins with the GTPase Sar1p being placed in the active form by its GTP Exchange Factor (GEF) Sec12p; this step reveals an amphipathic helix that inserts Sar1p into the ER membrane

while also generating membrane curvature. Active Sar1-GTP is then able to recruit the inner COPII coat, consisting of Sec23p/Sec24p. An interaction with the cargo and Sec24p helps sequester cargo into the pre-budding complex while Sar1p continues to generate a small amount of membrane curvature. This nascent inner coat is collected and ordered by binding of the outer coat proteins, Sec13p/Sec31p, allowing enough membrane curvature to generate a vesicle. Docking and fusion of the vesicle to the Golgi complex is mediated by the TRAPPI complex through its binding to Sec23p after the coat protein hydrolyzes Sar1-GTP in its role as a GTPase Activating Protein (GAP). This step then recruits the early Golgi GTPase Ypt1p to the vesicle, which subsequently recruits the tethering protein Uso1p. Finally, vesicle fusion with the Golgi can occur following SNARE (SNAP (Soluble NSF Attachment Protein)) REceptor assembly (Cao, 1998; Jensen and Schekman, 2010).

Regulation of GTPases

It has been known for some time that the Golgi complex serves several roles in the cell. In most cells other than *S. cerevisiae*, about 6-10 cisternae are in close proximity to one another, with the side closer to the ER known as the cis-Golgi and the side further from the ER known as the trans-Golgi. The Golgi complex was first known as a protein modification organelle, as numerous modifications occur to proteins as they move through the Golgi complex. These modifications include phosphorylation by kinases and sequential addition of carbohydrates as the proteins move through the organelle (Dunphy and Rothman, 1985). Its secondary function, which most concerns this thesis, is its role as a central trafficking hub; proteins that exit the trans-Golgi are sorted and packaged for destinations throughout the cell (Griffiths and Simons, 1986).

Proteins mature through the Golgi complex via cisternal maturation. That is, the maturing proteins remain in individual cisterna throughout their time in the Golgi while modifying enzymes and Golgi-resident proteins that provide membrane identity shuttle between stacks. This model was first shown beautifully in yeast by the Glick and Nakano labs, where they showed that individual cisterna acquire and lose Golgi-resident proteins (Losev et al., 2006; Matsuura-Tokita et al., 2006). However, this begs the question how individual cisterna mature and how the proteins that provide membrane identity can so consistently cycle on and off of membranes.

The proteins widely believed to give membrane identity are the Rab GTPases. This is accomplished by their ability to "switch" on and off by binding to specific nucleotides, GTP or GDP, which then controls which downstream effectors they can bind to. These effectors are as diverse as coat proteins, tethering complexes, molecular motors, and SNARE proteins. Eleven Rab proteins are found in yeast (and than 60 in humans) on different organelles, but they primarily function at different stages of the secretory pathway (Hutagalung and Novick, 2011). Crystal structures exist for nearly all classes of Rabs, which give insight into their precise molecular function.

Rab GTPases are generally small proteins no more than about 30 kDa. They all have the same characteristic structure, termed the "GTPase fold," consisting of a six-stranded beta sheet surrounded by five alpha helixes (Lee et al., 2009). Two regions, termed switch I and switch II, are the major determinants of effector binding and their structure is controlled by the specific nucleotide that is bound. When GDP is bound, these regions primarily consist of unstructured loops; when GTP is bound, these two regions undergo a conformational change that makes them more structured to bind downstream effectors (Vetter, 2001). Further, analysis of the crystal structures of different Rab proteins in both active and inactive states shows that both the residues

present in this region and the conformation they adopt are diverse; this explains how different Rab proteins are able to bind to specific effectors (Eathiraj et al., 2005; Hutagalung and Novick, 2011).

Their membrane insertion ability is controlled by their C-terminal CAAX motif; *in vivo*, this allows one or (usually) two geranyl moieties to be post-translationally covalently attached. When this is removed, the function of the protein is compromised; loss of function of essential Rabs will render the cell unable to live (Calero et al., 2003). Other regions, at the extreme N-terminus or C-terminus just upstream of the CAAX box, are the most divergent and can also play a role in membrane targeting. This was elegantly shown in yeast where the secretory vesicle Rab, Sec4p, had its C-terminal hypervariable region replaced with that of the cis-Golgi Rab Ypt1p; localization of this chimera was now cis-Golgi despite having a general Sec4p structure (Brennwald and Novick, 1993).

The ability of Rabs to exist in two states, with GTP bound or GDP bound, is controlled by a host of different proteins. Likewise, their function is controlled by their ability to exist in or out of a membrane. After Rabs are first translated by the ribosome, they will complex with the Rab escort protein (REP) and then be prenylated by the Rab geranylgeranyl transferase (GGT). Upon delivery to its target membrane, its ability to exist in an active GTP-bound state or inactive GDP-bound state are controlled by Guanine-nucleotide Exchange Factors (GEFs) and GTPase Activating Proteins (GAPs). GEF proteins, which are highly divergent but have the same basic function, stimulate the Rab proteins to bind GTP, allowing it to bind to downstream effectors. The ability to turn "off" and lose their interaction with effectors is controlled by GAPs. These proteins, which are well conserved and consist of a TBC (Tre2/Bub2/Cdc16) domain, catalyze the hydrolysis of GTP to GDP to return the Rab to its inactive state. Other proteins, such as

Guanine-nucleotide Dissociation Inhibitors (GDIs) can now remove this inactive Rab from one compartment and reinsert it into the target membrane via a GDI Dissociation Factor (GDF) for another round of action (Hutagalung and Novick, 2011).

Diseases caused by loss-of-function mutants for particular players in this pathway underscore the importance of these proteins in a normal functioning secretory system. This includes choroideremia, caused by human REP-1 mutation, and is characterized by atrophy of the retinal pigment epithelium leading to blindness (Seabra et al., 1993). Mutations in GDI1 can lead to X-linked mental retardation (D'Adamo et al., 1998), while mutations in Rab3GAP can lead to defects in eye, nervous system, and genitalia development (Aligianis et al., 2005; 2006).

Rab GTPases Control Membrane Identity in the Golgi Complex

The process that gives secretory membranes their individual identity is largely mediated by Rab proteins correctly localizing and activating via a GEF cascade and being inactivated by a countercurrent GAP cascade. This ensures both directionality of the secretory pathway and proper localization of effectors. It has been shown for some time that certain Rabs, such as Ypt1p, localize to membranes early in the secretory pathway while other Rabs, such as Ypt31/32p and Sec4p, localize to later membranes (Benli et al., 1996; Jedd et al., 1995; Salminen and Novick, 1987). However, studies from the Novick Lab have elegantly shown exactly how this occurs. The GEF cascade uses an already active Rab protein to recruit the next GEF in the pathway; this will serve to activate the following Rab. The previous Rab is then shut off by the countercurrent GAP cascade, where the next Rab in the pathway will recruit the GAP for the previous Rab.

In the yeast Golgi, Ypt31p and Yp32p are both incredibly well conserved Rabs that were

first shown to be involved in secretory trafficking within (or out of) the Golgi (Benli et al., 1996; Jedd et al., 1997). The Novick lab found that overexpression of either of these Rabs can suppress the growth defect of *sec2-78*, a mutant allele to the GEF for Sec4p, the Rab present on secretory vesicles (Ortiz et al., 2002; Walch-Solimena et al., 1997). They further showed (1) that overexpression of Ypt32p relocalizes the mutant Sec2p allele from the cytosol to a polarized state similar to the wildtype protein, (2) that binding of Sec2p occurs only with GTP bound, (3) that the overexpression does not effect its normal exchange activity with Sec4p, and (4) that Ypt32p and Sec4p bind to different sites on Sec2p. These results suggested that Ypt32p was responsible for localizing Sec2p to the Golgi complex and allow it to recruit and activate the next Rab in the pathway, Sec4p. Conversely, it has been shown that Ypt1p and Ypt6p (the early-Golgi Rabs) are inactivated via a GAP cascade. In this system, active Ypt32p recruits both Gyp1p and Gyp6p, the GAP protein for Ypt1p and Ypt6p, respectively. When these GAPs are deleted, the transition between Rab compartments is delayed and there is an increase in time that two Rabs are active on one membrane as analyzed by time-lapse microscopy of Golgi cisternae (Rivera-Molina and Novick, 2009; Suda et al., 2013). A similar type of cascade has been seen in mammalian cells, suggesting a conserved mechanism. In this system, Rabex5 (the GEF for Rab5) is recruited to a membrane by a Rab5 effector, Rabaptin5. This allows subsequent recruitment and activation of Rab5 at the proper location (Horiuchi et al., 1997).

A natural extension of the GEF cascade occurs in the example given above, where Sec2p recruits Sec4p and another effector, the exocyst component Sec15p. This system is critical as it sets up the transition from trans-Golgi to secretory vesicle and allows for the association of Myo2p. In the GEF cascade, Sec2p is recruited to the membrane via its interaction with Ypt32p; based on differences in localization experiments and *in vitro* binding experiments, this Ypt32p

binding region in Sec2p was predicted to be between amino acids 160-374 (Ortiz et al., 2002). Sec4p, meanwhile, was understood to require only the N-terminal exchange domain (amino acids 1-160) for binding. However, a third region C-terminal to these other regions existed that was also implicated in Sec2p localization. Mutations in this region (amino acids 450-508) or its deletion lead to cells with mislocalized Sec2p.

The finding that the exocyst tethering complex component Sec15p also binds to Sec2p solved this interesting regulatory puzzle. Mutations or deletions to this third C-terminal region yielded tighter binding of to Sec15p and reduced binding to Ypt32p; there was also significantly less Sec15p in the cytoplasm, further suggesting tighter binding to the secretory vesicle-localized Sec2p. Strikingly, the Ypt32p and Sec15p binding sites on Sec2p overlapped and suggested a mechanism for switching from late-TGN to secretory vesicles. As discussed before, Ypt32p recruits Sec2p to the late-Golgi. This in turn allows Sec2p to recruit and activate Sec4p. At this point, there is a regulatory switch in the Sec2p C-terminal domain that controls Ypt32p/Sec15p binding partners. This switch seems to be dependent on a number of things. First, since Sec15p is an effector for Sec4p, having an additional effector present implied that the GEF would replace Ypt32p for Sec15p (Medkova et al., 2006). Other experiments also showed that this regulatory switch was dependent on falling PI4P levels, as high PI4P levels (present at the late-Golgi) inhibit the Sec2p-Sec15p interaction. This is due to a series of basic patches present in this third C-terminal switch domain that bind to and sense PI4P levels. When levels are hypothesized to fall as secretory vesicles mature, this inhibitory effect was relieved, allowing Sec15p binding (Mizuno-Yamasaki et al., 2010). Finally, data published last year have shown that a group of residues (in 180-188) undergo phosphorylation by an unknown kinase after this regulatory switch is completed, which further strengthens the Sec2p-Sec15p interaction and prevent it from

reverting (Stalder et al., 2013). The dephosphorylation event at the cortex was then theorized to relieve Sec15 binding, allowing recycling of Sec2p from the plasma membrane.

As should be clear now, Rab proteins allow for (1) the fidelity of membrane identity throughout the Golgi and (2) aid in the maturation of Golgi membranes into secretory vesicle membranes. Unlike earlier steps in the secretory pathway, the transit of secretory cargo to the bud is an active process and requires their association with the motor Myo2p. How they physically interact with the motor is still an active area of research. Before discussing the transport of secretory vesicles by Myo2p, I will begin with a general overview of cargo transport.

Cargo Transport by Myo2p

With the exception of secretory vesicles, Myo2p transports specific cargoes at specific times during the cell cycle. Cargo association is mediated by binding to distinct receptor proteins, which physically link the cargo to the C-terminal tail domain (Figures 1.4, 1.5). Non-essential cargo receptors include the vacuole receptor complex Vac17p-Vac8p (Ishikawa et al., 2003), the peroxisome receptor Inp2p (Fagarasanu et al., 2006), the trans-Golgi receptors Ypt31/32p (Lipatova et al., 2008), and the astral microtubule receptor Kar9p-Bim1p (Yin et al., 2000). Essential cargoes of Myo2p include mitochondria, with the interaction dependent on Ypt11p and Mmr1p (Chernyakov et al., 2013; Itoh et al., 2002; 2004), and secretory vesicles, which are dependent on Sec4p and an unknown component binding to PI4P (Jin et al., 2011; Santiago-Tirado and Bretscher, 2011; Schott et al., 1999). Regulation of the timing of cargo inheritance (with the exception of secretory vesicles, which are constitutively transported) is largely done at the receptor level. The method of regulation is varied and includes phosphorylation of specific residues (Peng and Weisman, 2008), degradation of the receptor at

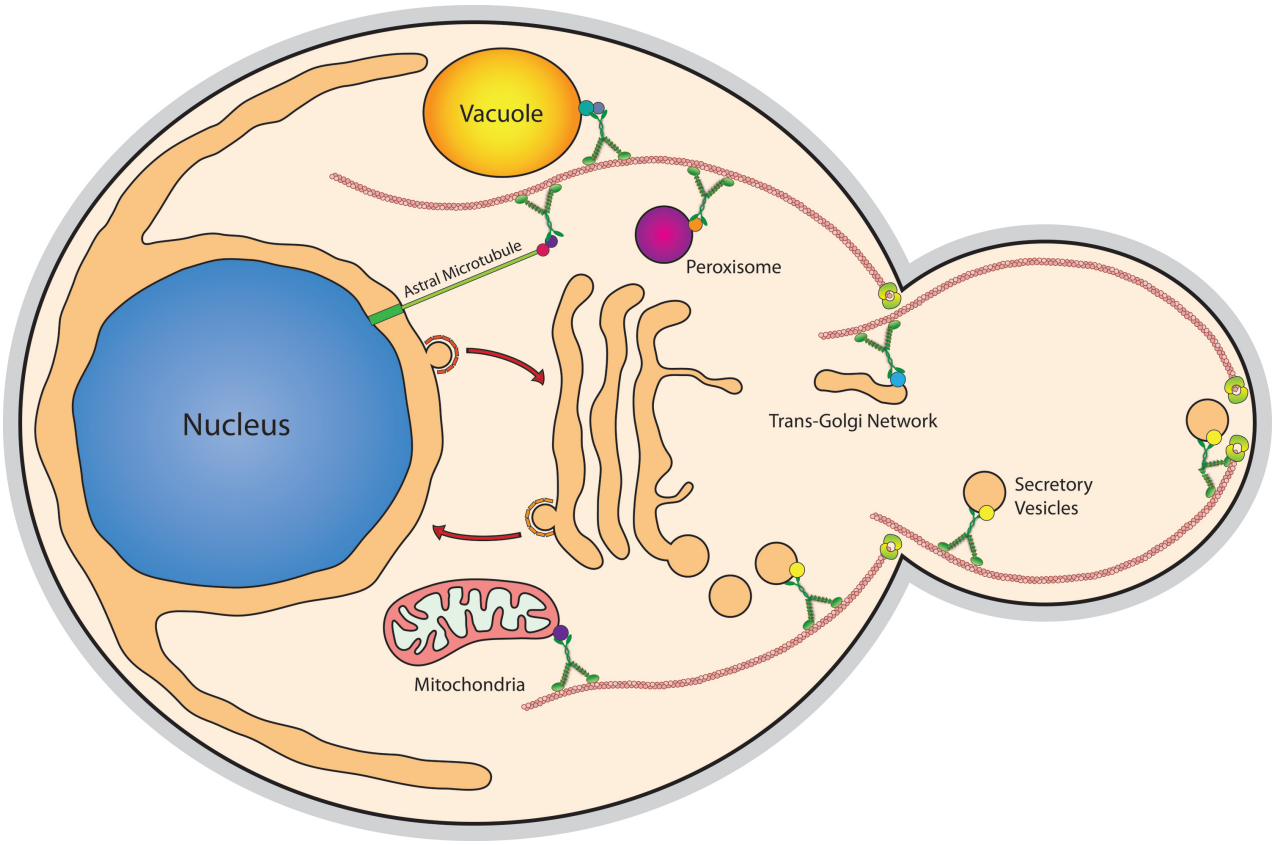

Figure 1.5. Model of Myo2p cargo transport in budding yeast. Myo2p transports cargoes on actin cables nucleated by formin proteins at the bud tip and neck (actin cables shown in red, formins shown in yellow-green). Myosin motors transport specific cargoes by binding to specific receptor proteins (colored circles). Secretory vesicles and mitochondria are its only essential cargos.

different times in the cell cycle (Fagarasanu et al., 2006; Tang et al., 2003), or the nucleotide binding state of the receptor (Lipatova et al., 2008; Santiago-Tirado and Bretscher, 2011).

Additional regulation occurs at the level of the Myo2p tail, as certain binding sites overlap; this implies that cargos compete for access. Residues for binding Mmr1p and Vac17p overlap on subdomain I, while residues for binding Kar9, Inp2p, and the Rab GTPases Ypt11p/Ypt31p/Ypt32p/Sec4p overlap on the more highly conserved subdomain II (Figure 1.4). Thus, binding to the receptor site on either subdomain effectively prevents other cargoes that use that subdomain from binding. This competition has recently been detected *in vivo* with very specific point mutants that disturb either Vac17p or Mmr1p binding to subdomain I (Eves et al., 2012). Mutations blocking mitochondrial receptor binding lead to a greater volume of vacuole in the bud, and vice versa. Further, it has been proposed that the helices and loops that fall between binding sites may modulate binding across the tail; that is, a receptor that binds to subdomain I will cause a conformational change in the tail that will cause other receptors from binding subdomain II.

Since this work is devoted to how Myo2p coordinates its actions with its essential cargo of secretory vesicles, I will refrain from going too in-depth on its role in transporting other cargoes. Nevertheless, I will go into some detail on vacuolar inheritance because it can give important insights into the regulation of Myo2p.

Vacuolar Membranes

The inheritance of the vacuole is not an essential function in yeast, but its inheritance and release from Myo2p is well characterized. Vacuoles can be generated *de novo* (most likely from earlier endosomal components) and this feature allowed for the quick isolation of vacuole morphology mutants, most of which were defective in the inheritance of the vacuole (Shaw and

Wickner, 1991; Weisman et al., 1990). During the yeast's life cycle, it was noticed that the vacuole becomes disrupted and smaller components move into the bud to reform following cytokinesis. The class I set of *vac* mutants had apparently normal functioning vacuoles but were unable to be inherited (Wang et al., 1996). This analysis, and the finding that the vacuole was not inherited in a subset of actin alleles and in the *myo2-66* allele, suggested that Myo2p was actively transporting them into the bud (Hill et al., 1996). Additional work with the *myo2-2* allele in the tail confirmed that Myo2p moves the vacuole into the bud (Catlett and Weisman, 1998).

The receptor for the vacuole is now known to be Vac8p-Vac17p. Vac8p is modified at its amino terminus with myristoyl and palmitoyl groups, and these modifications are necessary for the inheritance of the vacuole (Wang et al., 1998). This suggested it might bind to Myo2p as a direct receptor, but no interaction was found. The Vac17p intermediary was found through several parallel experiments, including overexpression suppression screens of the *myo2-2* allele, an intergenic suppressor screen to revert the effects of a second Myo2p tail point mutant, and a yeast two-hybrid screen for Vac8p interactions (Ishikawa et al., 2003). Further work showed that Myo2p binds Vac17p directly (which in turn binds Vac8p on the vacuole membrane) and that disruption of any of these interactions leaves vacuoles unable to be inherited.

The mechanism behind the release of the vacuole from the motor is well characterized and pertinent to this thesis. It was noticed that Vac17p levels, as well as movement of the vacuole itself, was coordinated with the cell cycle. Vac17p levels peak in G1 and S phase (corresponding to unbudded/newly budded cells) and are lowest during cytokinesis. Blocking vacuole inheritance with different mutants increased Vac17p levels, suggesting that inheritance was somehow regulated by protein expression or turnover. Sequence analysis of Vac17p revealed a PEST degradation sequence, which when deleted abrogated the cell cycle regulation of Vac17p

and, importantly, vacuoles were inherited but not deposited correctly near the bud tip (Tang et al., 2003). Further work showed that phosphorylation events can regulate the degradation of Vac17p. The Weisman lab found that a specific residue in the PEST domain (T240) is phosphorylated in the mother cell and is required for binding of the ubiquitin ligase Dma1p, which only binds the vacuole once it enters the bud (Yau et al., 2014). This targets Vac17p for degradation via the ubiquitin-proteasome system and provides a mechanism for the targeted release of the vacuole at the proper place and time. Additionally, another phospho-region of Vac17p may control Myo2p binding (Peng and Weisman, 2008). Two residues in the Myo2p binding domain of Vac17p are phosphorylated by CDK and this phosphorylation is correlated with Vac17p levels and vacuole transport; this led to the hypothesis that association of Vac17p is at least in part regulated by CDK, though additional work remains to be done to show this.

Secretory Membranes

The ability of the bud to grow is directly related to the delivery of secretory membranes, including late-Golgi elements and secretory vesicles. These membrane-bound compartments contain lipids that will become integral to the growing bud and enzymes that will remodel the cell wall at all stages of growth. Secretory vesicles in particular are by far the most frequently transported cargo of Myo2p; given the size of the bud, rates of growth, and the rate of endocytosis, I have estimated that about 2000 vesicles are required for sufficient membrane surface to generate a new bud (Donovan and Bretscher, 2012). Therefore, the importance of coordinating secretory vesicle delivery by Myo2p with their tethering and fusion to the plasma membrane cannot be overstated. Evidence that secretory vesicles are required for bud growth was found in the very first paper that showed a genetic underpinning for the secretory system. In that paper, *sec1-1* cells showed a buildup of secretory vesicles in the bud when shifted to the

restrictive temperature (Novick and Schekman, 1979). Shifting back to the permissive temperature allowed these vesicles (and those in most other *sec* mutants) to be fusion competent. How these vesicles got to the bud, however, was a mystery.

The paper that discovered that the temperature sensitive gene product of *cdc66* was actually a class-V myosin also first suggested that it is involved in the vectoral transport of vesicles. At the restrictive temperature, this mutant (now termed *myo2-66*, whose mutation is in the head domain of the motor) saw a large buildup of vesicles in the mother cell that could still grow isotropically but were not transported to the bud (Johnston et al., 1991). These findings were later extended by the Novick group, who showed that *myo2-66* is synthetically lethal with a number of late-acting, but not early-acting, *sec* mutants (Govindan et al., 1995). Crucially, they also found that late-*sec* mutants that normally show a buildup of vesicles in the bud instead showed a depolarized distribution when combined with the *myo2-66* mutant at the restrictive temperature. These results strongly implied that Myo2p had a role in the targeting of secretory vesicles. Later experiments in our lab conclusively showed that tropomyosin-containing actin cables are required for both Sec4p and Myo2p polarization (Pruyne et al., 1998).

Some controversy emerged around this time when it was suggested that Myo2p might not be an active motor moving cargo to the bud, but instead that the tail domain functioned as the localization domain; the motor domain was then able to either organize actin cables, capture diffusing cargo, or both (Reck-Peterson et al., 1999). This was supported by the finding that overexpression of the tail domain resulted in a polarized fragment after a short expression time (it was probably just binding to secretory vesicles and transported there) and that some Myo2p remains polarized in LatA treated cells (which may have been Myo2p still docked to secretory vesicles after fixation) (Ayscough et al., 1997).

However, our lab generated conditional mutants to the tail of Myo2p that specifically affect secretory vesicle binding (Schott et al., 1999). In these mutants, vesicles became depolarized from the motor within five minutes, which remained polarized. This showed that the tail domain of Myo2p binds to secretory vesicles and that the motor brings them into the bud through an active process. While this was the correct conclusion supported by the data, my work actually casts doubt on the fidelity of these conditional motors with regards to their ability to turn on and off. I was able to exploit this misregulation in Chapter 2 to better understand how class-V myosins function. Lastly, our lab was the first to show unequivocally that a class-V myosin motor directly moves a cargo *in vivo* by generating motors with 0, 2, 4, 6, and 8 IQ domains and watching the characteristic changes in velocity of GFP-Sec4 marked vesicles (Schott et al., 2002).

Receptors for Secretory Membranes

Due to the Sec2p regulatory switch described above (where Sec2p controls Ypt31/32p binding, Sec4p binding and activation, and recruitment of the exocyst through Sec15p), the exact point where Myo2p interacts with the membrane is a little murky. It seems likely that the transition is a continuum. This is supported by the fact that Myo2p binds to and colocalizes with both Ypt31/32p and Sec4p (Lipatova et al., 2008; Santiago-Tirado et al., 2011; this thesis). Microscopy data from our lab has shown that a compartment labeled by GFP-Ypt32p shows a more tubular appearance indicative of the TGN; this compartment moves in a bud directed manner and has been seen to break up into smaller vesicles (Felipe Santiago, unpublished data). Further, evidence presented at a conference showed that at least some Ypt31/32p remained on vesicles positive for Sec4p in time-lapse microscopy experiments (Yui Jin, unpublished data).

All of this suggests that Myo2p binding and transport operates on a continuum with additional proteins shuffling on and off.

The receptor for Myo2p on secretory membranes eluded researchers for more than 10 years after it was shown that the motor transports them. The first evidence that Myo2p binds a Rab in the secretory pathway was presented by both the Segev and Ragnini-Wilson Labs in 2008. They showed conclusively that Ypt31/32p, homologs of the mammalian Rab11, bind to the C-terminal domain and that this interaction is required for viability (Casavola et al., 2008; Lipatova et al., 2008). Through yeast two-hybrid experiments and *in vitro* binding assays, they showed that this interaction is GTP-dependent and requires only the globular tail domain of Myo2p. When cells were made to overexpress GDP-locked Ypt32p, vesicles accumulated in the cytoplasm that were not polarized. This implies that cells require the Myo2p-Ypt31/32p interaction for polarized transport. Further, Lipatova et al. (2008) created a *ypt31Δ/ypt32*^{ts} strain (which is weakly temperature sensitive) that qualitatively mislocalized the Myo2p motor at the restrictive temperature. However, Ypt31/32p is probably not the first binding partner of Myo2p in the Ypt31/32p-Sec4p handoff mechanism because overexpression of active *YPT32* in *sec2-59* cells still accumulates secretory membranes in the mother cell (Casavola et al., 2008), implying that Ypt32p alone cannot recruit the motor and ensure transport.

Once trans-Golgi membranes have matured into secretory vesicles, there are several components on the vesicle that ensure Myo2p stays bound. The first is the Rab Sec4p, whose interaction is essential (Jin et al., 2011; Santiago-Tirado et al., 2011). Like Ypt31p/Ypt32p, this occurs in a GTP dependent manner as shown by both yeast two-hybrid and *in vitro* binding assays. Unlike Ypt31p/Ypt32p, the coiled-coil domain of Myo2p is required for binding as detected by yeast two-hybrid experiments. However, the primary binding site still appears to be

the cluster of residues centered on the Y1415 site, which has been shown to be the binding site for other Rab proteins (Figure 1.4). Mutation of this residue results in either extremely temperature-sensitive growth or death depending on what the change is (Pashkova et al., 2006). Further details of the Myo2p-Sec4p interaction will be discussed later in this chapter.

Results from our lab have also shown a role for the lipid PI4P in linking Myo2p to the secretory vesicle membrane, but in an indirect manner dependent on an unknown component (Santiago-Tirado et al., 2011). This was first found by showing that increasing Golgi PI4P levels by overexpressing the kinase *PIK1* could rescue certain conditional Myo2p tail mutants defective in vesicle binding discussed above. Further, it was shown that PI4P is critical for vesicle transport and that the Rab component of the receptor could be bypassed and vesicle transport could still be achieved by enhancing the PI4P interaction. This led to the development of a 'coincidence detection' model for secretory vesicle selection, where Sec4p and PI4P together are responsible for recruitment of Myo2p.

We have some *in vitro* evidence that this unknown PI4P receptor is also the GEF Sec2p. It was found that the Myo2p interaction with dominant active Sec4p-decorated PI4P-positive liposomes is enhanced when Sec2p is added (Felipe Santiago, unpublished data). However, *in vivo* Sec2p is depolarized in the conditional *pik1-101* kinase mutant after 1 hour at the restrictive temperature while Sec6p is still polarized, indicating vesicles are still transported (Mizuno-Yamasaki et al., 2010). More research is clearly needed on the identity of this PI4P-dependent component of the secretory vesicle receptor.

A third component on the secretory vesicle that binds to Myo2p is Sec15p; this interaction is also found using recombinant mammalian homologs (Jin et al., 2011). This essential 113 kDa component of the exocyst complex binds to a basic patch of Myo2p present on

the opposite face of the Rab binding domain (as previously described, see Figure 1.4). These residues are also required for autoinhibition in higher myosin-V motors. It is interesting that it binds on the opposite face of the tail as Sec4p, given that Sec15p is also an effector for Sec4p (Guo et al., 1999); how the geometry of this interaction works is unknown. Because the Sec15p binding site shares the residues that may be involved in autoinhibition, it was proposed that Sec15 binding might compete for access and therefore aid in activating the motor (Jin et al., 2011). This seems unlikely though, as secretory vesicles are still polarized in exocyst complex mutants *sec6-4* and *sec15-1*, where the exocyst is completely disassembled (Govindan et al., 1995; Salminen and Novick, 1987; TerBush and Novick, 1995).

One last player on the secretory vesicle that may play a role in the vesicle receptor is the kinesin-related protein Smy1p. Yeast two-hybrid experiments consistently show that it has one of the strongest interactions of any protein with Myo2p, yet it has never been detected as a binding partner in an immunoprecipitation experiment (Beningo et al., 2000; unpublished data). First discovered as an overexpression suppressor of the *myo2-66* allele (Lillie and Brown, 1992), data has been published showing it performing a variety of different roles in the cell. Various reports have proposed different roles for the protein, including functioning as an electrostatic tether that aids in Myo2p processivity (Hodges et al., 2009) and as a modulator of formin Bnr1p activity at the bud neck (Chesarone-Cataldo et al., 2011). However, since its deletion is synthetic lethal with a number of late-acting secretion mutants (including *sec4-8*) it seems likely that Smy1p is somehow involved in the secretory pathway. Results from our lab have shown that Myo2p still undergoes transport at normal speeds in *smy1Δ* cells, but is hyperpolarized when overexpressed, perhaps suggesting a role for it in modulating dynamics of the motor (my unpublished data, Kyaw Myo Lwin unpublished data).

The Late Stages of the Secretory Pathway and the Role of Myo2p

Secretory vesicles, as we have seen, bud from the Golgi and are then transported to sites of growth along filamentous actin cables by the motor protein Myo2p. What happens once they get to the cell cortex, the order of events to fusion, and how that is integrated with the role of Myo2p is a large part of this thesis.

The Exocyst Complex

As described above, the Sec2p regulatory switch allows for the binding of Sec15p to the vesicle as it matures. Sec15p is a member of a large (~750 kDa), multi-subunit complex known as exocyst. The exocyst complex is believed to physically tether vesicles to the cortex in the step immediately preceding vesicle fusion. However, despite nearly 20 years of research, this function has not been shown conclusively as the complex is notoriously difficult to reconstitute *in vitro*. Much of the functional data of the exocyst complex comes from *in vivo* work with temperature sensitive mutants. In fact, six of the original 23 *sec* screen mutants are exocyst complex proteins, all of which show a buildup of vesicles in the bud at the restrictive temperature (Novick et al., 1981). This demonstrates the importance of the exocyst complex *in vivo* since nearly all of its component members are required for proper function.

The exocyst complex was first identified in the Novick Lab as a multi-subunit complex consisting of Sec6p, Sec8p, and Sec15p, which localized to the tips of small buds as observed by immuno-electron microscopy (Bowser et al., 1992; TerBush and Novick, 1995). Subsequent genetic work, immunoprecipitation experiments and mass spectrometry identified the additional members of the complex, Sec3p, Sec5p, Sec10p, Exo70p and Exo84p (TerBush et al., 1996). It appears that the exocyst complex remains relatively stable as a single complex in fractionation

experiments. However, the composition of the exocyst can be disturbed in some *sec* mutants, including *sec6-4* and *sec15-1*; as described in the following chapters, I have exploited this finding in my work.

The interactions the members of the exocyst complex make with one another has been worked out through a series of yeast-two hybrid and immunoprecipitation experiments. The basic scheme shows that Sec15p binds in a GTP-dependent manner to Sec4p on secretory vesicles (Guo et al., 1999). The other members of the complex have various interactions with Sec15p and among themselves (Figure 1.6). However, the opposite face of the complex shows that Sec3p and Exo70p bind to components present on the cortex. The Sec3p N-terminal domain has been shown to bind to GTPases Rho1p and Cdc42p as well as the lipid $PI(4,5)P_2$; Exo70p also binds to Cdc42p and $PI(4,5)P_2$ but instead binds Rho3p (Adamo et al., 1999; 2001; Guo et al., 2001; He et al., 2007; Robinson et al., 1999; Zhang et al., 2001). Rho GTPase nucleotide cycling does not appear to be critical for exocyst polarization or function (Roumanie et al., 2005). However, $PI(4,5)P_2$ binding is critical, as mutants lacking the ability to bind the lipid (or in Mss4p kinase mutants that create the lipid) show diffuse exocyst staining or death (He et al., 2007; Hutagalung et al., 2009; Zhang et al., 2008).

The dynamics of the exocyst complex was revealed through fluorescence recovery after photobleaching (FRAP) experiments and showed that two sub-groups of the exocyst come together, likely at the plasma membrane (Boyd et al., 2004). One group, consisting of Sec5p, Sec6p, Sec8p, Sec10p, Sec15p, Exo70p, and Exo84p, requires actin to recover its localization after photobleaching and all showed the same recovery kinetics as the vesicle Rab Sec4p. They also were able to visualize puncta of these components moving at rates consistent with Sec4p-vesicle mediated transport (Schott et al., 2002). Another group of components, namely Sec3p but

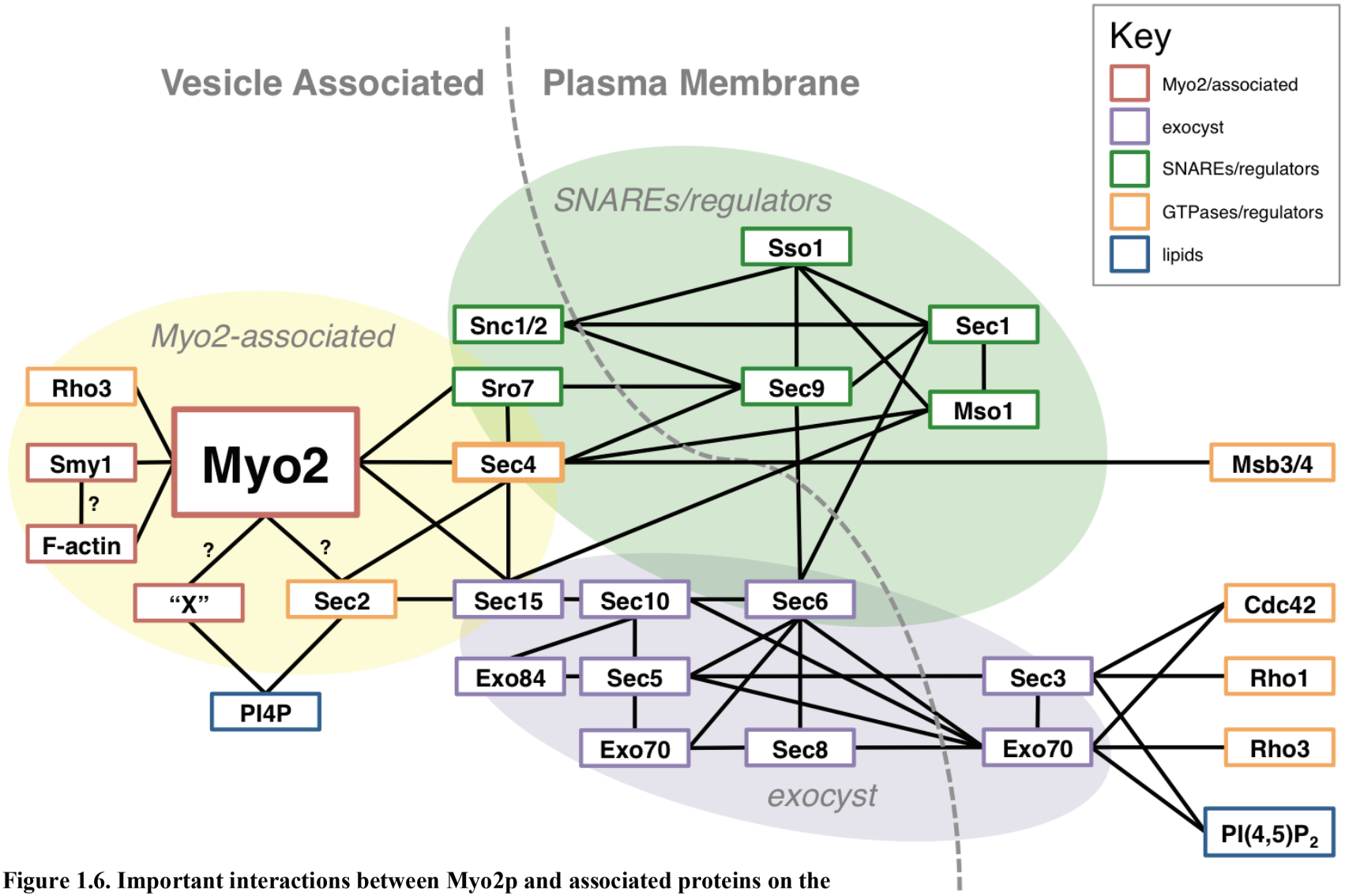

Figure 1.6. Important interactions between Myo2p and associated proteins on the vesicle and at the bud tip. Solid lines represent direct binding and regulatory events. Question marks ("?") represent potential interactions.

also a pool of Exo70p, showed actin-independent localization and recovery. This makes sense, as there were already reports that these members interact with Rho proteins at the cortex. In fact, Sec3p was initially thought to be the landmark protein on the cortex that targets exocyst and vesicles properly (Finger et al., 1998); this was based on the finding that Sec3-GFP was unaffected by secretory disruptions. However, observing the endogenous Sec3p protein by antibody probe suggests that this is not the case, and mutants depolarizing Sec3p localization does not affect secretion rates or the polarization of Sec4p, Myo2p, and Sec15p (Roumanie et al., 2005). Exo70p may also play a role in the localization of the exocyst, as mutants defective in $PI(4,5)P_2$ binding (but not Rho3p binding) result in depolarized exocyst components (He et al., 2007).

Recent structural studies and deep-etch electron microcopy has given insight into how the exocyst functions and even how it might be integrated with Myo2p. Crystal structures from both yeast and *Drosophila* complex members have been determined; though their sequences show almost no similarity, there is overall structural homologies in the form of 3-4 helical bundles in tandem repeats (Dong et al., 2005; Hamburger et al., 2006; Sivaram et al., 2006; Wu et al., 2005). Most surprisingly, this motif also manifests itself in the Myo2p tail, with subdomains I and II forming largely separate helical bundles (Jin et al., 2011; Pashkova et al., 2006). This observation, and the fact that Myo2p binds to the exocyst component Sec15p, makes an argument that the motor is better integrated into the complex than previously appreciated; this could have implications for the motor's ability to release from secretory vesicles. The composition of the exocyst was also revealed through quick-etch deep freeze electron microscopy. These images suggest that the helical bundles are splayed open in a 'flower petal motif' in one conformation and closely packed together in another (Hsu et al., 1998). This

closely packed bundle, with dimensions of ~5x5x25 nanometers, may be the 'tethering conformation' while the more open conformation may exist on secretory vesicles. Lastly, the size of the tethered exocyst complex compared to the 80-100 nm vesicle might mean that there needs to be some disassembly of the complex in order for fusion to occur. How this would occur is not known.

SNARE-Mediated Fusion

Membrane fusion requires two adjacent phospholipid bilayers to fuse into one; thus, a large energy barrier must be overcome in order to join them. The SNARE hypothesis, first proposed in 1993, suggested that cognate SNARE proteins on opposing membranes link together to physically drive membrane fusion (Söllner et al., 1993). SNARE proteins contain the ~70 amino acid coiled-coil SNARE motif adjacent to the C-terminal trans-membrane anchor (Weimbs et al., 1997). This structure places hydrophobic residues toward the interior of a four-helix bundle, with one hydrophilic residue per helix (Q or R) next to each other that are proposed to stabilize and help dictate which SNAREs may join the bundle. The t/Q-SNARE members participating at the yeast plasma membrane are syntaxin-like Sso1p (which contributes two helices to the bundle) and SNAP-25-like Sec9p. Vesicles contain the synaptobrevin/VAMP-like v/R-SNARE proteins Snc1/2p (Aalto et al., 1993; Brennwald et al., 1994; Protopopov et al., 1993).

Note that in yeast, the exact SNARE partnering does not convey specificity to membrane trafficking. Snc2p, for instance, can bind *in vitro* to a wide variety of t/Q-SNARE partners at trafficking steps throughout the cell (Grote and Novick, 1999); various SNARE proteins of the same class can be swapped if the replacement is overexpressed (Darsow et al., 1997; Liu and

Barlowe, 2002). Regulation of SNARE assembly occurs at numerous levels. First, individual SNAREs can undergo autoinhibitory actions that prevent their incorporation unless they are activated by some external stimulus. This is most evident in yeast with Sso1p, which can close up into a three-helix bundle that prevents binding to the other cognate SNAREs *in vivo* and *in vitro* (Munson and Hughson, 2002). Secondly, SM (Sec1/Munc18 class) proteins can physically interact with completed ternary bundles (SNAREpins). At the plasma membrane, Sec1p can bind to Sso1p-Sec9p-Snc2p complexes and has been proposed to drive SNARE-mediated membrane fusion (Scott et al., 2004; Togneri et al., 2006), though unlike most other SM-family members it interacts weakly with individual SNAREs.

Towards a Timeline of Events in Exocytosis

In working on this project and writing this thesis, I was surprised to find that there was no complete resource that definitively orders the events in exocytosis. This is probably because a lot of the important facts are scattered over 25 years of research and some of the data are contradictory. Most surprisingly, the critical step required for efficient exocytosis, Sec4-GTP hydrolysis, is hardest to pinpoint (Walworth et al., 1992). At least five different effectors bind to Sec4-GTP at the bud tip and the order in which they bind is difficult to put in one framework; however, since upwards of 75 molecules of Sec4p are present on a secretory vesicle being moved by Myo2p (this thesis), it seems highly unlikely that all molecules are binding to all effectors and that a definite order to the timeline exists. Nevertheless, I will attempt to distill what is known so far into a timeline of events.

As detailed above, Myo2p interacts with late-Golgi/secretory elements via its interaction with Ypt31/32p and Sec4p. This handoff is likely controlled through binding to additional

factors; otherwise, the motor would fall off the membrane during the switch. A nice candidate for this factor is Sec2p, since it binds to both Ypt31/32p and Sec4p and can bind PI4P (which our model suggests an additional Myo2p receptor is dependent on). There are, however, some problems with using Sec2p as a Myo2p receptor as discussed above. A second factor that could help link the motor to the membrane during the Rab switch is the exocyst component Sec15p, but this would require that Sec15p binds Sec4-GTP before Myo2p does. The exocyst complex probably binds before vesicle transport occurs though, as moving puncta of exocyst complex proteins have been seen moving at speeds consistent with Myo2p movement (Boyd et al., 2004). Once one motor or several binds to receptor(s), the secretory vesicle with the bound exocyst is then shuttled to sites of growth along polarized actin cables at about 3 μm/sec (Schott et al., 2002).

Before beginning this thesis project, it was not known when, where, or how Myo2p is released from secretory vesicles. A first step in the fusion process is the tethering of the vesicle to the cortex via interaction of the vesicle-associated exocyst with the cortex-associated components. Tethering likely occurs first because in certain exocyst mutants (*sec6-4*, *sec15*-1) the complex is completely disassembled and vesicles do not fuse; further, SNARE complex formation is inhibited in these exocyst mutants (Grote et al., 2000; TerBush and Novick, 1995). This is interesting, as it suggests that the exocyst complex might regulate SNARE assembly (Figure 1.6). There is good evidence that the exocyst component Sec6p binds to t-SNARE Sec9p to inhibit the Sec9p-Sso1p interaction. However, this can only occur when Sec6p is *not* binding to the rest of the exocyst, suggesting that there is some uncharacterized rearrangement of the exocyst complex when it engages that might release the t-SNARE Sec9p for action only when the exocyst is assembled (Morgera et al., 2012; Sivaram et al., 2005). This same series of

experiments also uncovered a role for a Sec6p-Sec1p interaction that could help target Sec1p to sites of growth to promote SNARE assembly only when the exocyst is present. Concurrent with this Sec9p-Sso1p-Sec6p regulation, it is likely that another SNARE regulatory event comes into play. Sro7/77p are conserved lethal giant larva (*lgl*) homologs that are redundantly required for viability. These proteins normally sequester t-SNARE Sec9p from its associate t-SNARE, Sso1p (Grosshans et al., 2006). When active Sec4-GTP interacts with Sro7/77p, it repositions a 60-residue amino-terminal "tail" that displaces Sec9p and allows for SNARE complex formation (Hattendorf et al., 2007). This release is also consistent with the data above regarding the Sec9p-Sec6p interaction. Presumably, exocyst assembly at sites of growth releases Sec9p at the same time that Sec4-GTP (also in the vicinity) stimulates the release of Sec9p from Sro7/77p.

Now that vesicles have tethered to the membrane, it is likely that initial SNARE assembly occurs. This is suggested by analysis of several mutants. First, SNARE assembly has been shown to be dependent on functional Sec4p. This information comes from the fact that SNARE ternary complexes do not form in *sec2-41* cells at the restrictive temperature, where Sec4p is largely inactive; unfortunately, this result is complicated by the fact that vesicles are not transported to sites of growth (Carr et al., 1999; Grote et al., 2000; Walch-Solimena et al., 1997). However, it has been shown that SNARE ternary complexes are greatly diminished at the permissive temperature in *sec4-8* cells too (where secretory vesicles are transported to sites of growth) though these cells are rather sick and do not secrete material at the same rate as wildtype cells at the permissive temperature (Grote and Novick, 1999; Novick et al., 1980). Regardless, it seems likely from this data that functional Sec4p is required for SNARE complex formation.

A clue to when Sec4-GTP is hydrolyzed comes from the action of the founding member of the SM-like proteins, Sec1p. *In vitro*, Sec1p interacts preferentially with the t-SNAREs

Sso1p/Sec9p but also the completed ternary SNARE bundles; unlike neuronal SM-like proteins, the presence of Sec1p stimulates fusion assays suggesting a positive role in SNARE complex formation (Scott et al., 2004). Critically, it is thought to be targeted to SNARE complexes through binding to Mso1p, which is recruited to sites of growth by its C-terminus through an interaction with Sec4-GTP. Thus, the recruitment of Sec1p to SNARE bundles likely occurs while Sec4-GTP still exists. This is also supported by the finding that the primary action of Sec1p occurs downstream of SNARE bundle formation, as SNARE ternary complexes can still form in *sec1-1* mutants at the restrictive temperature though vesicles do not fuse (Grote and Novick, 1999; Novick and Schekman, 1979).

Hydrolysis of Sec4-GTP is stimulated by GTPase Activating Proteins (GAPs) Msb3p and Msb4p (Gao et al., 2003). These redundant TBC (Tre2/Bub2/Cdc16) domain-containing proteins localize to sites of growth and when disrupted (or mutated to be non-functional) cause secretory defects including large numbers of vesicles in the bud. However, deletion of both of the GAP proteins is not lethal; this may be due to intrinsic hydrolysis of Sec4-GTP or through off-target effects of other GAP proteins; for instance, the cis-Golgi GAP Gyp1p has been shown to have moderate GAP activity on Sec4p *in vitro* (Du et al., 1998). Further, Sec4p has a particularly high intrinsic GDP off-rate, which may indicate a propensity of the Rab to undergo several rounds of cycling at sites of exocytosis (Kabcenell et al., 1990). Regardless, this hydrolysis event is required for efficient exocytosis (Salminen and Novick, 1987; Walworth et al., 1992; Gao et al., 2003) and would likely occur following vesicle tethering and SNARE assembly.

The conformational change that occurs during hydrolysis would likely affect downstream Sec4p binding partners present at the bud tip. The Sec15p binding interaction required Sec4-GTP in yeast two-hybrid experiments, but it is unknown if its release is dependent on this event (Guo

et al., 1999; Heider and Munson, 2012). Secondly, the Myo2p-Sec4p interaction is dependent on GTP *in vitro*, but it was not known before starting this work if Sec4p hydrolysis results in release of the motor from the vesicle; it is complicated by the finding that the motor is also well integrated with the exocyst complex through Sec15p and possibly binds to the GEF Sec2p.

To summarize the potential order of events at the bud tip, vesicles are first delivered in a Myo2-dependent manner. Tethering of vesicles can then occur through the exocyst complex, through contact of cortex and vesicle localized pools. The presence of an assembled exocyst and Sec4-GTP at the cortex set off a number of SNARE regulatory events that allows for SNARE ternary complex formation. Following hydrolysis of Sec4-GTP, vesicle fusion can then proceed though SNARE mediated mechanisms. Finally, individual components are likely recycled for another round of vesicle transport and fusion.

Overview of Dissertation Project

Research over the past three decades has revealed the mechanisms of polarity establishment, transport of organelles and secretory cargo, and the regulatory mechanisms that occur during the fusion of secretory cargo with the cortex. Incredibly, the molecular machinery underlying these processes is well conserved through evolution, making the genetically tractable budding yeast a good model system for which to tease apart mechanisms relevant to human health and disease. Perhaps the best vote of confidence for this research approach was the awarding of the 2013 Nobel Prize in Medicine to Randy Schekman for "discoveries of machinery regulating vesicle traffic."

Many studies have focused on specific steps in the secretory pathway, such as tethering or fusion; while this approach has been fruitful, certain proteins such as Myo2p are present at a

number of vesicle trafficking steps. Missing from such segmented analysis has been the dynamic properties of the motor and how the motor is regulated at the molecular level. While some information on the dynamic nature of the motor was known before starting this project, how its dynamics is integrated with the secretory pathway was less certain. As work will show in the following chapters, I have dissected the role of Myo2p at all stages of post-Golgi vesicle trafficking, from cargo capture to delivery and recycling. Due to the immense similarities between yeast and human post-Golgi trafficking, the results presented in the following chapters are likely widely applicable.

REFERENCES

Aalto, M.K., Ronne, H., and Keränen, S. (1993). Yeast syntaxins Sso1p and Sso2p belong to a family of related membrane proteins that function in vesicular transport. EMBO J. *12*, 4095–4104.

Adamo, J.E., Moskow, J.J., Gladfelter, A.S., Viterbo, D., Lew, D.J., and Brennwald, P.J. (2001). Yeast Cdc42 functions at a late step in exocytosis, specifically during polarized growth of the emerging bud. J. Cell Biol. *155*, 581–592.

Adamo, J.E., Rossi, G., and Brennwald, P. (1999). The Rho GTPase Rho3 has a direct role in exocytosis that is distinct from its role in actin polarity. Mol. Biol. Cell *10*, 4121–4133.

Adams, A.E., and Pringle, J.R. (1984). Relationship of actin and tubulin distribution to bud growth in wild-type and morphogenetic-mutant Saccharomyces cerevisiae. J. Cell Biol. *98*, 934–945.

Adams, A., Botstein, D., and Drubin, D. (1989). A yeast actin-binding protein is encoded by SAC6, a gene found by suppression of an actin mutation. Science *243*, 231–233.

Adams, A.E., Botsteinf, D., and Drubint, D.G. (1991). Requirement of yeast fimbrin for actin organization and morphogenesis in vivo. Nature *354*, 404–408.

Aligianis, I.A., Johnson, C.A., Gissen, P., Chen, D., Hampshire, D., Hoffmann, K., Maina, E.N., Morgan, N.V., Tee, L., Morton, J., et al. (2005). Mutations of the catalytic subunit of RAB3GAP cause Warburg Micro syndrome. Nat. Genet. *37*, 221–224.

Aligianis, I.A., Morgan, N.V., Mione, M., Johnson, C.A., Rosser, E., Hennekam, R.C., Adams, G., Trembath, R.C., Pilz, D.T., Stoodley, N., et al. (2006). Mutation in Rab3 GTPase-Activating Protein (RAB3GAP) Noncatalytic Subunit in a Kindred with Martsolf Syndrome. Am. J. Hum. Gen. *78*, 702–707.

Amatruda, J.F., Cannon, J.F., Tatchell, K., Hug, C., and Cooper, J.A. (1990). Disruption of the actin cytoskeleton in yeast capping protein mutants. Nature *344*, 352–354.

Au, J.S.-Y., and Huang, J.-D. (2002). A tissue-specific exon of myosin Va is responsible for selective cargo binding in melanocytes. Cell Motil. Cyto. *53*, 89–102.

Ayscough, K.R., Stryker, J., Pokala, N., Sanders, M., Crews, P., and Drubin, D.G. (1997). High rates of actin filament turnover in budding yeast and roles for actin in establishment and maintenance of cell polarity revealed using the actin inhibitor latrunculin-A. J. Cell Biol. *137*, 399–416.

Beningo, K.A., Lillie, S.H., and Brown, S.S. (2000). The Yeast Kinesin-related Protein Smy1p Exerts Its Effects on the Class V Myosin Myo2p via a Physical Interaction. Mol. Biol. Cell *11*, 691–702.

Benli, M., Döring, F., Robinson, D.G., Yang, X., and Gallwitz, D. (1996). Two GTPase isoforms, Ypt31p and Ypt32p, are essential for Golgi function in yeast. EMBO J. *15*, 6460–6475.

Berg, J.S., and Cheney, R.E. (2002). Myosin-X is an unconventional myosin that undergoes intrafilopodial motility. Nat. Cell Biol. *4*, 246.

Bi, E., Maddox, P., Lew, D.J., Salmon, E.D., McMillan, J.N., Yeh, E., and Pringle, J.R. (1998). Involvement of an actomyosin contractile ring in Saccharomyces cerevisiae cytokinesis. J. Cell Biol. *142*, 1301–1312.

Bobola, N., Jansen, R.-P., Shin, T.H., and Nasmyth, K. (1996). Asymmetric Accumulation of Ash1p in Postanaphase Nuclei Depends on a Myosin and Restricts Yeast Mating-Type Switching to Mother Cells. Cell *84*, 699–709.

Bowser, R., Müller, H., Govindan, B., and Novick, P. (1992). Sec8p and Sec15p are components of a plasma membrane-associated 19.5S particle that may function downstream of Sec4p to control exocytosis. J. Cell Biol. *118*, 1041–1056.

Boyd, C., Hughes, T., Pypaert, M., and Novick, P. (2004). Vesicles carry most exocyst subunits to exocytic sites marked by the remaining two subunits, Sec3p and Exo70p. J. Cell Biol. *167*, 889–901.

Brennwald, P., Kearns, B., Champion, K., Keränen, S., Bankaitis, V., and Novick, P. (1994). Sec9 is a SNAP-25-like component of a yeast SNARE complex that may be the effector of Sec4 function in exocytosis. Cell *79*, 245–258.

Brennwald, P., and Novick, P. (1993). Interactions of three domains distinguishing the Ras-related GTP-binding proteins Ypt1 and Sec4. Nature *362*, 560–563.

Brockerhoff, S.E., Stevens, R.C., and Davis, T.N. (1994). The unconventional myosin, Myo2p, is a calmodulin target at sites of cell growth in Saccharomyces cerevisiae. J. Cell Biol. *124*, 315–323.

Buttery, S.M., Yoshida, S., and Pellman, D. (2007). Yeast Formins Bni1 and Bnr1 Utilize Different Modes of Cortical Interaction during the Assembly of Actin Cables. Mol. Biol. Cell *18*, 1826–1838.

Calero, M., Calero, M., Chen, C.Z., Zhu, W., Winand, N., Havas, K.A., Gilbert, P.M., Burd, C.G., and Collins, R.N. (2003). Dual Prenylation Is Required for Rab Protein Localization and Function. Mol. Biol. Cell *14*, 1852–1867.

Cao, X. (1998). Initial docking of ER-derived vesicles requires Uso1p and Ypt1p but is independent of SNARE proteins. EMBO J. *17*, 2156–2165.

Carr, C.M., Grote, E., Munson, M., Hughson, F.M., and Novick, P.J. (1999). Sec1p binds to SNARE complexes and concentrates at sites of secretion. J. Cell Biol. *146*, 333–344.

Casavola, E.C., Catucci, A., Bielli, P., Di Pentima, A., Porcu, G., Pennestri, M., Cicero, D.O.,

and Ragnini-Wilson, A. (2008). Ypt32p and Mlc1p bind within the vesicle binding region of the class V myosin Myo2p globular tail domain. Mol. Microbiol. *67*, 1051–1066.

Catlett, N.L., and Weisman, L.S. (1998). The terminal tail region of a yeast myosin-V mediates its attachment to vacuole membranes and sites of polarized growth. Proc. Natl. Acad. Sci. USA *95*, 14799–14804.

Cheney, R.E., O'Shea, M.K., Heuser, J.E., Coelho, M.V., Wolenski, J.S., Espreafico, E.M., Forscher, P., Larson, R.E., and Mooseker, M.S. (1993). Brain myosin-V is a two-headed unconventional myosin with motor activity. Cell *75*, 13–23.

Chernyakov, I., Santiago-Tirado, F., and Bretscher, A. (2013). Active segregation of yeast mitochondria by Myo2 is essential and mediated by Mmr1 and Ypt11. Curr. Biol. *23*, 1818–1824.

Chesarone, M., Gould, C.J., Moseley, J.B., and Goode, B.L. (2009). Displacement of Formins from Growing Barbed Ends by Bud14 Is Critical for Actin Cable Architecture and Function. Dev. Cell *16*, 292–302.

Chesarone-Cataldo, M., Guérin, C., Yu, J.H., Wedlich-Soldner, R., Blanchoin, L., and Goode, B.L. (2011). The Myosin Passenger Protein Smy1 Controls Actin Cable Structure and Dynamics by Acting as a Formin Damper. Dev. Cell *21*, 217–230.

Coureux, P.-D., Sweeney, H.L., and Houdusse, A. (2004). Three myosin V structures delineate essential features of chemo-mechanical transduction. EMBO J. *23*, 4527–4537.

Coureux, P.-D., Wells, A.L., Ménétrey, J., Yengo, C.M., Morris, C.A., Sweeney, H.L., and Houdusse, A. (2003). A structural state of the myosin V motor without bound nucleotide. Nature *425*, 419–423.

D'Adamo, P., Menegon, A., Nigro, Lo, C., Grasso, M., Gulisano, M., Tamanini, F., Bienvenu, T., Gedeon, A.K., Oostra, B., Wu, S.-K., et al. (1998). Mutations in GDI1 are responsible for X-linked non-specific mental retardation. Nat. Gen. *19*, 134–139.

Darsow, T., Rieder, S.E., and Emr, S.D. (1997). A multispecificity syntaxin homologue, Vam3p, essential for autophagic and biosynthetic protein transport to the vacuole. J. Cell Biol. *138*, 517–529.

Dong, G., Hutagalung, A.H., Fu, C., Novick, P., and Reinisch, K.M. (2005). The structures of exocyst subunit Exo70p and the Exo84p C-terminal domains reveal a common motif. Nat. Struct. Mol. Biol. *12*, 1094–1100.

Donovan, K.W., and Bretscher, A. (2012). Myosin-V Is Activated by Binding Secretory Cargo and Released in Coordination with Rab/Exocyst Function. Dev. Cell *23*, 769–781.

Drees, B., Brown, C., Barrell, B.G., and Bretscher, A. (1995). Tropomyosin is essential in yeast, yet the TPM1 and TPM2 products perform distinct functions. J. Cell Biol. *128*, 383–392.

Du, L.L., Collins, R.N., and Novick, P.J. (1998). Identification of a Sec4p GTPase-activating protein (GAP) as a novel member of a Rab GAP family. J. Biol. Chem. *273*, 3253–3256.

Dunphy, W.G., and Rothman, J.E. (1985). Compartmental organization of the Golgi stack. Cell *42*, 13–21.

Eathiraj, S., Pan, X., Ritacco, C., and Lambright, D.G. (2005). Structural basis of family-wide Rab GTPase recognition by rabenosyn-5. Nature *436*, 415–419.

Espindola, F.S., Espreafico, E.M., Coelho, M.V., Costa, F.R., Mooseker, M.S., and Larson, R.E. (1992). Biochemical and immunological characterization of p190-calmodulin complex from vertebrate brain: a novel calmodulin-binding myosin. J. Cell Biol. *118*, 359–368.

Espindola, F.S., Suter, D.M., Partata, L.B.E., Cao, T., Wolenski, J.S., Cheney, R.E., King, S.M., and Mooseker, M.S. (2000). The light chain composition of chicken brain myosin-Va: Calmodulin, myosin-II essential light chains, and 8-kDa dynein light chain/PIN. Cell Motil. Cyto. *47*, 269–281.

Espreafico, E.M., Cheney, R.E., Matteoli, M., Nascimento, A.A., de Camilli, P.V., Larson, R.E., and Mooseker, M.S. (1992). Primary structure and cellular localization of chicken brain myosin-V (p190), an unconventional myosin with calmodulin light chains. J. Cell Biol. *119*, 1541–1557.

Estrada, P., Kim, J., Coleman, J., Walker, L., Dunn, B., Takizawa, P., Novick, P., and Ferro-Novick, S. (2003). Myo4p and She3p are required for cortical ER inheritance in Saccharomyces cerevisiae. J. Cell Biol. *163*, 1255–1266.

Eves, P.T., Jin, Y., Brunner, M., and Weisman, L.S. (2012). Overlap of cargo binding sites on myosin V coordinates the inheritance of diverse cargoes. J. Cell Biol. *198*, 69–85.

Fagarasanu, A., Fagarasanu, M., Eitzen, G.A., Aitchison, J.D., and Rachubinski, R.A. (2006). The Peroxisomal Membrane Protein Inp2p Is the Peroxisome-Specific Receptor for the Myosin V Motor Myo2p of Saccharomyces cerevisiae. Dev. Cell *10*, 587–600.

Finger, F.P., Hughes, T.E., and Novick, P. (1998). Sec3p Is a Spatial Landmark for Polarized Secretion in Budding Yeast. Cell *92*, 559–571.

Gao, L., Liu, W., and Bretscher, A. (2010). The yeast formin Bnr1p has two localization regions that show spatially and temporally distinct association with septin structures. Mol. Biol. Cell *21*, 1253–1262.

Gao, X.-D., Albert, S., Tcheperegine, S.E., Burd, C.G., Gallwitz, D., and Bi, E. (2003). The GAP activity of Msb3p and Msb4p for the Rab GTPase Sec4p is required for efficient exocytosis and actin organization. J. Cell Biol. *162*, 635–646.

Geli, M.I., and Riezman, H. (1996). Role of Type I Myosins in Receptor-Mediated Endocytosis in Yeast. Science *272*, 533–535.

Goode, B.L., and Eck, M.J. (2007). Mechanism and Function of Formins in the Control of Actin

Assembly. Annu. Rev. Biochem. *76*, 593–627.

Govindan, B., Bowser, R., and Novick, P. (1995). The role of Myo2, a yeast class V myosin, in vesicular transport. J. Cell Biol. *128*, 1055–1068.

Griffiths, G., and Simons, K. (1986). The trans Golgi network: sorting at the exit site of the Golgi complex. Science *234*, 438–443.

Grosshans, B.L., Andreeva, A., Gangar, A., Niessen, S., Yates, J.R., Brennwald, P., and Novick, P. (2006). The yeast lgl family member Sro7p is an effector of the secretory Rab GTPase Sec4p. J. Cell Biol. *172*, 55–66.

Grote, E., and Novick, P. (1999). Promiscuity in Rab-SNARE interactions. Mol. Biol. Cell *10*, 4149.

Grote, E., Carr, C.M., and Novick, P.J. (2000). Ordering the Final Events in Yeast Exocytosis. J. Cell Biol. *151*, 439.

Guo, W., Roth, D., Walch-Solimena, C., and Novick, P. (1999). The exocyst is an effector for Sec4p, targeting secretory vesicles to sites of exocytosis. EMBO J. *18*, 1071–1080.

Guo, W., Tamanoi, F., and Novick, P. (2001). Spatial regulation of the exocyst complex by Rho1 GTPase. Nat. Cell Biol. *3*, 353–360.

Haarer, B.K., Lillie, S.H., Adams, A.E., Magdolen, V., Bandlow, W., and Brown, S.S. (1990). Purification of profilin from Saccharomyces cerevisiae and analysis of profilin-deficient cells. J. Cell Biol. *110*, 105–114.

Hamburger, Z.A., Hamburger, A.E., West, A.P., and Weis, W.I. (2006). Crystal structure of the S.cerevisiae exocyst component Exo70p. J. Mol. Biol. *356*, 9–21.

Hammer, J.A., and Sellers, J.R. (2011). Walking to work: roles for class V myosins as cargo transporters. Nat. Rev. Mol. Cell Biol. *13*, 13–26.

Hartwell, L.H. (1971). Genetic control of the cell division cycle in yeast *1IV. Genes controlling bud emergence and cytokinesis. Exp. Cell Res. *69*, 265–276.

Hartwell, L.H., Culotti, J., Pringle, J.R., and Reid, B.J. (1974). Genetic control of the cell division cycle in yeast. Science *183*, 46–51.

Hattendorf, D., Andreeva, A., Gangar, A., Brennwald, P., and Weis, W. (2007). Structure of the yeast polarity protein Sro7 reveals a SNARE regulatory mechanism. Nature *446*, 567–571.

He, B., Xi, F., Zhang, X., Zhang, J., and Guo, W. (2007). Exo70 interacts with phospholipids and mediates the targeting of the exocyst to the plasma membrane. EMBO J. *26*, 4053–4065.

Heider, M.R., and Munson, M. (2012). Exorcising the exocyst complex. Traffic *13*, 898–907.

Herskowitz, I. (1988). Life cycle of the budding yeast Saccharomyces cerevisiae. Microbiol.

Rev. *52*, 536.

Heuck, A., Fetka, I., Brewer, D.N., Hüls, D., Munson, M., Jansen, R.-P., and Niessing, D. (2010). The structure of the Myo4p globular tail and its function in ASH1 mRNA localization. J. Cell Biol. *189*, 497–510.

Hill, K.L., Catlett, N.L., and Weisman, L.S. (1996). Actin and myosin function in directed vacuole movement during cell division in Saccharomyces cerevisiae. J. Cell Biol. *135*, 1535–1549.

Hodges, A.R., Bookwalter, C.S., Krementsova, E.B., and Trybus, K.M. (2009). A nonprocessive class V myosin drives cargo processively when a kinesin- related protein is a passenger. Curr. Biol. *19*, 2121–2125.

Hodges, A.R., Krementsova, E.B., Bookwalter, C.S., Fagnant, P.M., Sladewski, T.E., and Trybus, K.M. (2012). Tropomyosin is essential for processive movement of a class V myosin from budding yeast. Curr. Biol. *22*, 1410–1416.

Horiuchi, H., Lippé, R., McBride, H.M., Rubino, M., Woodman, P., Stenmark, H., Rybin, V., Wilm, M., Ashman, K., Mann, M., et al. (1997). A novel Rab5 GDP/GTP exchange factor complexed to Rabaptin-5 links nucleotide exchange to effector recruitment and function. Cell *90*, 1149–1159.

Howell, A.S., Savage, N.S., Johnson, S.A., Bose, I., Wagner, A.W., Zyla, T.R., Nijhout, H.F., Reed, M.C., Goryachev, A.B., and Lew, D.J. (2009). Singularity in Polarization: Rewiring Yeast Cells to Make Two Buds. Cell *139*, 731–743.

Hsu, S.-C., Hazuka, C.D., Roth, R., Foletti, D.L., Heuser, J., and Scheller, R.H. (1998). Subunit Composition, Protein Interactions, and Structures of the Mammalian Brain sec6/8 Complex and Septin Filaments. Neuron *20*, 1111–1122.

Hutagalung, A.H., and Novick, P.J. (2011). Role of Rab GTPases in Membrane Traffic and Cell Physiology. Physiol. Rev. *91*, 119–149.

Hutagalung, A.H., Coleman, J., Pypaert, M., and Novick, P.J. (2009). An internal domain of Exo70p is required for actin-independent localization and mediates assembly of specific exocyst components. Mol. Biol. Cell *20*, 153–163.

Ishikawa, K., Catlett, N.L., Novak, J.L., Tang, F., Nau, J.J., and Weisman, L.S. (2003). Identification of an organelle-specific myosin V receptor. J. Cell Biol. *160*, 887–897.

Itoh, T., Watabe, A., Toh-E, A., and Matsui, Y. (2002). Complex Formation with Ypt11p, a rab-Type Small GTPase, Is Essential To Facilitate the Function of Myo2p, a Class V Myosin, in Mitochondrial Distribution in Saccharomyces cerevisiae. Mol. Cell Biol. *22*, 7744–7757.

Itoh, T., Toh-e, A., and Matsui, Y. (2004). Mmr1p is a mitochondrial factor for Myo2p-dependent inheritance of mitochondria in the budding yeast. EMBO J. *23*, 2520–2530.

Jamieson, J.D., and Palade, G.E. (1966). Role of the Golgi complex in the intracellular transport of secretory proteins. Proc. Natl. Acad. Sci. USA *55*, 424–431.

Jamieson, J.D., and Palade, G.E. (1967). Intracellular transport of secretory proteins in the pancreatic exocrine cell. II. Transport to condensing vacuoles and zymogen granules. J. Cell Biol. *34*, 597–615.

Jedd, G., Mulholland, J., and Segev, N. (1997). Two new Ypt GTPases are required for exit from the yeast trans-Golgi compartment. J. Cell Biol. *137*, 563–580.

Jedd, G., Richardson, C., and Robert Litt, A.N.S. (1995). The Ypt1 GTPase is essential for the first two steps of the yeast secretory pathway. J. Cell Biol. *131*, 583–590.

Jensen, D., and Schekman, R. (2010). COPII-mediated vesicle formation at a glance. J. Cell Sci. *124*, 1–4.

Jin, Y., Taylor Eves, P., Tang, F., and Weisman, L.S. (2009). PTC1 Is Required for Vacuole Inheritance and Promotes the Association of the Myosin-V Vacuole-specific Receptor Complex. Mol. Biol. Cell. *20*, 1312–1323.

Jin, Y., Sultana, A., Gandhi, P., Franklin, E., Hamamoto, S., Khan, A.R., Munson, M., Schekman, R., and Weisman, L.S. (2011). Myosin V Transports Secretory Vesicles via a Rab GTPase Cascade and Interaction with the Exocyst Complex. Dev. Cell *21*, 1156–1170.

Johnson, J.M., Jin, M., and Lew, D.J. (2011). Symmetry breaking and the establishment of cell polarity in budding yeast. Curr. Opin. Genet. Dev. *21*, 740–746.

Johnston, G.C., Prendergast, J.A., and Singer, R.A. (1991). The Saccharomyces cerevisiae MYO2 gene encodes an essential myosin for vectorial transport of vesicles. J. Cell Biol. *113*, 539–551.

Kabcenell, A. K., Goud, J., Northup, J.K., and Novick, P.J. (1990). Binding and hydrolysis of guanine nucleotides by Sec4p, a yeast protein involved in the regulation of vesicular traffic. J. Biol. Chem. *265,* 9366-9372.

Karcher, R.L., Roland, J.T., Zappcosta, F., Huddleston, M.J., Annan, R.S., Carr, S.A., and Gelfand, V.I. (2001). Cell Cycle Regulation of Myosin-V by Calcium/Calmodulin-Dependent Protein Kinase II. Science *293*, 1317–1320.

Karpova, T.S., McNally, J.G., Moltz, S.L., and Cooper, J.A. (1998). Assembly and Function of the Actin Cytoskeleton of Yeast: Relationships between Cables and Patches. J. Cell Biol. *142*, 1501–1517.

Kovar, D.R., Wu, J.-Q., and Pollard, T.D. (2005). Profilin-mediated Competition between Capping Protein and Formin Cdc12p during Cytokinesis in Fission Yeast. Mol. Biol. Cell *16*, 2313–2324.

Kozubowski, L., Saito, K., Johnson, J.M., Howell, A.S., Zyla, T.R., and Lew, D.J. (2008).

Symmetry-breaking polarization driven by a Cdc42p GEF-PAK complex. Current Biol. *18*, 1719–1726.

Krementsov, D.N., Krementsova, E.B., and Trybus, K.M. (2004). Myosin V: regulation by calcium, calmodulin, and the tail domain. J. Cell Biol. *164*, 877–886.

Krementsova, E., Hodges, A., Lu, H., and Trybus, K. (2006). Processivity of chimeric class V myosins. J. Biol. Chem. *281*, 6079.

Krementsova, E.B., Hodges, A.R., Bookwalter, C.S., Sladewski, T.E., Travaglia, M., Sweeney, H.L., and Trybus, K.M. (2011). Two single-headed myosin V motors bound to a tetrameric adapter protein form a processive complex. J. Cell Biol. *195*, 631–641.

La Cruz, De, E.M., Wells, A.L., Rosenfeld, S.S., Ostap, E.M., and Sweeney, H.L. (1999). The kinetic mechanism of myosin V. Proc. Natl. Acad. Sci. USA *96*, 13726–13731.

La Cruz, De, E.M., Wells, A.L., Sweeney, H.L., and Ostap, E.M. (2000). Actin and Light Chain Isoform Dependence of Myosin V Kinetics. Biochem. *39*, 14196–14202.

Lamson, R.E., Winters, M.J., and Pryciak, P.M. (2002). Cdc42 Regulation of Kinase Activity and Signaling by the Yeast p21-Activated Kinase Ste20. Mol. Cell Biol. *22*, 2939–2951.

Layton, A.T., Savage, N.S., Howell, A.S., Carroll, S.Y., Drubin, D.G., and Lew, D.J. (2011). Modeling Vesicle Traffic Reveals Unexpected Consequences for Cdc42p-Mediated Polarity Establishment. Curr. Biol. *21*, 184–194.

Leberer, E., Wu, C., Leeuw, T., Fourest-Lieuvin, A., and Segall, J.E. (1997). Functional characterization of the Cdc42p binding domain of yeast Ste20p protein kinase. EMBO J. *16*, 83–97.

Lee, M.-T.G., Mishra, A., and Lambright, D.G. (2009). Structural mechanisms for regulation of membrane traffic by rab GTPases. Traffic *10*, 1377–1389.

Legesse-Miller, A., Zhang, S., Santiago-Tirado, F.H., Van Pelt, C.K., and Bretscher, A. (2006). Regulated phosphorylation of budding yeast's essential myosin V heavy chain, Myo2p. Mol. Biol. Cell *17*, 1812–1821.

Li, X.-D., Ikebe, R., and Ikebe, M. (2005). Activation of Myosin Va Function by Melanophilin, a Specific Docking Partner of Myosin Va. J. Biol. Chem. *280*, 17815–17822.

Li, X.-D., Jung, H.S., Mabuchi, K., Craig, R., and Ikebe, M. (2006). The globular tail domain of myosin Va functions as an inhibitor of the myosin Va motor. J. Biol. Chem. *281*, 21789–21798.

Li, X.-D., Jung, H.S., Wang, Q., Ikebe, R., Craig, R., and Ikebe, M. (2008). The globular tail domain puts on the brake to stop the ATPase cycle of myosin Va. Prot. Nat. Acad. Sci. USA *105*, 1140–1145.

Li, X.-D., Mabuchi, K., Ikebe, R., and Ikebe, M. (2004). Ca2+-induced activation of ATPase

activity of myosin Va is accompanied with a large conformational change. Biochem. Biophys. Res. Comm. *315*, 538–545.

Lillie, S.H., and Brown, S.S. (1994). Immunofluorescence localization of the unconventional myosin, Myo2p, and the putative kinesin-related protein, Smy1p, to the same regions of polarized growth in Saccharomyces cerevisiae. J. Cell Biol. *125*, 825–842.

Lillie, S.H., and Brown, S.S. (1992). Suppression of a myosin defect by a kinesin-related gene. Nature *356*, 358–361.

Lin, C.-H., and Forscher, P. (1995). Growth cone advance is inversely proportional to retrograde F-actin flow. Neuron *14*, 763–771.

Lipatova, Z., Tokarev, A.A., Jin, Y., Mulholland, J., Weisman, L.S., and Segev, N. (2008). Direct interaction between a myosin V motor and the Rab GTPases Ypt31/32 is required for polarized secretion. Mol. Biol. Cell *19*, 4177–4187.

Liu, H., and Bretscher, A. (1989). Disruption of the single tropomyosin gene in yeast results in the disappearance of actin cables from the cytoskeleton. Cell *57*, 233–242.

Liu, J., Taylor, D.W., Krementsova, E.B., Trybus, K.M., and Taylor, K.A. (2006). Three-dimensional structure of the myosin V inhibited state by cryoelectron tomography. Nature *442*, 208–211.

Liu, Y., and Barlowe, C. (2002). Analysis of Sec22p in endoplasmic reticulum/Golgi transport reveals cellular redundancy in SNARE protein function. Mol. Biol. Cell *13*, 3314–3324.

Losev, E., Reinke, C.A., Jellen, J., Strongin, D.E., Bevis, B.J., and Glick, B.S. (2006). Golgi maturation visualized in living yeast. Nature *441*, 1002–1006.

Martin, S.R., and Bayley, P.M. (2004). Calmodulin bridging of IQ motifs in myosin-V. FEBS Lett. *567*, 166–170.

Matsuura-Tokita, K., Takeuchi, M., Ichihara, A., Mikuriya, K., and Nakano, A. (2006). Live imaging of yeast Golgi cisternal maturation. Nature *441*, 1007–1010.

Medkova, M., France, Y.E., Coleman, J., and Novick, P. (2006). The rab exchange factor Sec2p reversibly associates with the exocyst. Mol. Biol. Cell *17*, 2757–2769.

Mizuno-Yamasaki, E., Medkova, M., Coleman, J., and Novick, P. (2010). Phosphatidylinositol 4-Phosphate Controls Both Membrane Recruitment and a Regulatory Switch of the Rab GEF Sec2p. Dev. Cell *18*, 828–840.

Moon, A.L., Janmey, P.A., Louie, K.A., and Drubin, D.G. (1993). Cofilin is an essential component of the yeast cortical cytoskeleton. J. Cell Biol. *120*, 421–435.

Morgera, F., Sallah, M.R., Dubuke, M.L., Gandhi, P., Brewer, D.N., Carr, C.M., and Munson, M. (2012). Regulation of exocytosis by the exocyst subunit Sec6 and the SM protein Sec1. Mol.

Biol. Cell *23*, 337–346.

Moseley, J.B., and Goode, B.L. (2005). Differential Activities and Regulation of Saccharomyces cerevisiae Formin Proteins Bni1 and Bnr1 by Bud6. Journal of Biological Chemistry *280*, 28023–28033.

Munson, M., and Hughson, F.M. (2002). Conformational regulation of SNARE assembly and disassembly in vivo. J. Biol. Chem. *277*, 9375–9381.

Müller, T., Hess, M.W., Schiefermeier, N., Pfaller, K., Ebner, H.L., Heinz-Erian, P., Ponstingl, H., Partsch, J., Röllinghoff, B., Köhler, H., et al. (2008). MYO5B mutations cause microvillus inclusion disease and disrupt epithelial cell polarity. Nat. Genet. *40*, 1163–1165.

Nascimento, A.F.Z., Trindade, D.M., Tonoli, C.C.C., de Giuseppe, P.O., Assis, L.H.P., Honorato, R.V., de Oliveira, P.S.L., Mahajan, P., Burgess-Brown, N.A., Delft, von, F., et al. (2013). Structural insights into functional overlapping and differentiation among myosin V motors. J. Biol. Chem. *288*, 34131–34145.

Ng, R., and Abelson, J. (1980). Isolation and sequence of the gene for actin in Saccharomyces cerevisiae. Proc. Natl. Acad. Sci. USA *77*, 3912–3916.

Novick, P., and Schekman, R. (1979). Secretion and cell-surface growth are blocked in a temperature-sensitive mutant of Saccharomyces cerevisiae. Proc. Natl. Acad. Sci. USA *76*, 1858–1862.

Novick, P., Ferro, S., and Schekman, R. (1981). Order of events in the yeast secretory pathway. Cell *25*, 461–469.

Novick, P., Field, C., and Schekman, R. (1980). Identification of 23 complementation groups required for post-translational events in the yeast secretory pathway. Cell *21*, 205–215.

Ortiz, D., Medkova, M., Walch-Solimena, C., and Novick, P. (2002). Ypt32 recruits the Sec4p guanine nucleotide exchange factor, Sec2p, to secretory vesicles; evidence for a Rab cascade in yeast. J. Cell Biol. *157*, 1005–1015.

Pashkova, N., and Weisman, L.S. (2005). Myosin V attachment to cargo requires the tight association of two functional subdomains. J. Cell Biol. *168*, 359–364.

Pashkova, N., Jin, Y., Ramaswamy, S., and Weisman, L.S. (2006). Structural basis for myosin V discrimination between distinct cargoes. EMBO J. *25*, 693–700.

Pastural, E., Barrat, F.J., Dufourcq-Lagelouse, R., Certain, S., Sanal, O., Jabado, N., Seger, R., Griscelli, C., Fischer, A., and de Saint Basile, G. (1997). Griscelli disease maps to chromosome 15q21 and is associated with mutations in the myosin-Va gene. Nat. Genet. *16*, 289–292.

Peng, Y., and Weisman, L.S. (2008). The Cyclin-Dependent Kinase Cdk1 Directly Regulates Vacuole Inheritance. Dev. Cell *15*, 478–485.

Protopopov, V., Govindan, B., Novick, P., and Gerst, J.E. (1993). Homologs of the synaptobrevin/VAMP family of synaptic vesicle proteins function on the late secretory pathway in S. cerevisiae. Cell *74*, 855–861.

Pruyne, D.W., Schott, D.H., and Bretscher, A. (1998). Tropomyosin-containing actin cables direct the Myo2p-dependent polarized delivery of secretory vesicles in budding yeast. J. Cell Biol. *143*, 1931–1945.

Pruyne, D., Legesse-Miller, A., Gao, L., Dong, Y., and Bretscher, A. (2004). Mechanisms of polarized growth and organelle segregation in yeast. Annu. Rev. Cell Dev. Biol. *20*, 559–591.

Purcell, T.J., Morris, C., Spudich, J.A., and Sweeney, H.L. (2002). Role of the lever arm in the processive stepping of myosin V. Proc. Natl. Acad. Sci. USA *99*, 14159–14164.

Reck-Peterson, S.L., Novick, P.J., and Mooseker, M.S. (1999). The Tail of a Yeast Class V Myosin, Myo2p, Functions as a Localization Domain. Mol. Biol. Cell *10*, 1001.

Reck-Peterson, S.L., Tyska, M.J., Novick, P.J., and Mooseker, M.S. (2001). The Yeast Class V Myosins, Myo2p and Myo4p, Are Nonprocessive Actin-Based Motors. J. Cell Biol. *153*, 1121.

Rivera-Molina, F.E., and Novick, P.J. (2009). A Rab GAP cascade defines the boundary between two Rab GTPases on the secretory pathway. Proc. Natl. Acad. Sci. USA *106*, 14408–14413.

Robinson, N.G., Guo, L., Imai, J., Toh-E, A., Matsui, Y., and Tamanoi, F. (1999). Rho3 of Saccharomyces cerevisiae, which regulates the actin cytoskeleton and exocytosis, is a GTPase which interacts with Myo2 and Exo70. Mol. Cell Biol. *19*, 3580–3587.

Romero, S., Le Clainche, C., Didry, D., Egile, C., Pantaloni, D., and Carlier, M.-F. (2004). Formin Is a Processive Motor that Requires Profilin to Accelerate Actin Assembly and Associated ATP Hydrolysis. Cell *119*, 419–429.

Rossi, G., and Brennwald, P. (2011). Yeast homologues of lethal giant larvae and type V myosin cooperate in the regulation of Rab-dependent vesicle clustering and polarized exocytosis. Mol. Biol. Cell *22*, 842–857.

Roumanie, O., Wu, H., Molk, J.N., Rossi, G., Bloom, K., and Brennwald, P. (2005). Rho GTPase regulation of exocytosis in yeast is independent of GTP hydrolysis and polarization of the exocyst complex. J. Cell Biol. *170*, 583–594.

Sabatini, B.L., Oertner, T.G., and Svoboda, K. (2002). The Life Cycle of Ca2+ Ions in Dendritic Spines. Neuron *33*, 439–452.

Sakamoto, T., Yildiz, A., Selvin, P.R., and Sellers, J.R. (2005). Step-Size Is Determined by Neck Length in Myosin V. Biochem. *44*, 16203–16210.

Salminen, A., and Novick, P. (1987). A ras-like protein is required for a post-Golgi event in yeast secretion. Cell *49*, 527–538.

Santiago-Tirado, F.H., and Bretscher, A. (2011). Membrane-trafficking sorting hubs: cooperation between PI4P and small GTPases at the trans-Golgi network. Trends Cell Biol. *21*, 515–525.

Santiago-Tirado, F.H., Legesse-Miller, A., Schott, D., and Bretscher, A. (2011). PI4P and Rab inputs collaborate in myosin-V-dependent transport of secretory compartments in yeast. Dev. Cell *20*, 47–59.

Savage, N.S., Layton, A.T., and Lew, D.J. (2012). Mechanistic mathematical model of polarity in yeast. Mol. Biol. Cell *23*, 1998–2013.

Schott, D., Ho, J., Pruyne, D., and Bretscher, A. (1999). The COOH-terminal domain of Myo2p, a yeast myosin V, has a direct role in secretory vesicle targeting. J. Cell Biol. *147*, 791–808.

Schott, D.H., Collins, R.N., and Bretscher, A. (2002). Secretory vesicle transport velocity in living cells depends on the myosin-V lever arm length. J. Cell Biol. *156*, 35–39.

Scott, B.L., Van Komen, J.S., Irshad, H., Liu, S., Wilson, K.A., and McNew, J.A. (2004). Sec1p directly stimulates SNARE-mediated membrane fusion in vitro. J. Cell Biol. *167*, 75–85.

Seabra, M., Brown, M., and Goldstein, J. (1993). Retinal degeneration in choroideremia: deficiency of rab geranylgeranyl transferase. Science *259*, 377–381.

Sellers, J.R., Thirumurugan, K., Sakamoto, T., Hammer, J.A., III, and Knight, P.J. (2008). Calcium and cargoes as regulators of myosin 5a activity. Biochem. Biophys. Res. Comm. *369*, 176–181.

Shaw, J.M., and Wickner, W.T. (1991). vac2: a yeast mutant which distinguishes vacuole segregation from Golgi-to-vacuole protein targeting. EMBO J. *10*, 1741.

Shimada, Y., Gulli, M.-P., and Peter, M. (2000). Nuclear sequestration of the exchange factor Cdc24 by Far1 regulates cell polarity during yeast mating. Nat. Cell Biol. *2*, 117–124.

Shiroguchi, K., and Kinosita, K. (2007). Myosin V walks by lever action and Brownian motion. Science *316*, 1208–1212.

Sivaram, M.V.S., Furgason, M.L.M., Brewer, D.N., and Munson, M. (2006). The structure of the exocyst subunit Sec6p defines a conserved architecture with diverse roles. Nat. Struct. Mol. Biol. *13*, 555–556.

Sivaram, M.V.S., Saporita, J.A., Furgason, M.L.M., Boettcher, A.J., and Munson, M. (2005). Dimerization of the exocyst protein Sec6p and its interaction with the t-SNARE Sec9p. Biochem. *44*, 6302–6311.

Söllner, T., Whiteheart, S.W., Brunner, M., Erdjument-Bromage, H., Geromanos, S., Tempst, P., and Rothman, J.E. (1993). SNAP receptors implicated in vesicle targeting and fusion. Nature *362*, 318–324.

Stalder, D., Mizuno-Yamasaki, E., Ghassemian, M., and Novick, P.J. (2013). Phosphorylation of

the Rab exchange factor Sec2p directs a switch in regulatory binding partners. Prot. Natl. Acad. Sci. USA *110*, 19995–20002.

Stevens, R.C., and Davis, T.N. (1998). Mlc1p is a light chain for the unconventional myosin Myo2p in Saccharomyces cerevisiae. J. Cell Biol. *142*, 711–722.

Suda, Y., Kurokawa, K., Hirata, R., and Nakano, A. (2013). Rab GAP cascade regulates dynamics of Ypt6 in the Golgi traffic. Prot. Natl. Acad. Sci. USA *110*, 18976–18981.

Sweeney, H.L.H., Rosenfeld, S.S.S., Brown, F.F., Faust, L.L., Smith, J.J., Xing, J.J., Stein, L.A.L., and Sellers, J.R.J. (1998). Kinetic tuning of myosin via a flexible loop adjacent to the nucleotide binding pocket. J. Biol. Chem. *273*, 6262–6270.

Takizawa, P.A., Sil, A., Swedlow, J.R., Herskowitz, I., and Vale, R.D. (1997). Actin-dependent localization of an RNA encoding a cell-fate determinant in yeast. Nature *389*, 90–93.

Tang, F., Kauffman, E.J., Novak, J.L., Nau, J.J., Catlett, N.L., and Weisman, L.S. (2003). Regulated degradation of a class V myosin receptor directs movement of the yeast vacuole. Nature *422*, 87–92.

Taylor, K.A. (2007). Regulation and recycling of myosin V. Curr. O. Cell Biol. *19*, 67–74.

TerBush, D.R., and Novick, P. (1995). Sec6, Sec8, and Sec15 are components of a multisubunit complex which localizes to small bud tips in Saccharomyces cerevisiae. J. Cell Biol. *130*, 299–312.

TerBush, D.R., Maurice, T., Roth, D., and Novick, P. (1996). The Exocyst is a multiprotein complex required for exocytosis in Saccharomyces cerevisiae. EMBO J. *15*, 6483–6494.

Thirumurugan, K., Sakamoto, T., Hammer, J.A., Sellers, J.R., and Knight, P.J. (2006). The cargo-binding domain regulates structure and activity of myosin 5. Nature *442*, 212–215.

Togneri, J., Cheng, Y.-S., Munson, M., Hughson, F.M., and Carr, C.M. (2006). Specific SNARE complex binding mode of the Sec1/Munc-18 protein, Sec1p. Proc. Natl. Acad. Sci. USA *103*, 17730–17735.

Velvarska, H., and Niessing, D. (2013). Structural Insights into the Globular Tails of the Human Type V Myosins Myo5a, Myo5b, and Myo5c. PLoS ONE *8*, e82065.

Vetter, I.R. (2001). The Guanine Nucleotide-Binding Switch in Three Dimensions. Science *294*, 1299–1304.

Walch-Solimena, C., Collins, R.N., and Novick, P.J. (1997). Sec2p Mediates Nucleotide Exchange on Sec4p and is Involved in Polarized Delivery of Post-Golgi Vesicles. J. Cell Biol. *137*, 1495.

Walworth, N.C., Brennwald, P., Kabcenell, A.K., Garrett, M., and Novick, P. (1992). Hydrolysis of GTP by Sec4 protein plays an important role in vesicular transport and is stimulated by a

GTPase-activating protein in Saccharomyces cerevisiae. Mol. Cell Biol. *12*, 2017–2028.

Wang, F., Thirumurugan, K., Stafford, W., Hammer, J., Knight, P., and Sellers, J. (2004). Regulated conformation of myosin V. J. Biol. Chem. *279*, 2333.

Wang, Y.X., Zhao, H., Harding, T.M., Gomes de Mesquita, D.S., Woldringh, C.L., Klionsky, D.J., Munn, A.L., and Weisman, L.S. (1996). Multiple classes of yeast mutants are defective in vacuole partitioning yet target vacuole proteins correctly. Mol. Biol. Cell *7*, 1375–1389.

Wang, Y.-X., Catlett, N.L., and Weisman, L.S. (1998). Vac8p, a Vacuolar Protein with Armadillo Repeats, Functions in both Vacuole Inheritance and Protein Targeting from the Cytoplasm to Vacuole. J. Cell Biol. *140*, 1063–1074.

Wang, Z., Edwards, J.G., Riley, N., Provance, D.W., Karcher, R., Li, X.-D., Davison, I.G., Ikebe, M., Mercer, J.A., Kauer, J.A., et al. (2008). Myosin Vb Mobilizes Recycling Endosomes and AMPA Receptors for Postsynaptic Plasticity. Cell *135*, 535–548.

Warshaw, D.M., Kennedy, G.G., Work, S.S., Krementsova, E.B., Beck, S., and Trybus, K.M. (2005). Differential labeling of myosin V heads with quantum dots allows direct visualization of hand-over-hand processivity. Biophys. J. *88*, L30–L32.

Wei, Z., Liu, X., Yu, C., and Zhang, M. (2013). Structural basis of cargo recognitions for class V myosins. Proc. Natl. Acad. Sci. USA *110*, 11314–11319.

Weimbs, T., Low, S.H., Chapin, S.J., Mostov, K.E., Bucher, P., and Hofmann, K. (1997). A conserved domain is present in different families of vesicular fusion proteins: a new superfamily. Proc. Natl. Acad. Sci. USA *94*, 3046–3051.

Weisman, L.S., Emr, S.D., and Wickner, W.T. (1990). Mutants of Saccharomyces cerevisiae that block intervacuole vesicular traffic and vacuole division and segregation. Proc. Natl. Acad. Sci. USA *87*, 1076–1080.

Wu, S., Mehta, S.Q., Pichaud, F., Bellen, H.J., and Quiocho, F.A. (2005). Sec15 interacts with Rab11 via a novel domain and affects Rab11 localization in vivo. Nat. Struct. Mol. Biol. *12*, 879–885.

Wu, X.S., Rao, K., Zhang, H., Wang, F., Sellers, J.R., Matesic, L.E., Copeland, N.G., Jenkins, N.A., and Hammer, J.A. (2002). Identification of an organelle receptor for myosin-Va. Nat. Cell Biol. *4*, 271–278.

Yang, H.-C., and Pon, L.A. (2002). Actin cable dynamics in budding yeast. Proc. Natl. Acad. Sci. USA *99*, 751–756.

Yau, R.G., Peng, Y., Valiathan, R.R., Birkeland, S.R., Wilson, T.E., and Weisman, L.S. (2014). Release from Myosin V via Regulated Recruitment of an E3 Ubiquitin Ligase Controls Organelle Localization. Dev. Cell *28*, 520–533.

Yildiz, A., Forkey, J.N., McKinney, S.A., Ha, T., Goldman, Y.E., and Selvin, P.R. (2003).

Myosin V Walks Hand-Over-Hand: Single Fluorophore Imaging with 1.5-nm Localization. Science *300*, 2061–2065.

Yin, H., Pruyne, D., Huffaker, T.C., and Bretscher, A. (2000). Myosin V orientates the mitotic spindle in yeast. Nature *406*, 1013–1015.

Zhang, X., Bi, E., Novick, P., Du, L., Kozminski, K.G., Lipschutz, J.H., and Guo, W. (2001). Cdc42 interacts with the exocyst and regulates polarized secretion. J. Biol. Chem. *276*, 46745–46750.

Zhang, X., Orlando, K., He, B., Xi, F., Zhang, J., Zajac, A., and Guo, W. (2008). Membrane association and functional regulation of Sec3 by phospholipids and Cdc42. J. Cell Biol. *180*, 145–158.

CHAPTER 2

MYOSIN-V IS ACTIVATED BY BINDING SECRETORY CARGO AND RELEASED IN COORDINATION WITH RAB/EXOCYST FUNCTION

OVERVIEW

As detailed in Chapter 1, cell polarity in eukaryotic cells is maintained through the interplay of a polarized cytoskeleton and motor proteins that mediate cargo transport. For the essential cargo of secretory vesicles in budding yeast, transport via Myo2p is ensured through two receptors: vesicle bound Sec4-GTP and an unidentified component dependent on PI4P. In addition, there is some evidence that exocyst component Sec15p directly binds to Myo2p, though this does not appear to be essential for transport (Santiago-Tirado et al., 2011; Jin et al., 2011). While the association of Myo2p with secretory membranes has been well characterized, little is known about how the motor's transport cycle is coordinated with cargo association and delivery.

Before beginning this research, studies on the dynamics of Myo2p mostly concerned movement of cargo from the mother cell to the bud. It was shown that Myo2p colocalizes with secretory membranes, and that Myo2p transports secretory vesicles rapidly to sites of growth at 3 μm/s (Schott et al., 2002; Lipatova et al., 2008). Work with conditional mutants also showed that this happens constitutively, with secretory vesicles not influencing the polarization state of Myo2p (Schott et al., 1999). While this conclusion was supported by the available data, I will challenge this result and instead argue that Myo2p requires competent secretory vesicles to polarize.

Additionally, almost nothing was known about how the motor was released and recycled from secretory vesicles. Secretion occurs so persistently throughout the cell cycle that it seemed unlikely the motor was degraded after making one trip to a growth site, as certain Myo2p

receptors are. Western blot time-course experiments with cyclohexamide agreed with this (Stevens et al., 1998). Since both Myo2p and the vesicle marker Sec4p colocalize at sites of growth, it also seemed likely that Myo2p release from vesicles occurs at the plasma membrane and not just anywhere in the bud. And while experiments performed in our lab showed that Myo2p binds to Sec4p only in the GTP bound state, it was not known if the hydrolysis event was relevant to the release of the motor *in vivo* or how it integrated with the fusion machinery.

In this chapter, I will define the *in vivo* delivery cycle of a myosin-V in its essential function of secretory vesicle transport. I show that Myo2p is activated by binding to secretory vesicles and go on to define the number of motors that transport vesicles to sites of growth. In addition, I will show that efficient recycling of the motor from vesicles requires exocyst complex tethering and Sec4-GTP hydrolysis. Most of the results presented in this chapter have already been published in *Developmental Cell* (Donovan and Bretscher, 2012).

MATERIALS AND METHODS

Yeast Strains and Molecular Biology Techniques

Cells were grown using standard laboratory techniques (Sherman, 2001). Yeast transformations were performed using lithium acetate methods (Gietz et al., 2002). Actin patches and filaments were visualized using phalloidin staining using lab standard methods (Liu et al., 2012).

To generate Myo2-GFP and Myo2-3xGFP strains, I appended the tag at the 3' end of the *MYO2* open reading frame in the chromosome. The 3xGFP construct was a generous gift of the Glick Lab (University of Chicago). 3xGFP was cut and inserted into a pRS306 vector between the NotI and BamHI restriction endonuclease sites. The *MYO2* C-terminal coiled-coil

tail (nucleotides 2776-4725) was then amplified from genomic DNA preparations (YeaStar Genomic DNA kit). This fragment and the pRS306-3xGFP vector were then cut with XhoI and BamHI restriction enzymes and the fragment was ligated into the vector. A 495 nt region 3' to the *MYO2* gene was then inserted between NotI and Sac1 sites after PCR amplification. To disrupt the *MYO2* gene, I digested the unique HindIII site present in the Myo2-cctail, transformed the linear vector into wildtype or mutant strains, and grew on SD-Ura media to select for *MYO2-3xGFP::URA3*. In all cases, several clones were tested for proper Myo2-3xGFP localization and growth against wildtype before any experiments took place. A similar strategy was performed to generate Myo2-GFP clones, except a single GFP was amplified from the original pRS306-3xGFP vector using primers with NotI and BamHI restriction sites (5'-CAGGATCCATGTCTAAAGGTGAAGAATTATTC-3' and 5'-TATCAAATGCGGCCGCTAGGTACAATTCATCCATACCATG-3') to insert the GFP fragment C-terminal to the Myo2-cctail fragment. Mutant *myo2* constructs were generated using coiled-coil tail fragments amplified from genomic DNA sources containing the mutations. Sequencing reactions were performed to verify PCR accuracy in all cases where PCR was used to amplify products. Double mutants were generated using a diploid approach. In the case of *sec23-1 myo2-13-GFP*, a *sec23-1/sec23-1* mutant was generated followed by transformation of a linearized coiled-coil-tail-GFP vector containing the *myo2-13* mutations. This was then sporulated and dissected by standard techniques to acquire the double mutant.

To generate a chromosomally tagged GFP-Sec4, I appended GFP to the N-terminus of the *SEC4* gene. Briefly, I modified a *pRS315-pSEC4-GFP-SEC4* plasmid generously acquired from Ruth Collins at Cornell University. BamHI was used to cut upstream of the *SEC4* promoter and an internal HindIII site (present in *SEC4* at nucleotide 563) to liberate the *pSEC4-GFP-sec4*

fragment and placed it into a BamHI/HindIII cut pRS306 vector. To disrupt the *SEC4* gene, the vector was linearized by cutting with the unique BspEI site present in the *sec4* fragment. This was transformed into wildtype or mutant cells to generate *GFP-SEC4::URA3*. GFP localization was checked against the original CEN plasmid and growth assays comparing tagged and untagged strains were performed in all cases ahead of any experiments to verify fidelity of chromosomal GFP-Sec4. Endogenous tagging of other proteins was performed using standard PCR techniques as described in Longtine et al. (1998).

Microscopy and Photobleaching

Micrographs were acquired with a CSU-X spinning disc confocal microscope system (Intelligent Imaging Innovations) using a DMI600B microscope (Leica) and QuantEM EMCCD camera (Photometrics) controlled by Slidebook 5.0 Software (Intelligent Imaging Innovations). Strains shifted to high temperatures were imaged in an environmental chamber (Okolab) at the indicated temperature. Strains were imaged for short experiments on a 1.5% QSD agarose pad (Rossanese et al., 2001); for longer experiments or when photobleaching, a glass-bottomed dish with 0.5 mg/mL Concanavalin A (EY Laboratories) pre-spotted to adhere cells to the glass was used. Images were processed in either ImageJ or Slidebook 5.0 software. Panels were assembled after identical processing unless otherwise indicated.

Quantification of molecule numbers on secretory vesicles was done largely by following established protocols (Joglekar et al., 2008). The new assumption of ~5 molecules of Cse4p per kinetochore, or ~80 per anaphase cluster (Lawrimore et al., 2011) was used. An *RFP-SNC2* CEN plasmid acquired from Ruth Collins at Cornell University was used to determine if Myo2-4IQ-3xGFP was on secretory vesicles. This was coimaged with a Cse4-3xGFP strain (kindly provided

by Dr. Wei-Lih Lee, University of Massachusetts, Amherst) for direct comparison of fluorescence intensities. Similarly, a Cse4-GFP strain was directly compared to GFP-Sec4 strain. All cells were grown to log phase in synthetic media. Comparison of Cse4p foci intensity (with nuclear background subtracted) of cells in anaphase and vesicle foci intensity (with cytoplasm background subtracted) allowed for the determination of molecule number on vesicles. Several single plane movies centered on the bud neck were acquired for each strain. Vesicles diffusing around the cytoplasm were defined as those vesicles that don't make bud-directed movements over five frames (~2.2 seconds); the brightest intensity was used to determine molecule number per diffusing vesicle. Vesicles undergoing active transport to sites of growth were defined as vesicles that make rapid bud-directed movement over three frames; the brightest intensity was used to determine molecule number per vesicle.

Photobleaching experiments were performed using an argon laser and mosaic digital illumination system (Andor Scientific). Medium budded cells (defined as a bud diameter of 2 μm) were used throughout all photobleaching experiments for standardization purposes. FRAP experiments were conducted by photobleaching the central plane of the confocal z-section containing the bud of the bud for 2000 ms and determining the recovery kinetics of the GFP tagged protein for every second thereafter. In FLIP experiments, nearly the entire mother cell was photobleached for 750 ms every 6 seconds; micrographs and the intensity of GFP in the bud was determined every 2 seconds. FLIP experiments in temperature-sensitive strains were shifted to 35 °C for 1 hour unless otherwise indicated.

In all photobleaching experiments, the pre-bleach intensity of tagged protein in the bud was normalized to 1.0 to compare between cells. Further, the photobleaching caused by imaging was normalized using a nearby cell. The number of modes of action contributing to the recovery

of signal in a FRAP experiment was found using methods described in Boyd et al. (2004). The half-times of recovery were calculated using the equation $t_{1/2}$= (ln 2)/k (Salmon et al., 1984). To determine the modes of action in a FLIP experiment, the normalized intensity in the bud on an exponential scale was plotted against time. The presence of two discontinuous slopes was evidence for two rates constituting loss from the bud (Figure S3c). KaleidaGraph (Synergy Software) was used to generate single or double exponential curves to determine rates of recovery or loss. Rates for FLIP and FRAP experiments are summarized in Table S1.

Whole cell projections of log phase, medium budded cells were used to determine the fraction of tagged Myo2p or Sec4p found in the bud. Cells were imaged for 50 ms in each plane of a z-stack (0.5 μm step size), which was then used to create a summed projection for analysis of fluorescence in different cell regions. Background subtraction and quantification was performed in ImageJ. FLIP experiments in Figure 7F were conducted at 14 °C using a peristaltic pump (Rainin Instrument Co Inc.) that moved chilled media across the cells on the glass-bottomed dish. Cells were cooled to 14 °C for 15 minutes prior to conducting FLIP experiment. A temperature probe was used to ensure the temperature consistently remained at the cooled temperature.

Quantitative Immunoblots and Calculation of Molecule Number

Quantitative immunoblots of Myo2-GFP and GFP-Sec4 were performed using purified recombinant GST-eGFP and cell lysates containing chromosomally tagged proteins. To obtain yeast cell lysates, tagged GFP-Sec4 and Myo2-GFP strains were grown to log phase in SD media at 26°C in 8 mL cultures. A hemocytometer was used to determine the number of cells per culture. Cells were resuspended in 70 μL disruption buffer (20 mM Tris-Cl pH 7.9, 10 mM

$MgCl_2$ 1 mM EDTA, 5% glycerol, 1 mM dithiothreitol, 0.3 M ammonium sulfate, 1 mM PMSF, 1X Sigma yeast protease inhibitor cocktail) with 0.1 g acid-washed glass beads (Sigma). 6 X 1 minute vortex cycles at 8 °C (with one minute on ice between cycles) was used to disrupt cells. Empirical tests determined that nearly all cells were disrupted after six cycles. Sample buffer was then added directly, boiled for 1 minute, and clarified by centrifugation to obtain a crude lysate. Three independent preparations per protein were done when calculating number of molecules per cell.

To determine the number of proteins per cell, quantitative immunoblots were performed and analyzed using Odyssey infrared imaging system (LI-COR Biosciences). Essentially all proteins were transferred after a 1.5 hour semi-dry transfer. Mouse monoclonal antibody against GFP (Santa Cruz Biotechnology) was used to probe the membrane and the amount of GFP-tagged protein per cell was determined.

To obtain the number of molecules in different areas of the cell, whole cell z-projections of Myo2-GFP and GFP-Sec4 strains were obtained by confocal microscope using a 100X objective, 2X photomultiplier, and 0.4 μm step-size. It was assumed that the fluorescence intensity in the yeast cell is directly comparable to the number of molecules present (Wu, J-Q. and Pollard, 2005). Strains were grown in the dark to log phase at room temperature. Images were processed in ImageJ; after background subtraction, the intensity of signal in the mother, bud, and bud tip was then related to the number of proteins per cell obtained by quantitative immunoblot to determine molecule number in the mother, whole bud, and bud tip regions.

RESULTS

Myo2p has to deliver many organelles at appropriate times during the cell cycle. For the vacuole, timing is dictated by the cell cycle regulated synthesis and destruction of the vacuole receptor, Vac17p (Tang et al., 2003). Since Myo2p is polarized throughout the cell cycle in actively growing yeast, one model suggests that the motor is always active and transports any cargo for which a receptor is available. Alternatively, Myo2p might need to be activated by the presence of transport-competent cargo. To distinguish between these models, I examined Myo2p localization when transport-competent secretory cargo, Myo2p's most abundant and essential cargo, is eliminated.

Myo2p polarization requires competent secretory cargo

Myo2p was visualized in live cells by appending either *1xGFP* or *3xGFP* to the 3'-end of the *MYO2* open reading frame in the chromosome, neither of which had any detectable effect on cell growth or Myo2p localization. I first examined Myo2-3xGFP in wildtype cells and in cells harboring conditional mutations in essential secretory pathway genes. Sec23p is a component of COPII vesicles that transport secretory materials from the endoplasmic reticulum to the Golgi apparatus; in the conditional *sec23-1* mutant all export from the ER is blocked at the restrictive temperature, thereby also preventing post-Golgi secretory vesicles from being formed (Figure 2.1a; Kaiser and Schekman, 1990; Rexach and Schekman, 1991). Sec4p is the Rab GTPase associated with secretory vesicles that functions as part of the receptor for Myo2p; in the conditional *sec4-8* mutant secretory vesicles are made, but not transported at the restrictive temperature (Salminen and Novick, 1987; Ferro-Novick and Novick, 1993). In wildtype cells and the *sec23*-1 and *sec4-8* mutants growing at the permissive temperature, Myo2-3xGFP is

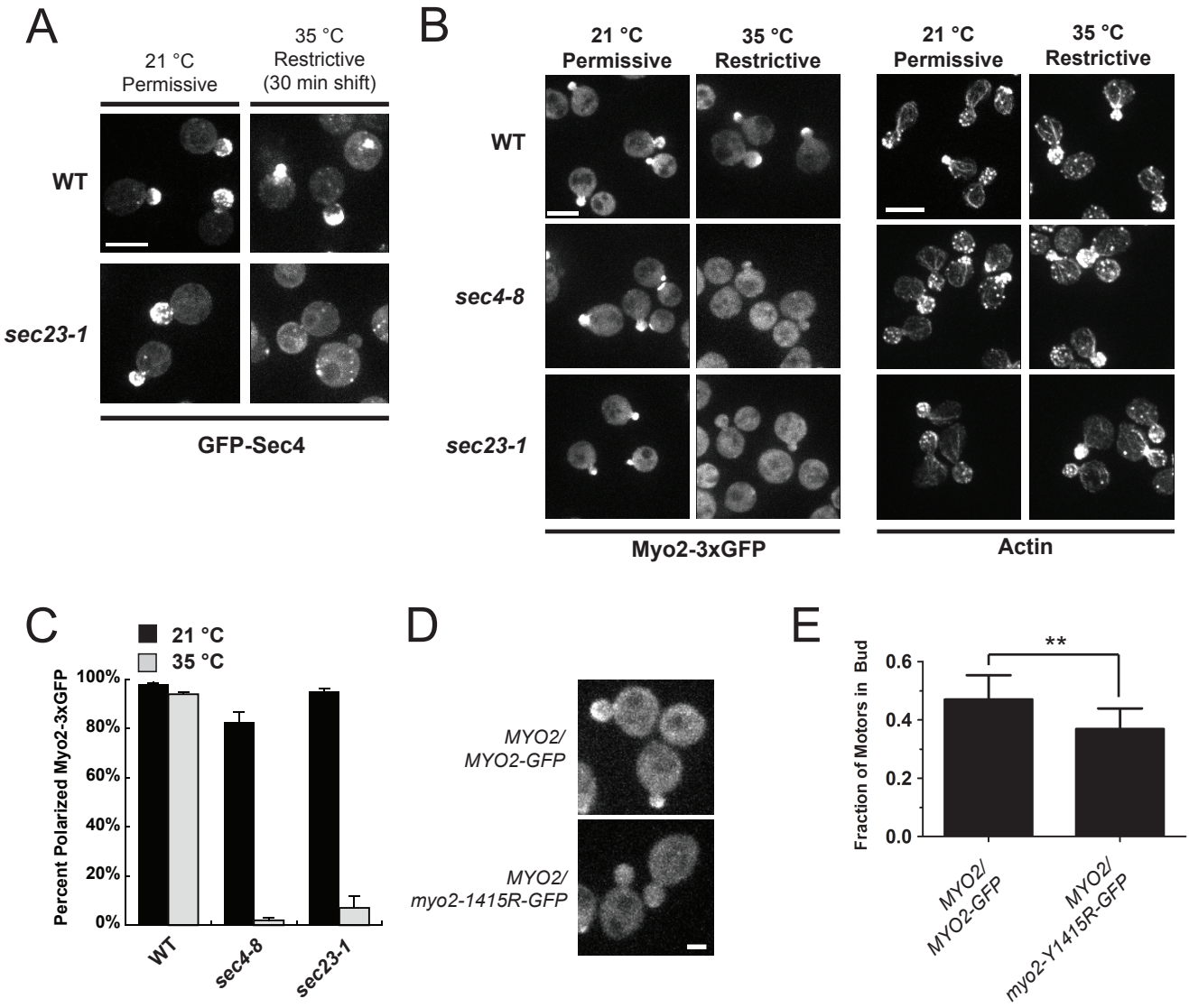

Figure 2.1. Myo2p polarization requires competent secretory cargo.

A. Endogenous GFP-Sec4 localization in wildtype and *sec23-1* cells at 21°C and 35°C following a 30 minute shift. GFP-Sec4 becomes enriched in the cytoplasm and in aggregates in *sec23-1* cells at the restrictive temperature. Scale bar represents 5 μm.
B. Polarization of Myo2-3xGFP and phalloidin-stained actin cables in wildtype, *sec4-8*, and *sec23-1* cells at the permissive temperature and after a 30 min shift to the restrictive temperature. Images adjusted for best presentation. Scale bar, 5 μm.
C. Quantification of Myo2-3xGFP polarization in (A). Three independent replicates of 150 small and medium buds were scored for each condition to determine the fraction of Myo2-3xGFP polarized. Error bars are standard deviation.
D. Diploids containing one copy of either *MYO2-GFP* or *MYO2-Y1415R-GFP*. Scale bar represents 2 μm.
E. Graph of (D) showing the fraction of total motors present in the bud. n=31 cells each. **, $p<0.01$

polarized to sites of growth. However, upon shifting to the restrictive temperature for 30 minutes Myo2-3xGFP became depolarized in both mutants whereas it remained polarized in wildtype cells (Figures 2.1b-c) This depolarization is not a result of an indirect defect of the actin cytoskeleton as normal actin cables were observed extending into the mother cell at both temperatures in all strains (Figure 2.1b). Thus, competent secretory vesicles are required to polarize a wildtype Myo2p motor.

How do secretory vesicles activate Myo2p? An attractive model for activation is the motor binding to a component of its receptor complex on secretory vesicles. Components of the complex include the Rab Sec4p and an unknown component dependent on PI4P (Santiago-Tirado et al., 2011). To determine if Sec4p has a role in activating Myo2p, I took advantage of the *myo2-Y1415R* mutation, which blocks Rab binding to the Myo2p tail (Pashkova et al., 2006; Lipatova et al., 2008; Santiago-Tirado et al., 2011). Since this is a lethal mutation, work with this allele was performed in a diploid. Strains with one copy of *MYO2* tagged with GFP (*MYO2/MYO2-GFP)* showed polarized motors similar to those seen in haploid cells. However, when one copy of *MYO2* was replaced with *myo2-Y1415R-GFP* (*MYO2/myo2-Y1415R-GFP*), observed motors showed minimal polarization and the fraction of total observable motors in the bud was significantly less (Figure 2.1d). While this result is complicated by the fact that wildtype/mutant heterodimers likely exist, the depolarization of Myo2-Y1415R-GFP motors strongly suggests that Myo2p is activated by binding to Sec4p.

Our lab has characterized conditional mutations in the Myo2p tail that fail to interact with receptors and fail to transport secretory vesicles at the restrictive temperature, but Myo2p nevertheless remains polarized (Figures 2.2a-b; Schott et al., 1999). Since this new work shows that competent secretory cargo is necessary to polarize wildtype Myo2p, tail mutants at the

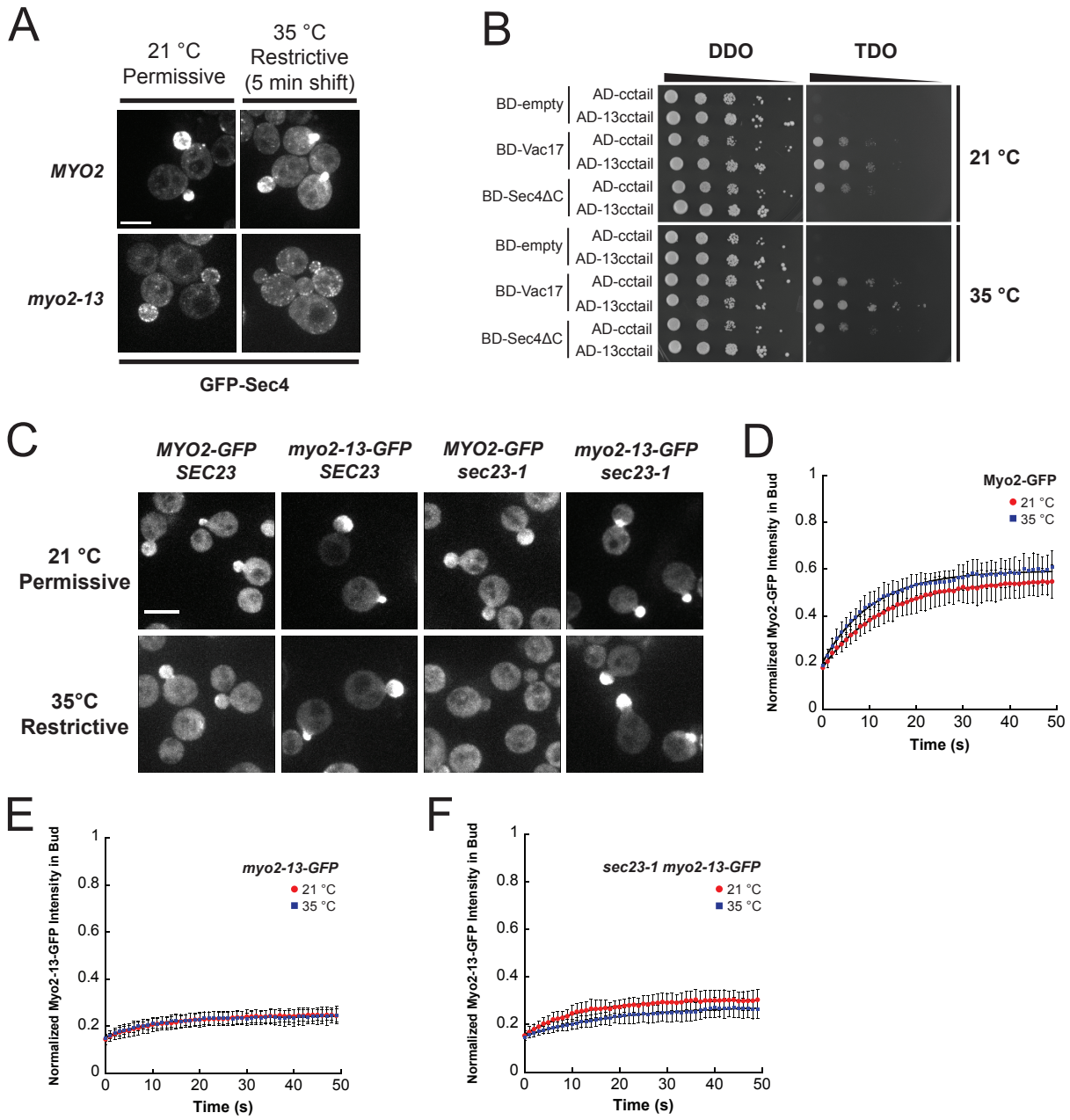

Figure 2.2. A mutant motor defective in cargo binding is constitutively active.

A. GFP-Sec4 localization in wildtype and *myo2-13* strains at 21 °C and 35 °C following a 5 minute shift. Scale bar represents 5 µm.
B. Yeast two-hybrid interactions of Myo2 or Myo2-13 coiled-coil region + tail (cctail, nucleotides 2776-4725) fused to the activation domain (AD), with Vac17p (1-258) or Sec4ΔCp fused to the binding domain (BD). Sec4p construct was mutated in the C-terminal CXC motif to prevent prenylation. Cells grown on double-dropout (DDO) SD-Trp-Leu media or triple-dropout (TDO) SD-Trp-Leu-His media.
C. Myo2-GFP and Myo2-13-GFP polarization in *SEC23* and *sec23-1* cells at 21°C and 35°C following a 30 minute shift. Images adjusted for best presentation. Scale bar, 5 µm.
D. Normalized Myo2-GFP intensity in the bud following bleach event at 21 °C and 35°C. The half-time of recovery was 10.3 ± 1.9 seconds at 21 °C (n=12) and 8.5 ± 2.4 seconds at 35°C (n=14). Error bars are standard deviation.
E. Normalized Myo2-13-GFP intensity in the bud following bleach event at 21 °C and 35°C. Note that wildtype recovery was not observed because the vast majority of motors are hyperpolarized to the bud. The half-time of recovery was 9.5 ± 3.2 seconds at 21 °C (n=14) and 9.1 ± 5.2 seconds at 35°C (n=14). Error bars are standard deviation.
F. Normalized Myo2-13-GFP intensity in the bud of *sec23-1* cell following bleach event at 21 °C and 35°C. The half-time of recovery was 10.2 ± 3.1 seconds at 21 °C (n=10) and 12.1 ± 3.5 seconds at 35°C (n=11). Error bars are standard deviation. Therefore, active recovery of Myo2-13-GFP into the bud is unaffected by the presence or absence of secretory vesicles.

restrictive temperature must be both defective in cargo binding and constitutively active. To test this model, I first introduced *myo2-13-GFP* into a *sec23-1* strain. Myo2-13-GFP was polarized in both *SEC23* and *sec23-1* cells at 21° and 35°, thereby indicating that Myo2-13-GFP is active in the presence and absence of secretory cargo (Figure 2.2c). Further, this polarization is actin dependent and the recovery of Myo2-13-GFP into the bud after photobleaching follows wildtype recovery kinetics (Figures 2.2d-f; data not shown); this indicates that Myo2-13-GFP polarization is due to motor activity. In summary, wildtype Myo2p needs to be activated to polarize, but a mutant defective in binding secretory vesicles is constitutively active and can polarize in the absence of cargo.

About 10 myosin-V motors associate with secretory vesicles

To investigate the delivery cycle of Myo2p, I first needed to quantify the number of motors in a yeast cell. Using quantitative immunoblots comparing purified GST-GFP with Myo2-GFP in total cell lysates, I estimate there are about 5800 Myo2-GFP molecules (2900 motors) per cell, which is in good agreement with a previous estimate (Figures 2.3a-c; Ghaemmaghami et al., 2003).

Timelapse micrographs of Myo2-3xGFP show diffusing puncta in the mother cell that then move abruptly towards the bud. To define the number of motors present on a secretory vesicle in different stages of its delivery cycle, I replaced chromosomal *MYO2* with *myo2-4IQ-3xGFP*. This allele contains four IQ motifs rather than the normal six in its lever arm, resulting in a truncated lever arm that reduces secretory vesicle transport speed (2.00 ± 0.56 μm/s, n= 25). Use of this slower-moving mutant was necessary to capture sufficient images of transported vesicles for quantitation, and does not affect protein expression, growth rate or Myo2p

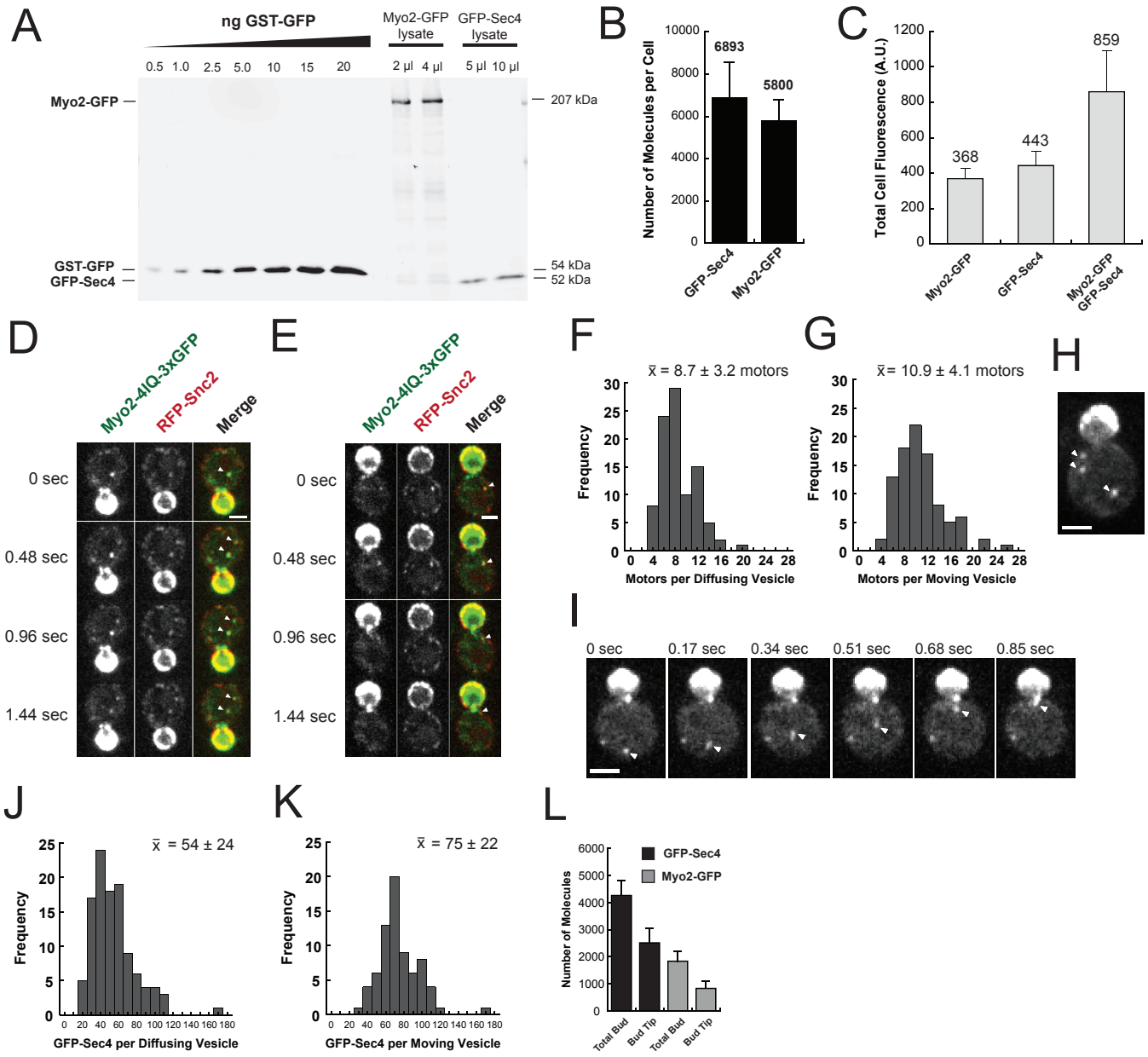

Figure 2.3. 10 Myo2p motors associate with vesicles undergoing active transport to sites of growth.

A. Quantitative immunoblot of Myo2-GFP and GFP-Sec4 lysates. Standard curve of GST-GFP (0.5 – 20 ng) was loaded onto 6-10% SDS-PAGE gel with indicated volumes of Myo2-GFP and GFP-Sec4 lysate and blotted with GFP antibodies.
B. Number of molecules of Myo2-GFP and GFP-Sec4 per cell, as determined from quantitative immunoblots. Note that monomers of Myo2-GFP are shown. Error bars are standard deviations from three independent cell lysates for both Myo2-GFP and GFP-Sec4.
C. Whole cell projection fluorescence (A.U.) of cells containing Myo2-GFP, GFP-Sec4, and both proteins tagged together.
D. Myo2-4IQ-3xGFP on RFP-Snc2 positive diffusing vesicles. Arrowheads show vesicle/motor puncta colocalization. Scale bar, 2 µm.
E. Myo2-4IQ-3xGFP transporting RFP-Snc2 positive vesicle to bud. Arrowheads show vesicle/motor puncta colocalization. Scale bar, 2 µm.
F. Histogram of number of motors on RFP-Snc2 positive diffusing vesicles, n= 94 puncta.
G. Histogram of number of motors on RFP-Snc2 positive vesicle undergoing active transport, n= 94 puncta.
H. GFP-Sec4 positive diffusing vesicles, as indicated by arrowheads. Scale bar, 2 µm.
I. GFP-Sec4 vesicle undergoing active transport, as shown by arrowheads. Scale bar, 2 µm.
J. Histogram of number of GFP-Sec4 molecules per diffusing vesicle, n= 98 puncta.
K. Histogram of number of GFP-Sec4 per puncta undergoing active transport, n = 72 puncta.
L. Number of molecules of Myo2-GFP and GFP-Sec4 in the total bud and bud tip of medium-budded cells, using total molecules per cell information obtained from quantitative immunoblots and whole cell fluorescence projections of cells. Error bars represent standard deviations for n= 55, 39 cells, respectively.

localization (Schott et al., 2002). The Myo2-4IQ-3xGFP puncta colocalize with RFP-Snc2 puncta, a tagged version of the post-Golgi v-SNARE that resides on secretory vesicles (Figure 2.3d; Protopopov et al., 1993). Nearly all Myo2-4IQ-3xGFP puncta were positive for RFP-Snc2, whereas about half of the RFP-Snc2 puncta were positive for Myo2-4IQ-3xGFP. Importantly, all rapidly moving RFP-Snc2 puncta had associated Myo2-4IQ-3xGFP (Figure 2.3e). Thus, secretory vesicles marked by RFP-Snc2 recruit Myo2p and are rapidly transported to growth sites, presumably when they encounter an actin cable.

I next sought to determine the number of motors involved in delivering secretory vesicles to sites of growth through *in vivo* quantitative microscopy. The number of molecules of Myo2-4IQ-3xGFP on RFP-Snc2 vesicle puncta were estimated by co-imaging with yeast expressing the centomeric histone protein Cse4-3xGFP as a molecular standard, assuming ~80 Cse4-3xGFP per anaphase cluster (Lawrimore et al., 2011). Using this method, there are 8.7 ± 3.2 motors per diffusing secretory vesicle (Figure 2.3f) and 10.9 ± 4.1 motors on vesicles being actively transported into the bud (Figure 2.2g). Because all rapidly moving vesicles were positive for Myo2-4IQ-3xGFP, it is unlikely I have under-sampled the number of motors per vesicle.

As Sec4p is part of the receptor for Myo2p on secretory vesicles, I also wanted to determine the number of Sec4p molecules on each secretory vesicle. Sec4p is C-terminally prenylated, so I appended GFP to the N-terminus of Sec4p at its chromosomal locus, which caused no deleterious effects. Quantitative immunoblotting indicates there are about 6,900 GFP-Sec4 molecules in a cell (Figure 2.3b). Confocal microscopy showed randomly diffusing puncta of GFP-Sec4 that, like Myo2p-3xGFP, were seen to abruptly move into the bud (Figures 2.3h-i). Using the same quantitative microscopy technique, I estimate there are about 54 ± 24 molecules of GFP-Sec4 per diffusing particle (Figure 2.3j) and 75 ± 22 molecules on puncta undergoing

active transport to sites of growth (Figure 2.3k). Thus, there is an excess of Sec4p molecules to accommodate the ~10 Myo2p motors on each puncta even if each Myo2p binds two Sec4p as would be expected.

Do the puncta of Myo2-4IQ-3xGFP, RFP-Snc2 and GFP-Sec4 correspond to single post-Golgi secretory vesicles, or clusters of them? A 5μm diameter yeast bud requires about 2000 secretory vesicles (~80-100 nm in diameter) to generate sufficient membrane surface. Post-Golgi secretory vesicles have to also provide membrane for endocytosis; given the number of endocytic patches and their lifetimes in the bud, a 30-50 nm endocytic vesicle is generated about every three seconds (Prescianotto-Baschong and Riezman, 1998; Kaksonen et al., 2003). If one assumes a doubling time of 90 minutes, cell growth and endocytosis would require the delivery of about one vesicle every 2-3 seconds, which is close to the observed number (0.29 ± 0.13 vesicles moving per second, n=10 movies). This rate implies that I am visualizing and quantifying the components of individual secretory vesicles.

Myo2p remains associated with secretory vesicles upon reaching sites of growth

Vesicles accumulate at sites of growth in the bud due to a kinetic delay before exocytosis; electron micrographs have shown that small growing buds accumulate a cluster of about 10-20 secretory vesicles (Mulholland et al., 1994). To explore the fate of Myo2p after secretory vesicle delivery to sites of growth, I determined the number of Sec4p and Myo2p molecules that accumulate in the bud using the previously obtained quantitative immunoblot data and full cell projections of Myo2-GFP and GFP-Sec4 fluorescence (Figure 2.3l) About 4260 Sec4p molecules accumulate within a medium sized bud, with 2510 concentrated at the bud tip (n= 39 cells). This tip-localized pool represents Sec4p molecules from approximately 34 vesicles. I also found 1834

molecules of Myo2p (917 motors) in the bud and 828 molecules (414 motors) at the bud tip (n= 55 cells). Strikingly, this represents 38 'vesicle complements' of Myo2p motors at the bud tip. This implies that a full complement of Myo2p motors remains associated with secretory vesicles until they undergo exocytosis.

Bulk movement of Myo2p motors into the bud is rapid

Since the foregoing analysis represents the steady state view of secretory vesicle transport, I used photobleaching approaches to examine the dynamics of Myo2p. Fluorescence recovery after photobleaching (FRAP) experiments were performed on medium-sized buds (2 μm in diameter) of wildtype cells expressing endogenous Myo2-GFP; after bleaching the bud, fluorescence recovery was monitored every second (Figure 2.4a). This approach therefore monitors a combination of diffusion and active transport into the bud. Myo2-GFP recovers quickly into the bud, with a Myo2-GFP recovery rate (k) of 0.070 ± 0.014 s^{-1} (n= 12; Figure 2.4b). This yields a half-time of recovery ($t_{1/2}$) of 10.3 ± 1.9 seconds. Similar recovery dynamics were obtained with GFP-Sec4 (Figures 2.4c-d), with a recovery rate (k) of 0.054 ± 0.007 s^{-1} and a half-time of recovery of 13.1 ± 1.7 seconds (n= 10). As expected, these values match other vesicle-associated proteins such as exocyst components (Boyd et al., 2004) and indicate that bulk transport of secretory vesicles to sites of growth is rapid.

Myo2p resides in the bud for a defined time and is then deactivated

To estimate the duration Myo2-GFP resides in the bud, I analyzed wildtype, medium-budded cells using the fluorescence loss in photobleaching (FLIP) technique. In this experiment, the mother cell was photobleached every six seconds and the loss of fluorescence from the bud

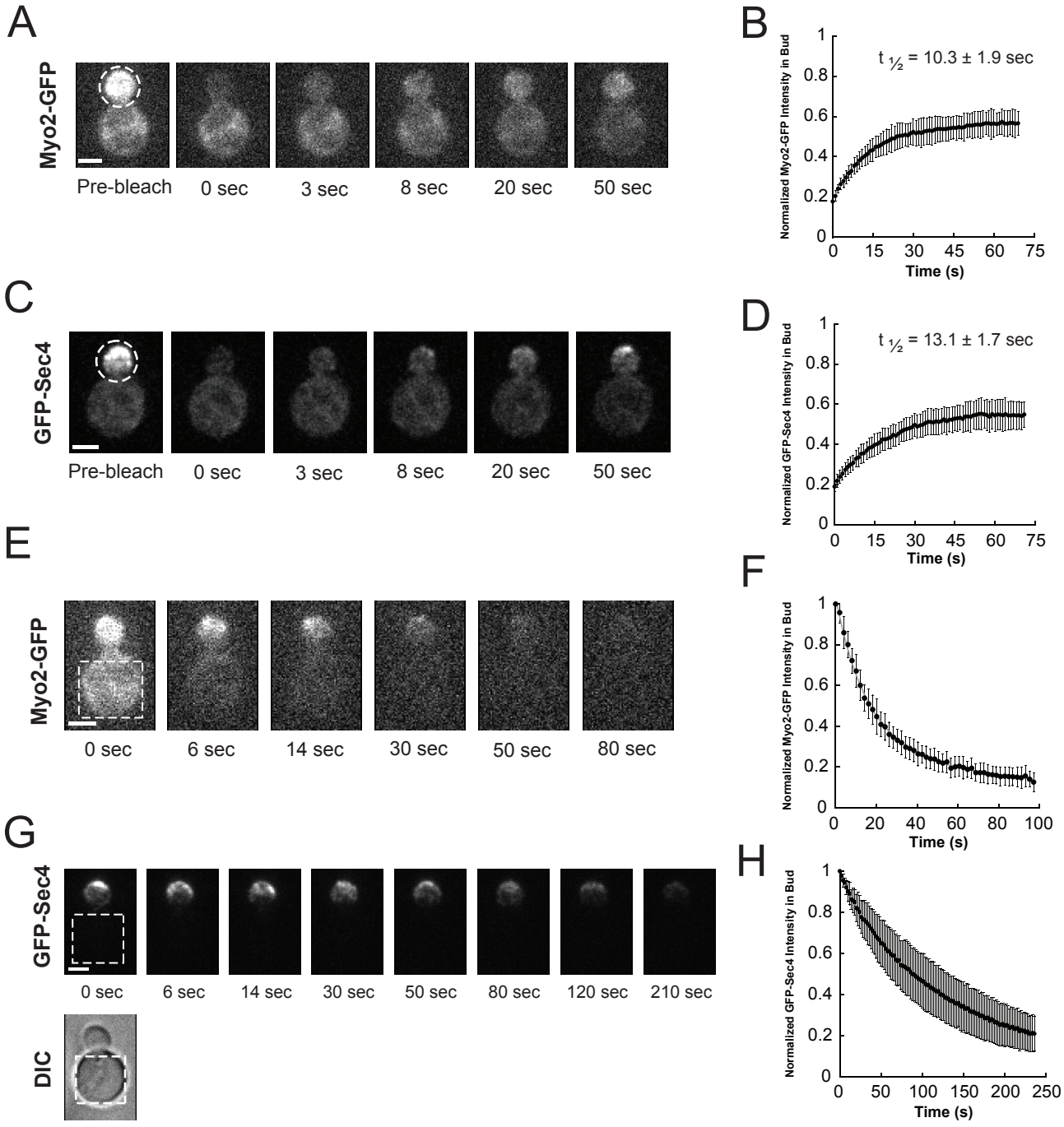

Figure 2.4. Bulk motor and Rab movement into and out of the bud reveals dynamic populations of proteins.

A. Still-frame micrographs of FRAP experiment shows rapid restoration of Myo2-GFP polarity. Circle indicates bleach area. Scale bar, 2 μm.
B. Normalized Myo2-GFP intensity in the bud following bleach event. Error bars are standard deviation of n= 12 cells. Full recovery not observed since about 33% of all Myo2-GFP is found in bud.
C. Representative still frame micrographs of GFP-Sec4 during FRAP experiment. Circle indicates bleach area. Scale bar, 2 μm.
D. Normalized GFP-Sec4 intensity in the bud following bleach event. Error bars are standard deviation of n= 10 cells. Full recovery of GFP-Sec4 not observed because a large fraction of GFP-Sec4 is found in the bud.
E. Still-frame micrographs of Myo2-GFP during FLIP experiment. Box indicates region bleached repeatedly. Scale bar, 2 μm.
F. Normalized Myo2-GFP intensity in the bud during FLIP experiment. Error bars indicate the standard deviation of n= 12 cells. Double exponential line of best fit shown in gray.
G. Still-frame micrographs of GFP-Sec4 during FLIP experiment. Box indicates region bleached repeatedly. Scale bar, 2 μm.
H. Normalized GFP-Sec4 intensity in the bud during FLIP experiment. Error bars indicate the standard deviation of n= 10 cells.

monitored every 2 seconds. Our lab's photobleaching setup allows for precise control over the region photobleached, and performing this experiment in fixed cells showed that the bud is not photobleached in FLIP experiments (data not shown). Further, an area of the field of view was used to subtract background and a separate unbleached cell to correct for the small amount of photobleaching that occurs during the observation period.

FLIP analysis revealed that Myo2-GFP fluorescence was lost from the bud in a highly reproducible manner over the course of 90 seconds (Figure 2.4e). To obtain rates of motor loss from the bud in such a FLIP experiment, the normalized fluorescence intensity of Myo2-GFP in the bud was plotted over time (Figure 2.4f). I determined that two components constitute an exponential loss of motors from the bud. A fast rate of motors leaving the bud yielded a Myo2-GFP half-time of loss ($t_{1/2}$) of 9.6 ± 2.1 sec, representing 57% of the motor population, while a slower rate of motors leaving the bud yielded a half-time of loss of 32.5 ± 13.7 sec, representing 36% of the population (n= 12). Approximately 10% of the total motor population in the bud remained immobile. An analysis of these rates is complicated by the fact that the mother cell could not be continually bleached, so some molecules could leave the bud and re-enter without being bleached. Nevertheless, an examination of individual time points shows that fluorescence is retained longer at the bud tip compared to the bud cytoplasm (Figure 2.4e). The motors at the bud tip (which the data presented in Figure 2.3 suggests are still bound to secretory vesicles at sites of growth) therefore correspond to the slower rate of loss while the faster rate corresponds to motors in the bud cytoplasm. These two fractions are also close to the steady-state data as approximately 45% of all motors in the bud reside at the bud tip, which is the sum of the immobile and tip localized populations. A similar analysis of GFP-Sec4 found only one rate

contributing to the loss of the Rab protein from the bud during a FLIP experiment, with a half-time of loss of 92.7 ± 39.1 sec (n=10; Figures 2.4g-h).

I next examined the recycling dynamics of the constitutively active Myo2-13-GFP mutant. Consistent with its constitutively active nature, Myo2-13-GFP is hyperpolarized to the bud tip, with about 70% of all motors residing in the bud, compared with only 35% for wildtype cells (Figure 2.5a). FLIP analysis at the permissive temperature shows that Myo2-13-GFP has a slight recycling defect with the tip-localized population having a half-time of loss of 46.3 ± 22.0 seconds (n= 13). After a 5 minute shift to the restrictive temperature it displays a greater recycling defect, with the tip-localized population having a half-time of loss of 99.5 ± 26.1 seconds (n= 16; Figures 2.5b-c). This tip-localized population also increases significantly from 53% to 66% of the total population, while there was no change in the fraction of motors in the 'immobile' population. These results show that a constitutively active motor gets trapped at sites of growth, indicating that wildtype Myo2p must be deactivated after release from cargo to allow it to recycle efficiently.

Myo2p recycling from vesicles requires exocyst function but not membrane fusion

The data show that Myo2p motors and secretory vesicles are intimately coupled until secretory vesicles reach sites of growth and that motors must deactivate to recycle efficiently. To dissect the steps necessary for efficient recycling of Myo2p from vesicles at sites of growth, I examined the behavior of Myo2-3xGFP in a panel of conditional mutants affecting events at the bud tip. Secretory mutants *sec6-4* and *sec15-1* are temperature-sensitive alleles of core exocyst complex proteins. At the permissive temperature, secretion is normal; upon shifting to the restrictive temperature, the exocyst complex disassembles and secretory vesicles accumulate in

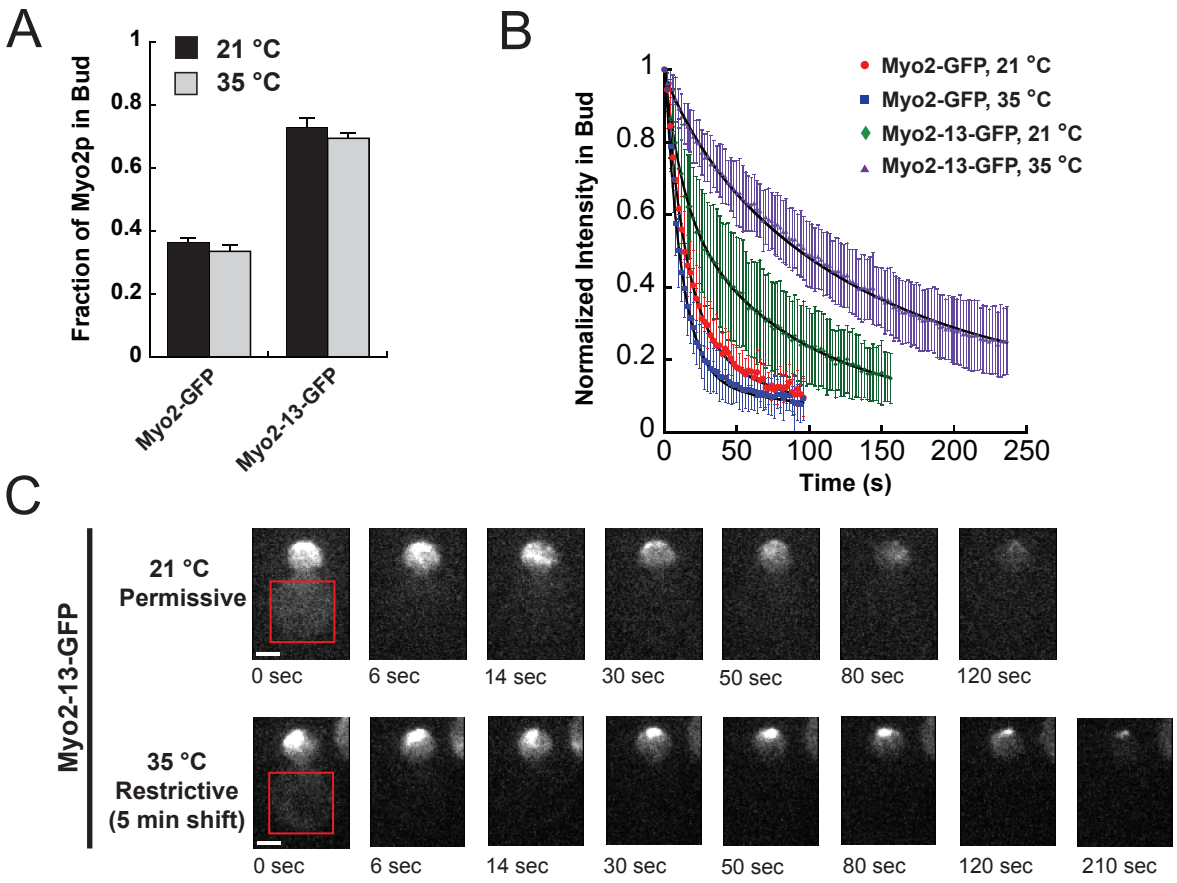

Figure 2.5. Myo2p must be deactivated for efficient recycling back into the mother cell.

A. Fraction of Myo2-GFP and Myo2-13-GFP in the bud at 21°C and 35°C (5 min shift). Error bars represent standard deviation.
B. Normalized Myo2-GFP and Myo2-13-GFP intensity in the bud during the FLIP experiment at indicated temperature. Error bars are standard deviation of n= 12 (wildtype), 13 (mutant permissive), and 16 (mutant restrictive) cells, respectively.
C. Still-frame micrographs of Myo2-13-GFP FLIP experiment at 21°C and 35°C. Boxed region indicates region bleached repeatedly. Scale bar, 2 μm.

the bud (Figures 2.6a-d; Salminen and Novick, 1987; Govindan et al., 1995; TerBush and Novick, 1995). Similarly, the *sec9-4* and *sec9-7* conditional t-SNARE mutants display relatively normal secretion at the permissive temperature; shifting to the restrictive temperature impairs the essential SNARE function in fusion and also causes the accumulation of secretory vesicles together with the exocyst complex (Figures 2.6a-d; Rossi et al., 1997; Katz et al., 1998). I reasoned that if Myo2p release from secretory vesicles required exocyst tethering and/or membrane fusion, there would be an increase in the amount of Myo2-3xGFP found in the bud of the relevant mutant during short shifts to the restrictive temperature due to a buildup of the motor with the vesicles.

Whole cell projection images of live wildtype and mutant cells showed that about 33% of all Myo2-3xGFP is present in the bud of medium-budded cells at the permissive temperature of all strains tested. However, there was a small but significant increase in the fraction of Myo2-3xGFP in the buds of *sec6-4* and *sec15-1* exocyst mutants following a shift to the restrictive temperature (Figure 2.6e) while there was no significant change in the *sec9-4* and *sec9-7* t-SNARE mutants (Figure 2.6f) There was also a small but significant increase in the amount of GFP-Sec4 in all mutants when shifted to the restrictive temperature as expected (Figures 2.6g-h). Critically, these results imply that recycling of motors is delayed when exocyst tethering is inhibited, but not when SNARE function is inhibited.

To address how the recycling dynamics of Myo2p change when essential exocyst tethering or SNARE functions are perturbed, I performed FLIP experiments with Myo2-GFP in wildtype, *sec6-4*, *sec15-1*, *sec9-4* and *sec9-7* strains at both the permissive and restrictive temperatures. In the *sec6-4* and *sec15-1* exocyst mutants, the vesicle-associated population of Myo2-GFP took 2 to 3-fold longer to leave the bud at the restrictive temperature (Figures 2.6i-j).

Figure 2.6. Efficient Myo2-GFP recycling from the bud requires exocyst complex tethering, but not SNARE action.

A. Quantification of Sec15-GFP polarization in wildtype, *sec6-4,* and *sec9-4* cells at the permissive and restrictive temperatures. 200 small and medium budded cells were scored for each strain and condition to determine fraction of polarization. Shifted to restrictive temperature for 15 minutes.
B. Representative images showing polarization of Sec15-GFP from (A).
C. Quantification of Sec6p polarization in wildtype, *sec6-4*, and *sec9-4* cells at the permissive and restrictive temperatures. 200 small and medium budded cells were scored for each strain and condition to determine fraction of polarization. Shifted to restrictive temperature for 15 minutes.
D. Representative images showing polarization of Sec6p from (A)
E. Fraction of Myo2-3xGFP in the bud from whole cell projections for exocyst complex conditional mutants. Temperature shifts were conducted for 15 minutes. *, $p<0.05$ significance.
F. Fraction of Myo2-3xGFP in the bud from whole cell projections for t-SNARE conditional mutants. Temperature shifts were conducted for 15 minutes.
G. Fraction of GFP-Sec4 in the bud from whole cell projections for exocyst complex conditional mutants. Temperature shifts were conducted for 15 minutes. *, $p<0.05$ significance.
H. Fraction of GFP-Sec4 in the bud from whole cell projections for t-SNARE conditional mutants. Temperature shifts were conducted for 15 minutes. *, $p<0.05$ significance.
I. Normalized Myo2-GFP intensity in the bud of *sec6-4* cells during a FLIP experiment at 21 °C and 35 °C. Error bars represent standard deviation of n= 10 cells.
J. Normalized Myo2-GFP intensity in the bud of *sec15-1* cells during a FLIP experiment at 21 °C and 35 °C. Error bars represent standard deviation of n= 11 and 15 cells, respectively.
K. Normalized Myo2-GFP intensity in the bud of *sec9-4* cells during a FLIP experiment at 21 °C and the restrictive 35 °C temperature. Error bars represent standard deviation of n= 12 cells (permissive), 16 cells (restrictive).
L. Normalized Myo2-GFP intensity in the bud of *sec9-7* cells during a FLIP experiment at 21 °C and the restrictive 35 °C temperature. Error bars represent standard deviation of n= 12 cells (permissive), 11 cells (restrictive).

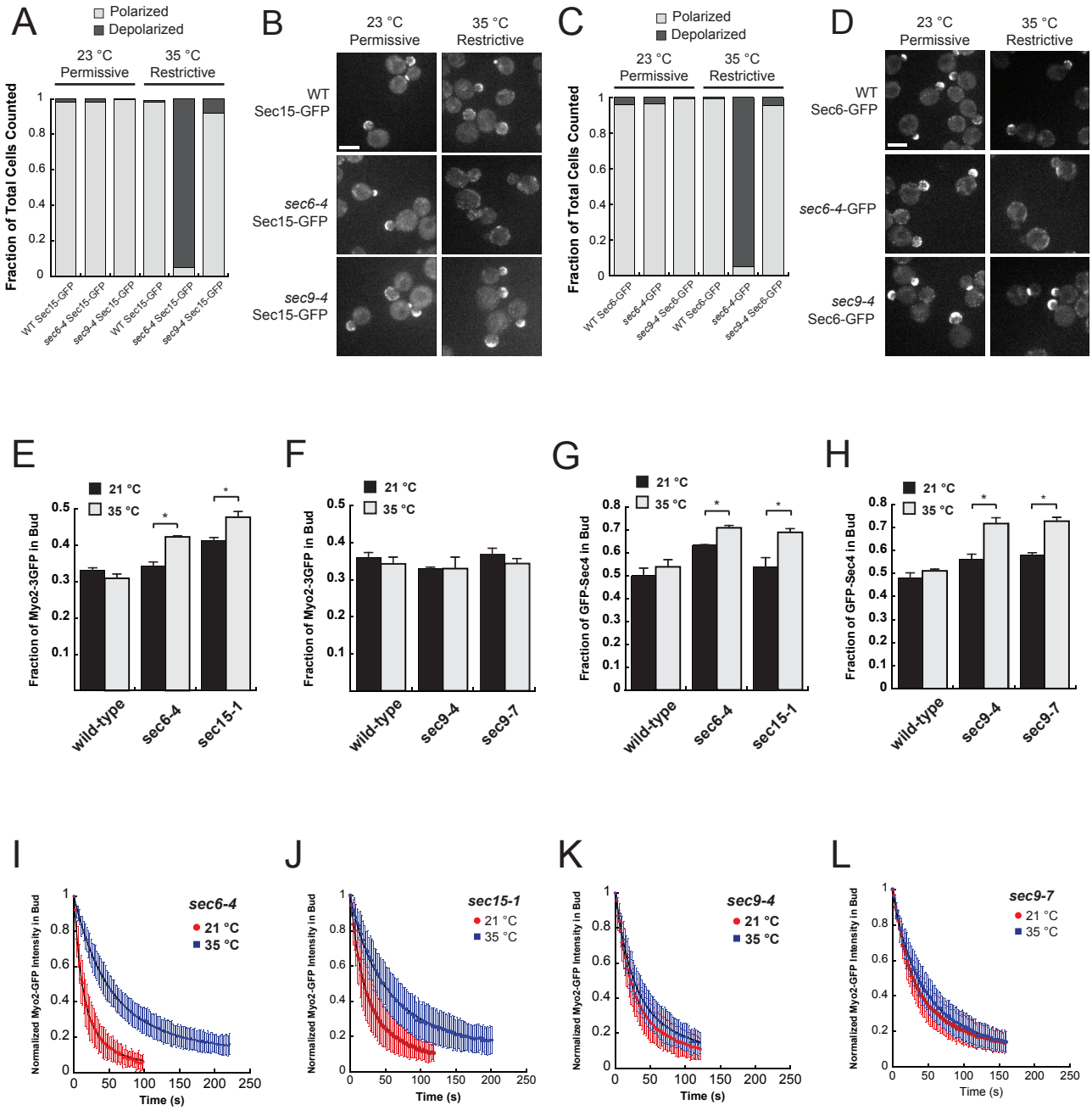

(see preceding page for Figure 2.6 caption)

This implies that efficient Myo2p recycling from sites of growth requires vesicle tethering to the plasma membrane through the exocyst complex. However, no significant difference was observed in the rates and half-times of loss of vesicle-bound Myo2-GFP leaving the bud in the *sec9-4* or *sec9-7* t-SNARE mutants at either temperature (Figures 2.6k-l). This shows that SNARE function is not required for efficient Myo2p recycling.

Delaying hydrolysis of Sec4-GTP slows Myo2p recycling

I next sought to explore which factors might contribute to efficient recycling of Myo2p motors from sites of growth. The Rab GTPase Sec4p coordinates many aspects of secretory vesicle transport, docking, and fusion, as its known effectors include Myo2p (Santiago-Tirado et al., 2011), the exocyst component Sec15p (Guo et al., 1999), the *lgl* homologs Sro7/77p (Gangar et al., 2005), and the Sec1p-targeting factor Mso1p (Weber-Boyvat et al., 2011). To explore if Sec4-GTP hydrolysis influences Myo2p recycling from growth sites, I examined the effect of delaying hydrolysis by deleting one or both of the bud-cortex localized, redundant GTPase Activating Proteins (GAPs) for Sec4p, Msb3p/Msb4p (Gao et al., 2003).

In FLIP experiments, no significant difference in the half-times of loss of Myo2-GFP from the bud were found between wildtype and the *msb3*Δ or *msb4*Δ single GAP mutants (Figures 2.7a-b). However, when both GAP proteins were deleted (*msb3*Δ *msb4*Δ), Myo2-GFP half-times of loss from bud of the vesicle-associated fraction increased 2 to 3-fold. This increase was not due to an increase in the immobile pool of motors and was concurrent with a build up of GFP-Sec4 and Myo2-3xGFP in the bud of the *msb3*Δ *msb4*Δ cells (Figures 2.7c-e); this suggests that delaying GTP hydrolysis results in both an accumulation of secretory vesicles and kinetic delay in motor recycling.

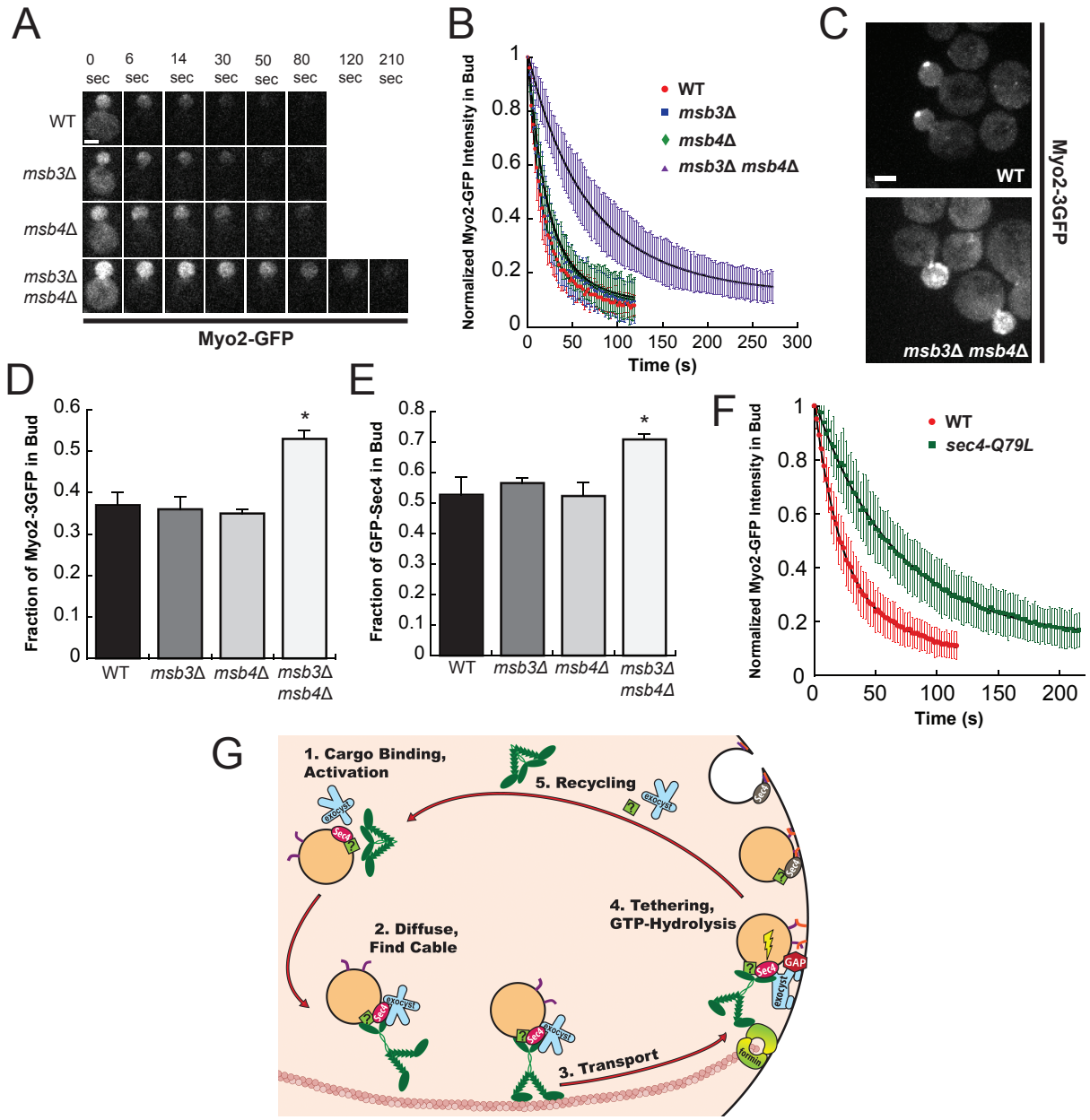

Figure 2.7. Deletion of Sec4-GAPs Msb4p and Msb4p or using the constitutively active *sec4-Q79L* mutant significantly delays Myo2-GFP recycling.

A. Representative summed projection micrographs of Myo2-GFP in bud during FLIP experiment for wildtype, *msb3*Δ, *msb4*Δ, and *msb3*Δ *msb4*Δ cells. Scale bar, 2 μm.
B. Normalized Myo2-GFP intensity in the bud of wildtype, *msb3*Δ, *msb4*Δ, and *msb3*Δ *msb4*Δ cells during FLIP experiment. Error bars represent standard deviation of n= 11 cells for each strain.
C. Maximum projection micrographs of Myo2-3GFP in wildtype and *msb3*Δ *msb4*Δ cells. Scale bar represents 2 μm.
D. Fraction of Myo2-3GFP in the bud from whole cell projections for wildtype, *msb3*Δ, *msb4*Δ, and *msb3*Δ *msb4*Δ cells. Error bars represent standard deviation. *, $p<0.05$ significance.
E. Fraction of GFP-Sec4 in the bud from whole cell projections for wildtype, *msb3*Δ, *msb4*Δ, and *msb3*Δ *msb4*Δ cells. Error bars represent standard deviation. *, $p<0.05$ significance.
F. Normalized Myo2-GFP intensity in the bud of wildtype and *sec4-Q79L* during FLIP experiment. Experiment done following 15 minute shift to the cold sensitive temperature of 14 °C. Error bars represent standard deviation of n= 13 cells for each strain.
G. Model of Myo2p activation, transport, and release from secretory cargo.

To examine the role of Sec4-GTP hydrolysis in another manner, I replaced the chromosomal copy of *SEC4* with the *sec4-Q79L* constitutively active mutant allele in which GTP hydrolysis is delayed. Previous analysis of the *sec4-Q79L* allele shows that it confers a cold sensitive phenotype, and *in vitro* Sec4-Q79L has 30% reduced hydrolysis activity compared to wildtype Sec4p (Walworth et al., 1992). FLIP experiments conducted between strains harboring wildtype *SEC4* and the *sec4-Q79L* mutant at the impaired temperature of 14 °C revealed that Myo2-GFP recycling from sites of growth in the bud was delayed similarly to the double *msb3Δ msb4Δ* GAP deletion mutant (Figure 2.7f). Thus, when GTP hydrolysis of Sec4p is delayed, exocytosis and the recycling of Myo2-GFP from sites of growth are also delayed.

DISCUSSION

Many studies of class-V myosins have focused on how they interact with their effectors and cargos. Missing from such analyses is the dynamic properties of the motor itself and how its dynamics is regulated at the molecular level. In this chapter, I have described the delivery cycle of a class-V myosin *in vivo*; a model summarizing the results is shown in Figure 2.7g. Myo2p motors are activated from an inactive pool through binding to a competent secretory vesicle and then the vesicle, in complex with ~10 motors, is shuttled to sites of growth. By quantitating molecules at the bud tip, I showed that docked vesicles retain a full complement of motors. Further, vesicle tethering by the exocyst complex and Sec4-GTP hydrolysis are required for efficient Myo2p recycling back into the mother cell, but efficient recycling does not require vesicle fusion. Since the myosin-V family of molecular motors is highly conserved, as are the Rab proteins they interact with and the exocyst complex that regulates their cargo dissociation, these findings are likely widely applicable.

Previous data has shown that in *myo2* conditional tail mutants shifted to the restrictive temperature, Myo2p polarizes to sites of growth without secretory cargo (Schott et al., 1999). However, wildtype Myo2-3xGFP fails to polarize when competent secretory cargo is not available, thereby demonstrating that motors are activated by binding cargo. Importantly, all *myo2* tail alleles examined that have conditionally lost their ability to transport secretory vesicles at the restrictive temperature remain polarized (Schott et al., 1999; this study), suggesting that the inability to bind secretory vesicles correlates with Myo2p activation. Consistent with this model, constitutively active Myo2-13p hyperpolarizes to sites of growth and is recycled from the bud incredibly slowly at the restrictive temperature. Thus, wildtype Myo2p needs to be activated by cargo, and deactivated upon cargo delivery.

How is Myo2p activated by secretory vesicles? *In vitro* studies with mammalian myosin-V have suggested that the motor undergoes autoinhibition through an interaction of the ATPase-containing head domain and the cargo-binding tail domain, and key residues in the tail mediating this regulation have been identified (Liu et al., 2006; Thirumurugan et al., 2006; Li et al., 2008). An attractive model is that autoinhibited Myo2p binds to a protein on the vesicle surface, thereby activating it only in the presence of competent secretory vesicles. Known interaction partners on vesicles include the exocyst component Sec15p, the Rab Sec4p, and an unidentified component dependent on PI4P (Santiago-Tirado et al., 2011; Jin et al., 2011). A recent study found that the Sec15p binding site on the Myo2p tail overlaps with the conserved residues believed to be involved in autoinhibition (Jin et al., 2011). However, the observation that secretory vesicles are still transported to sites of growth in the *sec6-4* and *sec15-1* mutants (Salminen and Novick, 1987; Govindan et al., 1995), where the exocyst is disassembled and Sec15p is depolarized (Terbush et al. 1995; Figure 2.6), makes it unlikely that Sec15p is critical

for Myo2p activation. A more likely regulator of the activation process is the Rab Sec4p. Evidence supporting this includes (1) the finding that Myo2p is not activated at the restrictive temperature in the *sec4-8* strain, (2) motors with the Y1415R mutation that are unable to bind to Sec4p are depolarized, and (3) Myo2p deactivation is slowed in mutants where Sec4-GTP hydrolysis is delayed. In addition, this work shows that Sec4p is a more critical activator of Myo2p than the unidentified component dependent on PI4P, as motors are still polarized in *pik1* kinase mutants deficient in PI4P creation at the Golgi (Santiago-Tirado et al., 2011). Evidence that Myo2p undergoes an autoinhibitory interaction is presented in Chapter 3, and the work presented in this chapter strongly argues that binding to Sec4p relieves the autoinhibition.

The association of ~10 motors with a transporting secretory vesicle raises the question of how many motors are needed and why there are so many. Longstanding work postulated that Myo2p was not a processive motor, and required at least 5 motors bound to cargo to ensure processive movement (Reck-Peterson et al., 2001). However, it was recently shown that Myo2p become processive on tropomyosin-containing actin cables (Hodges et al., 2012). It would appear that this *in vitro* result holds true *in vivo*, since I showed that constitutively active motors such as *myo2-13* can still move down actin cables toward the bud tip. This observation makes it likely that long run-lengths along actin cables can be achieved in the cell, but perhaps several motors are needed to allow for long-range transport of big cargoes. Gross et al. (2002) found 65 MyoV motors on aggregated *Xenopus* melanosomes and 88 when dispersed; perhaps larger cargoes require more motors to generate the force needed for transport. It would be interesting to determine if motor number increases with cargo size in yeast (peroxisomes, vacuoles, mitochondria, etc.).

I also found about 9 myosin-V motors on vesicles freely diffusing around the cytoplasm. This suggests that the rate-limiting step for transport is engaging an actin cable in the cytoplasm. Further, the normal distribution of the number of motors on this class of vesicles suggests that motors must be acquired rapidly; if they were acquired slowly one would expect to see more vesicles with smaller numbers of motors. Since there were also 75 molecules of Sec4p per transported vesicle, there are more than enough for the two Myo2p tail domains to bind, as might be expected. I should note here that the number of Cse4p molecules at anaphase centromere clusters has been estimated several times over the last 5 years; the number I used from Lawrimore et al. (2011) suggests ~80, but chIP data and a recent publication suggest it could be much lower at ~32 (Shivaraju et al., 2012). Lawrimore et al. (2011) cleverly showed that proteins bound to centromeric DNA are often undersampled in chIP experiments, but if a consensus in the field is ever achieved these numbers should be easy to scale.

When secretory vesicles arrive at sites of growth, they accumulate there because exocytosis is a kinetically slower process than transport. The docked vesicles, as marked by Sec4p, retain a full complement of Myo2p; this suggests that exocytosis is coupled with motor release and deactivation. This model derives from the observation that a constitutively active motor resides at the bud tip much longer than wildtype Myo2. I next investigated how Myo2p might be deactivated and released. Motor recycling back into the mother cell was significantly delayed when tethering via the exocyst complex was disrupted in the *sec6* and *sec15* mutants. Further, there was an increase in total Myo2p and Sec4p found in the bud of these mutants, consistent with vesicle accumulation and maintenance of the Sec4-GTP/Myo2p interaction. Analysis of t-SNARE *sec9* conditional mutants did not show a kinetic delay in the recycling of Myo2p, nor was there a buildup of total Myo2p in the bud compared to the non-permissive

condition. Critically, these results show that efficient Myo2p recycling requires exocyst complex tethering but is independent of the membrane fusion step requiring Sec9p. Further experiments demonstrate that delaying Sec4-GTP hydrolysis by deleting the redundant Sec4p GAP proteins Msb3/4p or using the constitutively active *sec4-Q79L* mutant also slows motor recycling, indicating that motor deactivation is related to Sec4-GTP hydrolysis.

The interpretation of these findings is not straightforward as there are at least four effectors of Sec4-GTP in the bud tip: Myo2p (Santiago-Tirado et al., 2011), the exocyst component Sec15p (Guo et al., 1999), the Sec1p-tartgeting factor Mso1p (Weber-Boyvat et al., 2011), and the Lgl homolog Sro7/77p that interacts with Sec9p and is involved in v-/t-SNARE fusion (Gangar et al., 2005). The functional relationships between these different effectors are not entirely known, especially if there is a temporal order in which Sec4-GTP interacts with its various effectors at the bud tip. Nevertheless, my results clearly show that motor recycling is influenced by the presence of Sec4-GTP and coordinated with events at the bud tip.

With this data, I will add Myo2p release to the timeline of events presented in Chapter 1. First, Myo2p delivers vesicles to the bud tip through its interaction with Sec4-GTP, and a component dependent on PI4P. Myo2p is also integrated with the vesicle-associated exocyst complex through its interaction with Sec15p (Jin et al., 2011). Second, the vesicle-transported and cortex-localized components of the exocyst tether the vesicle, together with Myo2p, at the cortex. The presence of Sec4-GTP and/or Myo2p stimulates Sro7/77p to displace Sec9p, priming the interaction between Sso1p and the v-SNARE Snc1/2p and perhaps recruiting Sec1p to the SNARE complex through its Mso1p interaction. Next, Sec4-GTP hydrolysis is activated by its GAP, Msb3/4p, resulting in release of Myo2p and Sec15p from Sec4p and eventual downstream fusion. An attractive possibility for coordinating this process would be if the assembled exocyst

complex stimulates the GAP activity of Msb3/4p. This model is more fully developed in Chapter 4 with results from single-vesicle tracking experiments.

It is interesting to note that defects in exocytosis result in the accumulation of hundreds of secretory vesicles as seen by electron microscopy, yet there is only about a 1.4-fold accumulation of Sec4 and Myo2 in conditional exocyst mutants. This implies that vesicles have a window of opportunity to fuse, and if they miss it, they either have to recruit fresh Sec4-GTP, or never fuse. Some evidence related to this is presented in Chapter 4, as vesicles in certain mutants (such as constitutively active *sec4-Q79L*) were observed 'falling off' the cortex after tethering. This implies an 'order of operations' exists with the fusion machinery that must be followed. How timing of events at the bud tip is determined will be a critical issue for future studies, but this data provides an outline for how Myo2p release is coordinated with events at sites of growth.

Post-Golgi secretory trafficking proteins are well conserved in higher eukaryotes, and it is likely that a closely related mechanism for activation and release of Myo2p seen in yeast exists for myosin-Vs in mammalian cells. The tail domain of myosin-Va was recently found to interact with the Sec4p homolog Rab3a, which resides on synaptic vesicles in neurons (Wöllert et al., 2011). This interaction allows for the mobilization of AMPA receptors after long-term potentiation and proper activation and release of the motor would be of obvious importance. Similarly, Glut4-positive vesicles are transported to the plasma membrane in muscle cells upon insulin stimulation through the interaction of myosin-Vb and the close Sec4p homolog Rab8a (Ishikura and Klip, 2008). Since the exocyst is likely linked to Rab8 through its interaction with Sec15 (Wu, S. et al., 2005), the same basic framework of tethering and release of the motor through Rab-GTP hydrolysis is likely to apply here as well. Further studies in mammalian cells

may show conservation of motor activation by competent secretory vesicles and release following tethering and Rab-GTP hydrolysis.

REFERENCES

Boyd, C., Hughes, T., Pypaert, M., and Novick, P. (2004). Vesicles carry most exocyst subunits to exocytic sites marked by the remaining two subunits, Sec3p and Exo70p. J. Cell Biol. *167,* 889-901.

Donovan, K.W. and Bretscher, A. (2012). Myosin-V is activated by binding secretory cargo and released in coordination with Rab/exocyst function. Dev. Cell., *23*, 769-781.

Ferro-Novick, S., and Novick, P. (1993). The role of GTP-binding proteins in transport along the exocytic pathway. Annu. Rev. Cell Biol. *9,* 575-599.

Gangar, A., Rossi, G., Andreeva, A., Hales, R., and Brennwald, P. (2005). Structurally conserved interaction of Lgl family with SNAREs is critical to their cellular function. Current Biology *15,* 1136-1142.

Gao, X.D., Albert, S., Tcheperegine, S.E., Burd, C.G., Gallwitz, D., and Bi, E. (2003). The GAP activity of Msb3p and Msb4p for the Rab GTPase Sec4p is required for efficient exocytosis and actin organization. J. Cell Biol. *162,* 635-46.

Ghaemmaghami, S., Huh, W.K., Bower, K., Howson, R.W., Belle, A., Dephoure, N., O'Shea, E.K., and Weissman, J.S. (2003). Global analysis of protein expression in yeast. Nature *425,* 737-741.

Gietz, R.D., Schiestl, R.H., Willems, A.R., and Woods, R.A. (1995). Studies on the transformation of intact yeast cells by the LiAc/SS-DNA/PEG procedure. Yeast *11,* 355-360.

Govindan, B., Bowser, R., and Novick, P. (1995). The role of Myo2, a yeast class V myosin, in vesicular transport. J. Cell Biol. *128,* 1055-1068.

Gross, S.P., Tuma, M.C., Deacon, S.W., Serpinskaya, A.S., Reilein, A.R., and Gelfand, V.I. (2002). Interactions and regulation of molecular motors in *Xenopus* melanophores. JCB *156*, 855-865.

Guo, W., Roth, D., Walch-Solimena, C., and Novick, P. (1999). The exocyst is an effector for Sec4p, targeting secretory vesicles to sites of exocytosis. EMBO J. *18,* 1071-80.

Hodges, A., Krementsova, E., Bookwalter, C., Fagnant, P., Sladewski, T., and Trybus, K. (2012). Tropomyosin is essential for processive movement of a class V myosin from budding yeast. Curr Biol. *22*, 1-7.

Ishikawa, K., Catlett, N.L., Novak, J.L., Tang, F., Nau, J.J., and Weisman, L.S. (2003). Identification of an organelle-specific myosin V receptor. J. Cell Biol. *160,* 887-897.

Ishikura, S., and Klip, A. (2008). Muscle cells engage Rab8A and myosin Vb in insulin-dependent GLUT4 translocation. Am. J Physiol. Cell Physiol. *295,* C1016-C1025.

Jin, Y., Sultana, A., Gandhi, P., Franklin, E., Hamamoto, S., Khan, A.R., Munson, M.,

Schekman, R., and Weisman, L.S. (2011). Myosin V Transports Secretory Vesicles via a Rab GTPase Cascade and Interaction with the Exocyst Complex. Dev. Cell *21,* 1156-1170.

Joglekar, A.P., Bouck, D., Finley, K., Liu, X., Wan, Y., Berman, J., He, X., Salmon, E., and Bloom, K.S. (2008). Molecular architecture of the kinetochore-microtubule attachment site is conserved between point and regional centromeres. J. Cell Biol. *181,* 587.

Kaiser, C.A., and Schekman, R. (1990). Distinct sets of SEC genes govern transport vesicle formation and fusion early in the secretory pathway. Cell *61,* 723-733.

Kaksonen, M., Sun, Y., and Drubin, D.G. (2003). A pathway for association of receptors, adaptors, and actin during endocytic internalization. Cell *115,* 475-487.

Katz, L., Hanson, P.I., Heuser, J.E., and Brennwald, P. (1998). Genetic and morphological analyses reveal a critical interaction between the C-termini of two SNARE proteins and a parallel four helical arrangement for the exocytic SNARE complex. EMBO J. *17,* 6200-6209.

Lawrimore, K., Bloom, K.S., and Salmon, E.D. (2011). Point centromeres contain more than a single centromer-specific Cse4 (CENP-A) nucleosome. J. Cell Biol. *195*, 573-582.

Li, X., Jung, H.S., Wang, Q., Ikebe, R., and Craig, R. (2008). The globular tail domain puts on the brake to stop the ATPase cycle of myosin Va. Prot. Natl. Acad. Sci. USA *105*, 1140-1145.

Lipatova, Z., Tokarev, A.A., Jin, Y., Mulholland, J., Weisman, L.S., and Segev, N. (2008). Direct interaction between a myosin V motor and the Rab GTPases Ypt31/32 is required for polarized secretion. Mol. Biol. Cell *19,* 4177-87.

Liu, W., Santiago-Tirado, F.H., and Bretscher, A. (2012). Yeast formin Bni1p has multiple localization regions that function in polarized growth and spindle orientation. Mol. Biol. Cell *23*, 412-422.

Liu, J., Taylor, D.W., Krementsova, E.B., and Trybus, K. (2006). Three-dimensional structure of the myosin V inhibited state by cryoelectron tomography. Nature *442*, 208-211.

Longtine, M.S., McKenzie, A., Demarini, D.J., Shah, N.G., Wach, A., Brachat, A., Philippsen, P., and Pringle, J.R. (1998). Additional modules for versatile and economical PCR-based gene deletion and modification in Saccharomyces cerevisiae. Yeast *14,* 953-961.

Mulholland, J., Preuss, D., Moon, A., Wong, A., Drubin, D., and Botstein, D. (1994). Ultrastructure of the yeast actin cytoskeleton and its association with the plasma membrane. J. Cell Biol. *125,* 381-391.

Müller, T., Hess, M.W., Schiefermeier, N., Pfaller, K., Ebner, H.L., Heinz-Erian, P., Ponstingl, H., Partsch, J., Röllinghoff, B., and Köhler, H. (2008). MYO5B mutations cause microvillus inclusion disease and disrupt epithelial cell polarity. Nat. Genet. *40,* 1163-1165.

Pashkova, N., Jin, Y., Ramaswamy, S., and Weisman, L.S. (2006). Structural basis for myosin V discrimination between distinct cargoes. EMBO J. *25*, 693-700.

Prescianotto-Baschong, C., and Riezman, H. (1998). Morphology of the yeast endocytic pathway. Mol. Biol. Cell *9,* 173-189.

Protopopov, V., Govindan, B., Novick, P., and Gerst, J.E. (1993). Homologs of the synaptobrevin/VAMP family of synaptic vesicle proteins function on the late secretory pathway in S. cerevisiae. Cell *74,* 855-861.

Rexach, M.F., and Schekman, R.W. (1991). Distinct biochemical requirements for the budding, targeting, and fusion of ER-derived transport vesicles. J. Cell Biol. *114*, 219–229.

Rossanese, O.W., Reinke, C.A., Bevis, B.J., Hammond, A.T., Sears, I.B., O'Connor, J., and Glick, B.S. (2001). A role for actin, Cdc1p, and Myo2p in the inheritance of late Golgi elements in Saccharomyces cerevisiae. J. Cell Biol. *153*, 47-62.

Rossi, G., Salminen, A., Rice, L.M., Brünger, A.T., and Brennwald, P. (1997). Analysis of a yeast SNARE complex reveals remarkable similarity to the neuronal SNARE complex and a novel function for the C terminus of the SNAP-25 homolog, Sec9. J. Biol. Chem. *272,* 16610-16617.

Salminen, A., and Novick, P.J. (1987). A ras-like protein is required for a post-Golgi event in yeast secretion. Cell *49,* 527-538.

Salmon, E., Leslie, R., Saxton, W., Karow, M., and McIntosh, J. (1984). Spindle microtubule dynamics in sea urchin embryos: analysis using a fluorescein-labeled tubulin and measurements of fluorescence redistribution after laser photobleaching. J. Cell Biol. *99,* 2165-2174.

Santiago-Tirado, F.H., Legesse-Miller, A., Schott, D., and Bretscher, A. (2011). PI4P and Rab inputs collaborate in myosin-V-dependent transport of secretory compartments in yeast. Dev. Cell *20,* 47-59.

Schott, D., Ho, J., Pruyne, D., and Bretscher, A. (1999). The COOH-terminal domain of Myo2p, a yeast myosin V, has a direct role in secretory vesicle targeting. J. Cell Biol. *147,* 791-808.

Schott, D.H., Collins, R.N., and Bretscher, A. (2002). Secretory vesicle transport velocity in living cells depends on the myosin-V lever arm length. J. Cell Biol. *156,* 35-40.

Sherman, F. (2002). Getting started with yeast. Meth. Enzymol. *350,* 3-41.

Shivaraju M, Unruh JR, Slaughter BD, Mattingly M, Berman J, Gerton JL (2012). Cell-cycle-coupled structural oscillation of centromeric nucleosomes in yeast. Cell *150*, 304–316.

Stevens R and Davis T. 1998. Mlc1p is a light chain for the unconventional myosin Myo2p in Saccharomyces cerevisiae. J. Cell Biol. *142*: 711.

Tang, F., Kauffman, E.J., Novak, J.L., Nau, J.J., Catlett, N.L., and Weisman, L.S. (2003). Regulated degradation of a class V myosin receptor directs movement of the yeast vacuole. Nature *422,* 87-92.

TerBush, D.R., and Novick, P. (1995). Sec6, Sec8, and Sec15 are components of a multisubunit complex which localizes to small bud tips in Saccharomyces cerevisiae. J. Cell Biol. *130,* 299-312.

Thirumurugan, K., Sakamoto, T., and Hammer III, J. (2006). The cargo-binding domain regulates structure and activity of myosin 5. Nature *442*, 212-215.

Wagner, W., Brenowitz, S.D., and Hammer III, J.A. (2010). Myosin-Va transports the endoplasmic reticulum into the dendritic spines of Purkinje neurons. Nat. Cell Biol. *13,* 40-48.

Walworth, N.C., Brennwald, P., Kabcenell, A., Garrett, M., and Novick, P. (1992). Hydrolysis of GTP by Sec4 protein plays an important role in vesicular transport and is stimulated by a GTPase-activating protein in Saccharomyces cerevisiae. Mol. Cell. Biol. *12,* 2017-2028.

Weber-Boyvat, M., Aro, N., Chernov, K.G., Nyman, T., and Jäntti, J. (2011). Sec1p and Mso1p C-terminal tails cooperate with the SNAREs and Sec4p in polarized exocytosis. Mol. Biol. Cell *22,* 230-244.

Wöllert, T., Patel, A., Lee, Y.L., Provance, D.W., Vought, V.E., Cosgrove, M.S., Mercer, J.A., and Langford, G.M. (2011). Myosin5a tail associates directly with Rab3A-containing compartments in neurons. J. Biol. Chem. *286,* 14352-14361.

Wu, J-Q., and Pollard, T.D. (2005). Counting cytokinesis proteins globally and locally in fission yeast. Science *310*, 310-314.

Wu, S., Mehta, S.Q., Pichaud, F., Bellen, H.J., and Quiocho, F.A. (2005). Sec15 interacts with Rab11 via a novel domain and affects Rab11 localization in vivo. Nat. Struct. Mol. Biol. *12*, 879–885.

CHAPTER 3

ESSENTIAL FUNCTIONS OF YEAST MYOSIN-V ARE IMPAIRED WHEN ITS REGULATORY HEAD-TAIL INTERACTION IS DISRUPTED

OVERVIEW

In the second chapter, I showed that a specific conditional allele, Myo2-13-GFP, is hyperactive and remains trapped at sites of growth for 3-4 fold longer than wildtype motors. From this, I reasoned that Myo2p must undergo a deactivation event to efficiently recycle from sites of growth. The identity of this deactivation event was unknown though there were numerous clues from vertebrate Myosin-V work. One potential avenue for inactivation was through a post-translational modification, such as phosphorylation. Phosphorylation of *Xenopus* MyoVa at residue S1650 plays a role in the regulated binding to membranes, and when removed causes the motor to dissociate from organelles; it is conceivable then that such an event could deactivate the motor (Karcher, 2001). While our lab showed that Myo2p is phosphorylated at several different residues, mutating them had no significant effect on the phenotype of the motor, the growth of cells, or cargo transport (Legesse-Miller et al., 2006).

A more attractive hypothesis is through the interaction of the head and tail domains, as has been shown for mammalian myosin-V motors. The strongest data for this interaction comes from direct observation via electron microscopy and ATPase activity assays being modulated by the presence or absence of the tail domain. The precise residues proposed to be involved in the interaction have also been mapped, and include (in mouse MyoVa) D136/K1706/K1779 (Li et al., 2008). However, despite a decade of research on the inactive motor *in vitro*, to my knowledge no one has looked at the transport cycle of a misregulated motor and the effects a misregulated motor has on its cargoes *in vivo.* Still, Myo2p has not been shown to undergo

inactivation through a head-tail interaction despite several attempts. In this chapter, I will present evidence that Myo2p undergoes an autoinhibitory event similar to MyoV motors through an interaction between the head and tail. These misregulated motors have wide-ranging effects on cargo association and delivery, as well as with their own transport cycle.

MATERIALS AND METHODS

Yeast Strains and Molecular Biology Techniques

Cells were grown and selected for using standard molecular biology techniques. Yeast transformations were performed using lithium acetate-based methods (Gietz et al., 1995). Dilution assays were spotted on appropriate media by 1:10 serial dilutions and put at the appropriate temperature listed in the figure legends.

Homology and Structural Work

Protein sequences of myosin-V motors were obtained from the Uniprot database and aligned with JalView software using the TCoffeeWS algorithm. The location of the basic patch on the Myo2p tail was found using the Myo2p tail crystal structure (PDB accession code 2F6H). Since a structure of the Myo2p head domain does not exist, a homology model was generated by threading the protein primary sequence of the Myo2p head domain (residues 1-785) around the chicken MyoVa head structure (without nucleotide; PDB accession code 1OE9) using the SWISS-MODEL server (University of Basel, Basel, Switzerland). The location of the acidic patch of residues is roughly similar to those found in the MyoVa structure.

Generation of Charge Mutants

To generate the *myo2-3DR* and *myo2-3DA* mutants, constructs were created where residues D123/E135/E137 were mutated to either arginine or alanine and would integrate them at the N-terminus of the *MYO2* locus. Li Xu in our lab created the initial wildtype construct. The region -500 to +750 (containing the promoter and the first 750 nucleotides of *MYO2*) was amplified from gDNA of a wildtype BY4741 strain with XhoI and BamHI sites at the end of the forward and reverse primers (respectively) using the Expand High Fidelity PCR kit. (Roche, Basel, Switzerland) This was then digested overnight with the appropriate enzymes and ligated into a similarly cut pRS303 vector. A second homology region containing nucleotides -968 to -500 was similarly amplified and ligated between the BamHI and NotI sites of the vector. To mutate residues in the head proposed to be involved in the interaction to either alanine or arginine, the QuikChange II XL kit (Agilent Technologies, Santa Clara, CA) was used with primers designed to introduce the appropriate mutations. Sequencing was performed on all amplified products as well as after site-directed mutagenesis to ensure fidelity. Following digestion of the unique BamHI site in the vector, the vectors containing the mutations were transformed into cells and selected for using SD-His media. Sequencing genomic DNA of the resulting colonies ensured the mutations were present at the *myo2* locus.

A similar strategy was used to mutate the R1402/K1473 residues in the tail to either alanine or glutamic acid, using the pRS303-Myo2tail-3'UTR plasmid initially created by Daniel Schott in our lab (Schott et al., 1999). In the *myo2-3DR-REKE* strain, this plasmid with mutations was swapped into the pRS305 vector to allow for its selection when transformed into *myo2-3DR::HIS*.

Motor and Cargo Phenotypes

To observe motors in the cell, strains were tagged with the pRS306-cctail-GFP plasmid used in Chapter 2. In the case of strains where the mutations were in the tail, the appropriate mutations were transferred into this construct prior to integration into the mutant strain to ensure the mutations were not selected against. Sequencing of genomic DNA was performed to ensure the mutations remained. Imaging was performed on a CSU-X spinning disc confocal microscope system (Intelligent Imaging Innovations, Denver, CO, USA) using a DMI600B microscope (Leica, Wetzlar, Germany) and either the CoolSnap HQ2 camera (Photometrics, Tuscon, AZ, USA) or QuantEM EMCCD camera (Photometrics). The fraction of motors in the bud was calculated by using summed whole cell projections of fluorescently tagged motors as described in Chapter 2. FLIP experiments performed in this chapter were performed as described in Chapter 2, with 2 second imaging intervals and bleach events occurring every six seconds. Bleaching was done using the Vector control system (Intelligent Imaging Innovations, Denver, CO) with raster block size of '10' and laser power at 60%.

Cargo phenotypes in charge mutants were observed and scored by transforming in the appropriate cargo marker. Secretory vesicles were imaged using the chromosomally integrated GFP-Sec4 marker developed in Chapter 2. Cells were scored as 'polarized' or 'not polarized.' Mitochondria were observed by transforming in the pRS306-mitoRFPff-ura3d plasmid developed in our lab (Chernyakov et al., 2013) and scored as either having 'aggregated mitochondria' or 'normal mitochondria.' Note that inheritance of mitochondria was not scored, as most cells still had some mitochondria transported to the bud. Spindle orientation was observed by using a GFP-Tub1 construct (pAFS125-GFP-Tub1) integrated into the *TUB1* locus

after being cut with XbaI (Yin et al., 2000). Cells were scored as either 'oriented' (with the spindle axis passing through the bud neck) or 'not oriented.'

Bgl2 assay

The fraction of internal Bgl2p, a constitutively transported cargo commonly used to probe for secretion defects, was determined by separating internal and external fractions. Cells were grown in 5 mL YPD at 26 °C to log phase. A control strain, *sec6-4*, was transferred to 37 °C for one hour. Cells were then killed in 'Killing Buffer' (10mM NaF/ 10mM NaN_3 in 10 mM Tris pH 7.4) and washed on ice in Buffer B (1.2 M sorbitol, 25 mM K-P_i, 25 mM BME, pH 7.4) containing killing buffer. Cells were then spheroplasted to remove the cell wall with 100 μL of 25 μM Zymolase 100T in Buffer B at 37 °C for 1 hour. Following a low speed spin at 500 G, the supernatent containing the external fraction was then gently harvested from the pellet containing the internal fraction. The pellet was resuspended in an equal volume of 10 mM MOPS buffer as the supernatent and both fractions were boiled following addition of Laemmli sample buffer. Fractions of all strains were run out on SDS-PAGE gels, transferred by semi-dry methods, and probed using an anti-Bgl2 antibody serum "02" at 1:4000. The internal fraction was found by dividing the internal fraction by the total amount of Bgl2 in both fractions.

RESULTS

Charge complementation strongly suggests that Myo2p undergoes a head-tail interaction

Residues D136/K1706/K1779 in mouse MyoVa have been shown to participate in the head to tail interaction, likely via an ionic bond (Li et al., 2008). Additionally, there is some evidence from biochemical and structural work that D134 and D121 in the head also play a role

in such an interaction (Li et al., 2008; Nascimento et al., 2013). To investigate the conservation of these five residues predicted to form the ionic bond between head and tail, I aligned vertebrate myosin-V protein sequences with those of Myo2p and Myo4p from budding yeast. Alignment showed that three acidic residues in the head are conserved in yeast Myo2p and Myo4p, while two basic charges in the tail are conserved in Myo2p but not Myo4p (Figure 3.1a). Since Myo4p is believed to be a monomer that functions differently than other unconventional myosins, this is unsurprising. It is important to note that even though the exact residues may change, the charges (shown with acidic in red and basic in blue) remain the same.

On the basis of this conservation, I next determined that these residues are found clustered in patches on the surface of the head and tail (Figure 3.1b). Note that the structure of the Myo2p head domain has not actually been solved; I generated this model by threading the Myo2p sequence around a MyoVa head structure. However, the tail residues adopt the same orientation and position as in the solved MyoVa tail structure (not shown), suggesting that the location of these basic residues is highly conserved.

Previous attempts to detect a Myo2p head-tail interaction in at least two labs have failed; these include trying to detect an interaction by co-immunoprecipitation of head and tail fragments and through yeast two-hybrid. To determine if Myo2p undergoes such a head-tail interaction via these residues, I took a charge complementation approach. Basic residues were mutated to glutamic acid (E) while acidic residues were mutated to arginine (R). Thus, mutating the three acidic residues in the head of Myo2p generated the *myo2-3DR* allele (so named because all three residues in MyoVa are aspartic acid) while mutating the two basic residues in the tail generated the *myo2-REKE* allele. These two mutations were combined into the *myo2-3DR-REKE* allele, which effectively swaps the charges at sites on the head and the tail.

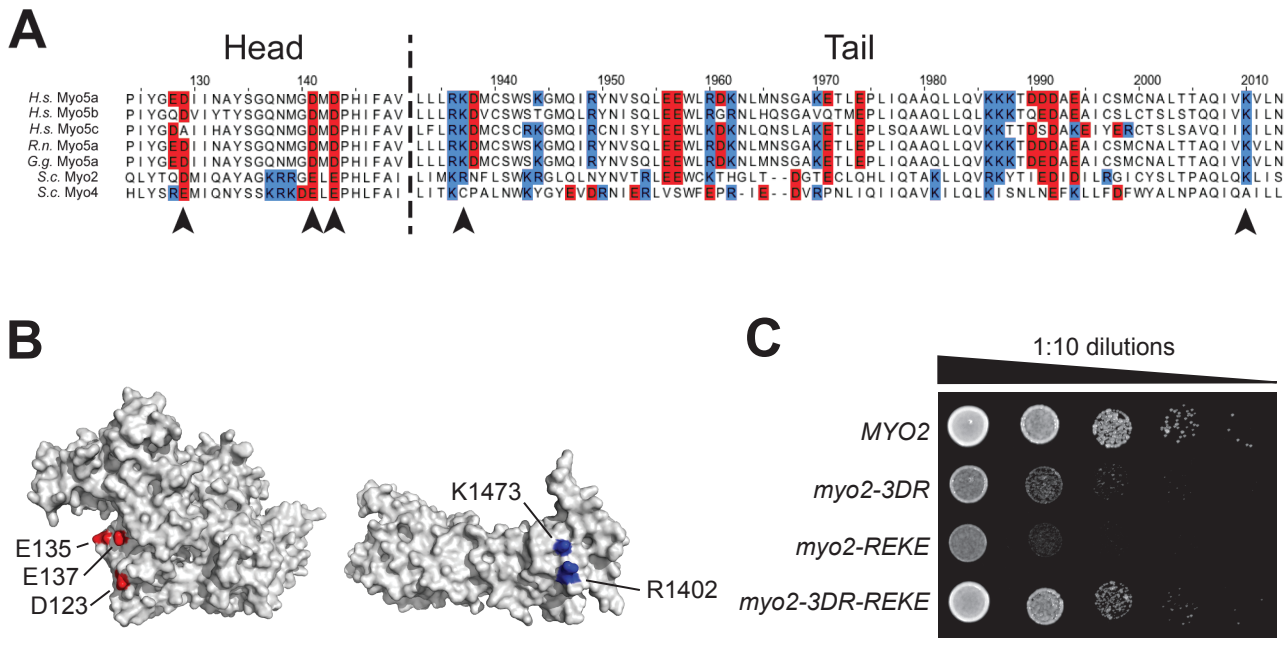

Figure 3.1. Charge complementation strongly suggests that Myo2p undergoes a head-tail interaction.

(A) Alignment of myosin-V motor protein sequences from vertebrates and budding yeast. Red-shaded letters are acidic residues while blue-shaded letters are basic residues. Numbers atop the sequence show the position along the consensus sequence. Arrowheads point to the three acidic residues and two basic residues that participate in the head-tail interaction in vertebrate myosins. *H.s.*, *Homo sapiens*; *R.n.*, *Rattus norvegicus; G.g., Gallus gallus; S.c. Saccharomyces cerevisiae*.

(B) Myo2p head and tail structures displaying the locations of the budding yeast residues from (A). Myo2p cargo binding tail, PDB accession number 2F6H. Head domain structural model was created from chicken MyoVa head (PDB #1OE9) as described in methods.

(C) 1:10 serial dilutions of wildtype and charge mutant strains. Spotted on YPD and incubated at 30 °C for 36 hours.

Mutant Myo2p alleles were spotted in 1:10 serial dilutions to assay for growth (Figure 3.1c). Both the *myo2-3DR* and *myo2-REKE* strains grew much slower than the wildtype control, suggesting that the residues in question are doing something important related to growth. Note that the strain containing *myo2-REKE* grew slightly slower than *myo2-3DR*; this was likely due to the fact that the R1402/K1473 basic patch is also the binding site for Sec15p, likely disturbing the interaction (Jin et al., 2011). To my great surprise, the charge-reversal *myo2-3DR-REKE* mutant grew nearly identical to wildtype, suggesting that charge complementation between the head and tail is sufficient to return Myo2p to wildtype-like growth. This information, coupled with work done on these homologous residues in MyoV, provides very strong evidence that Myo2p adopts a head-tail conformation.

Inhibiting Myo2 head-tail regulation causes Myo2p to become hyperpolarized and autoactive

To examine the state of the charge mutant motors *in vivo*, I tagged the endogenous *MYO2* locus with a single copy of GFP at its C-terminus in the wildtype and mutant strains. These tagged strains were functional across a broad range of temperatures and showed no difference in growth compared to the untagged alleles (not shown). As expected, Myo2-GFP is polarized towards sites of growth (Figure 3.2a). However, Myo2-3DR-GFP and Myo2-REKE-GFP motors appeared to be hyperpolarized towards the bud tip, with few motors remaining in the mother cell. I quantified this with summed whole-cell projections of medium buds, and found that about 37% of all wildtype motors were present in the bud (Figure 3.2b). Charge mutations in either the head or tail increase the number of motors in the bud to about 75% of the total. This shows that motors unable to undergo a head-tail interaction remain hyperpolarized. To validate this result, I also found that alanine mutants at the interaction sites will also hyperpolarize the motor (Figure 3.2c). Further, I disturbed the geometry of the motor by changing the length of its lever arm. Motors

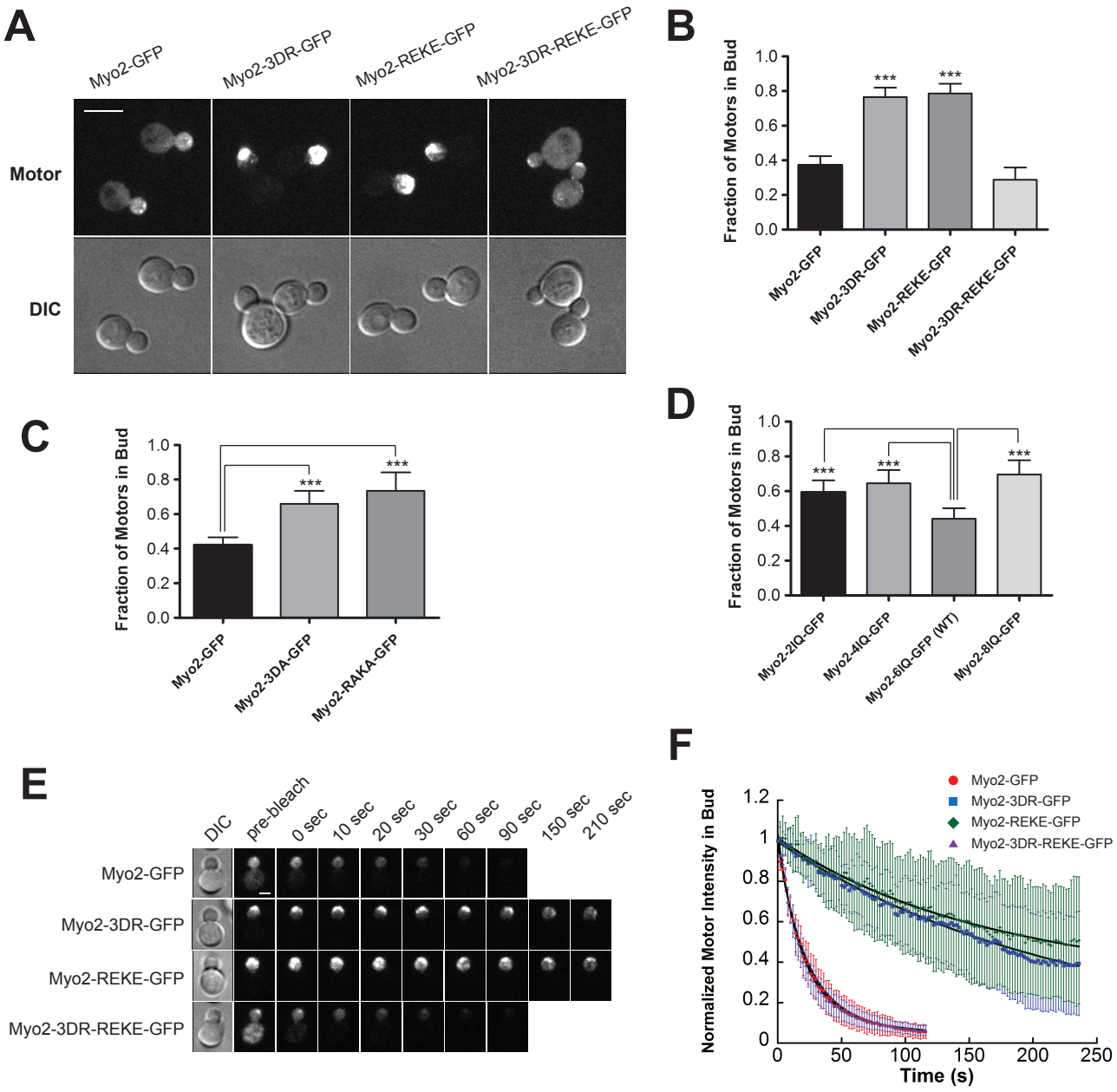

Figure 3.2. Inhibiting Myo2 head-tail regulation causes Myo2p to become hyperpolarized and auto-activated.

(A) Maximum projection images of wildtype and charge mutant motors tagged with GFP. DIC images shown for clarity. Scale bar is 2 µm.

(B) The fraction of motors in the bud of wildtype and charge mutants, as revealed by whole cell summed projection images. n= a minimum of 40 medium budded cells per strain. ***, $p<0.0001$ vs. wildtype.

(C) The fraction of motors in the bud of wildtype and alanine mutants, as revealed by whole cell summed projection images. n= a minimum of 45 medium budded cells per strain. ***, $p<0.0001$ vs. wildtype.

(D) The fraction of motors in the bud of wildtype and lever-arm IQ mutants, as revealed by whole cell summed projection images. n= a minimum of 40 medium budded cells per strain. ***, $p<0.0001$ vs. wildtype motor containing 6IQ domains.

(E) Representative still frame micrographs of FLIP experiments for wildtype and charge mutant motors. DIC image used to show outline of the cell. Scale = 2 µm.

(F) Graph of the normalized fluorescence intensity in the bud for wildtype and charge mutant motors. Myo2-GFP, n=12; Myo2-3DR-GFP, n= 14; Myo2-REKE-GFP, n= 12; Myo2-3DR-REKE-GFP, n= 15.

with 2, 4, or 8 IQ motifs on the lever arm showed significantly more motors polarized in the bud compared with wildtype 6IQ motors (Figure 3.2d). This last result suggests that the absolute length of the lever arm and coiled-coil (about 21 nm and 24 nm, respectively in wildtype) is important to maintain the interaction.

Strikingly, when charge reversal mutations in the head and tail were combined in the Myo2-3DR-REKE-GFP strain, the motor phenotype was similar to wildtype, with 32% of all motors present in the bud (Figures 3.2a-b). This strongly suggests that an interaction between these domains is both necessary and sufficient to regulate the delivery cycle of a myosin-V motor *in vivo*.

In Chapter 2, I showed that myosin-V motors in yeast must be deactivated for efficient recycling from sites of growth, and that this occurs when it releases its cargo. To determine if the head-tail interaction alone is sufficient to deactivate the motor and enable recycling, I performed fluorescence loss in photobleaching (FLIP) experiments. Motors in the mother cell were bleached every two seconds while the intensity of motor fluorescence in the bud was monitored over time. Wildtype motors followed known recycling kinetics, with the vast majority of motors leaving the bud after about 30 seconds (Figure 3.2e-f). Myo2-3DR-GFP or Myo2-REKE-GFP motors resided in the bud for much longer, with half-times of loss being ~2-3 minutes. This suggests that motors unable to form the head-tail interaction are hyperactive, similar to the *myo2-13* allele shown in Chapter 2. When both of these charges were combined, the Myo2-3DR-REKE-GFP motors recycled at rates matching wildtype motors. This indicates that the interaction between the head and tail is required for proper recycling dynamics.

Cargo transport functions of an unregulated myosin-V are severely compromised

Since I found that motor regulation occurs *in vivo* and when unregulated causes the motor to become hyperactive, I wanted to see the effects an unregulated myosin-V motor could have on its cargoes. Myo2p has two known essential cargoes it must transport into the bud for survival. These are the mitochondria, where Mmr1p and the Rab Ypt11p serve as receptors, and secretory vesicles, where the Rab Sec4p and an unknown component dependent on the lipid PI4P serve as receptors (Chernyakov et al., 2013; Jin et al., 2011; Santiago-Tirado et al., 2011). I also chose to observe the orientation of the mitotic spindle, a nonessential cargo for Myo2p mediated by the Kar9p-Bim1p interaction with astral microtubules (Yin et al., 2000). Importantly, these cargos bind to different locations on the tail (Figure 1.4); Mmr1p binds to subdomain I while Kar9p and the Rabs Sec4p/Ypt11p bind to subdomain II (and on the opposite face as Mmr1p). Thus, any failure to transport cargo is likely to be caused by a wide-scale defect in the motor's regulation and not due to the point mutations blocking receptor binding.

Wildtype cells show very robust polarization of the vesicle marker GFP-Sec4 (Figures 3.3a-b). However, when either the head or tail interacting regions had their charges reversed, there was a large build up of GFP-Sec4 marked vesicles in the mother cell and a large decrease in the fraction of cells with polarized GFP-Sec4. This does not appear to be a defect in Sec15p binding, also a feature of the R1402/K1473 site (Jin et al., 2011), because the result was phenocopied in the *myo2-3DR* strain. Since Myo2-3DR and Myo2-REKE motors are constitutively active and accumulate at the bud tip, it is likely that the vesicles are simply left behind in the mother cell due to a scarcity of available motors. When both charges are allowed to complement each other in the *myo2-3DR-REKE* strain, GFP-Sec4 polarization significantly increased, though not to quite the degree as wildtype (Figures 3.3a-b).

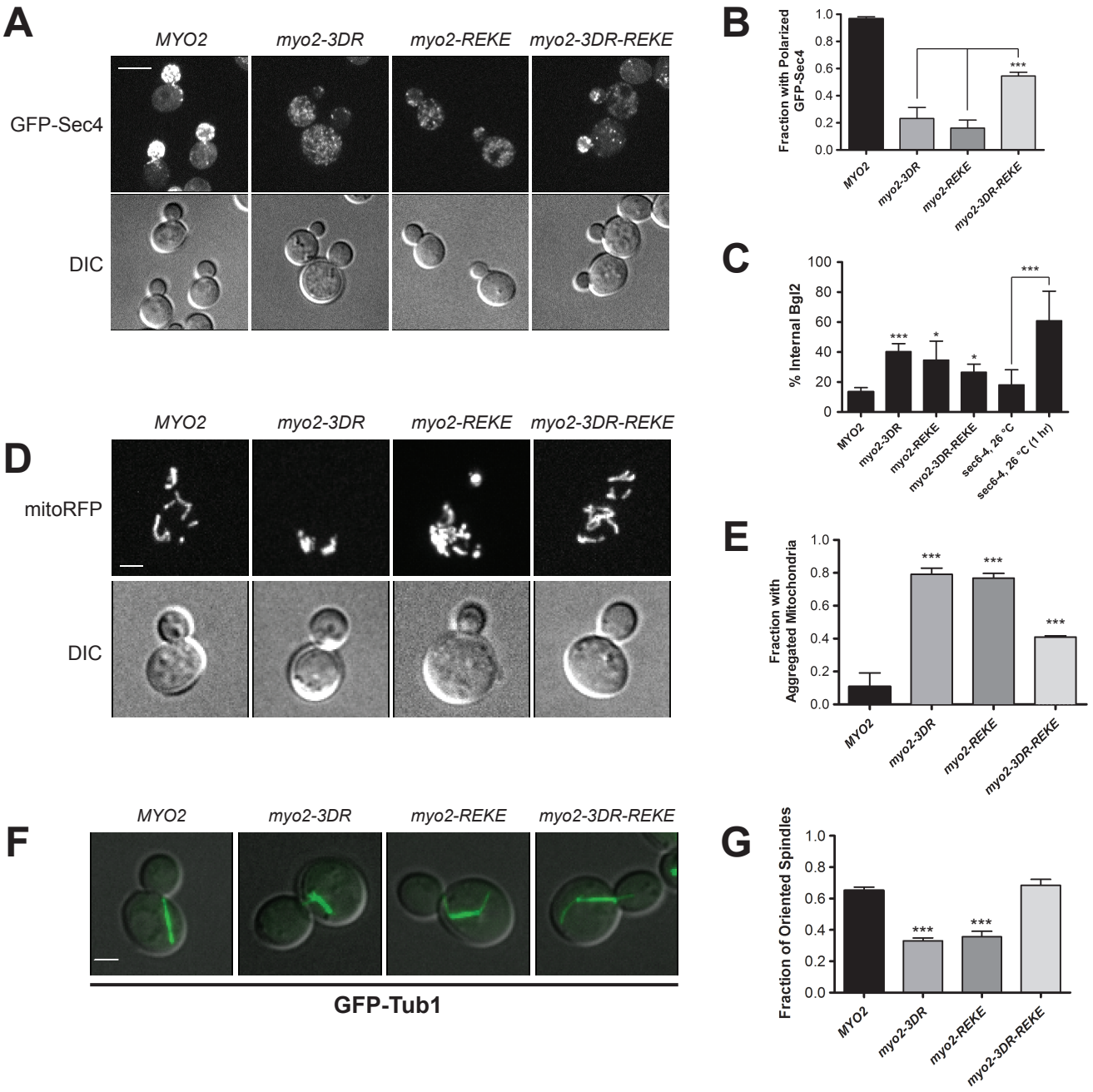

Figure 3.3. Cargo transport functions of an unregulated myosin-V are severely compromised.

(A) Maximum projection images of GFP-Sec4 in wildtype and charge mutant strains. DIC images shown for clarity. Scale = 5 μm.
(B) Fraction of cells with polarized GFP-Sec4 vesicles. 100+ medium budded cells were scored for each strain, n=3. ***, $p<0.0001$.
(C) Percent of Bgl2p found in the internal fraction of wildtype, *sec6-4*, and charge mutant strains. n=4 replicates. *, $p<0.05$. ***, $p<0.0001$.
(D) Maximum projection images of mitoRFP in wildtype and charge mutant strains. DIC images shown for clarity. Scale = 2 μm.
(E) Fraction of cells with aggregated mitochondria. 100+ medium budded cells were scored for each strain, n=3. ***, $p<0.0001$ vs. wildtype.
(F) Maximum projection images of GFP-Tub1 in wildtype and charge mutant strains. DIC images shown for clarity. Scale = 2 μm.
(G) Fraction of cells with oriented spindles, as defined by the axis of the spindle in line with the bud neck. 100+ medium budded cells were scored for each strain, n=3. ***, $p<0.0001$ vs. wildtype.

The defect in secretion was also detected using a Bgl2p assay, which shows the internal and external fractions of the constitutively transported cell wall enzyme endo-beta-1,3-glucanase (Figure 3.3c). Only 13% of the total Bgl2p population is present inside wild type cells. This rises more than 2.5-fold in the single-charge mutants, indicative of a secretion defect. However, there was still a significant difference between wildtype and the *myo2-3DR-REKE*; this could be due to vesicle fusion problems since the Sec15p binding site at R1402/K1473 is still mutated. While work presented in the next chapter argues against fusion problems, it is very clear that the essential process of secretory vesicle transport is compromised in mutants that disrupt the head-tail interaction.

I next turned to see how mitochondria are distributed in the cell. In wildtype cells, mitochondria appear as a network of tubes throughout the cell as marked with an RFP molecule fused to a mitochondrial localization sequence (Figures 3.3d-e). In either of the *myo2-3DR* or *myo2-REKE* strains, mitochondria adopted a distended and aggregated appearance toward the back of the mother cell. This phenotype has previously been seen in cells that are unable to transport mitochondria into the bud (Chernyakov et al., 2013). When both mutations were combined, there was a significant decrease in the fraction of cells with this phenotype and a majority of cells reverted to a normal mitochondrial distribution and appearance.

Similarly, the number of cells with properly aligned mitotic spindles was decreased in charge mutant strains (Figures 3.3f-g). Charge mutants had significantly fewer cells displaying oriented mitotic spindles, as scored by the spindle axis passing directly through the bud neck. Complementing charges in the *myo2-3DR-REKE* mutant fully restored this phenotype to wildtype levels. The combined results of vesicle polarization, mitochondrial distribution, and spindle orientation are important because the cargo receptors bind to different regions of the

Myo2p tail. It is unlikely that point mutations in the head or tail are causing such large-scale cellular changes, and are more likely caused by an unregulated myosin-V motor.

DISCUSSION

While mammalian myosin-V motors have been shown to undergo a specific head-tail interaction through acidic residues in the head and basic residues in the tail, no data exists on how misregulation of this event affects the cell *in vivo*. In this chapter, I have presented compelling evidence that yeast Myo2p also undergoes a head-tail interaction through acidic residues D123/E135/E137 in the head and basic residues R1402/K1473 in the tail. Mutation of either of these sites yields motors that are unable to recycle efficiently and unable to transport cargo. Further work will need to be done to show this interaction conclusively, perhaps through ATPase activity assays or observing conformational changes between wildtype and mutant motors through sedimentation analysis.

The central finding of this chapter is that an interaction between the head and tail of Myo2p is both necessary and sufficient to allow for Myo2p to recycle efficiently. These data also clarify the deactivation event in the bud tip shown in the previous chapter. In Chapter 2, I showed that the *myo2-13* allele is constitutively active and trapped at the bud tip, leading to the conclusion that wildtype motors must be deactivated in order to recycle efficiently. It would appear that the *myo2-13* allele is somehow defective in this head-tail regulatory event. The *myo2-13* allele contains four mutations generated by random PCR mutagenesis; while three of them are located on the surface of the tail in locations far removed from the basic patch, one of them (Y1389C) is buried in the tail within 2.5 nm of the R1402/K1473 basic patch. It is

conceivable that such a mutation could destabilize the tail enough to allow for misregulation of the motor.

The finding that mutating the basic patch in the tail domain results in motors that are defective in transporting at least three different cargoes is likely due to overall misregulation of the motor rather than specific defects in binding cargo. Because the motors are nearly all present in the bud tip, they are likely unable to transport cargo efficiently simply because they are not in the mother cytoplasm. That is, the vesicles, mitochondria and astral microtubules are left behind as the defective motors have already 'walked up' actin cables in an unregulated manner. Since they are unable to turn off, they are unable to recycle which exacerbates the situation. Misregulated motors are not lethal because the motors can still bind to essential cargoes, just not transport them at rates sufficient for rapid growth.

With this in mind, we can continue the discussion from Chapter 2 on how Myo2p motors are activated by secretory vesicles, and deactivated at the bud tip. It now seems likely that the 'default' state of Myo2p is actually the closed form. This is supported by (1) the finding that Myo2p motors are depolarized in mutants lacking competent secretory cargo, (2) motors that cannot bind Rab proteins are depolarized, and (3) hyperactive motors cannot transport cargo efficiently. Thus, autoinhibited motors diffusing in the cytoplasm are activated through cargo binding where they then transport the cargo to the proper place in the daughter cell. With secretory vesicles, the Sec4-GTP hydrolysis event releases the motor from the membrane, where it then intrinsically folds back up into its default state as an inactive motor. Data presented in the appendix suggests that it then diffuses back to the mother cell for another transport cycle. Recent biophysical data may lend support to the idea that the folded form is the default state, as the mouse MyoVa head-tail interaction is quite strong with a K_d of 30 nM (Velvarska and Niessing,

2013). In contrast, the Myo2-Sec4-GTP interaction has a weaker dissociation constant, at 4.6 μM (Jin et al., 2011). While this is comparing across species, the head-tail interaction is ~150x stronger than the interaction with a myosin-V receptor and supports the notion that its default state is in the closed conformation. Further, it may be that cooperative effects of cargo binding (such as both Myo2p monomer tails each interacting with a Sec4p molecule) could overcome the strong head-tail interaction to open the motor.

One interesting result that may not be appreciated is the control the length of the lever arm and coiled-coil domains are likely play in autoinhibition. Shortening the lever arm in IQ mutants also resulted in hyperpolarized motors (Figure 3.2d). Though I didn't perform photobleaching experiments or observe cargo-transport phenotypes, my experience with them suggests that these hyperpolarized motors would be unable to recycle efficiently. The lever arm of Myo2p is predicted to be an uninterrupted alpha helix of ~21 nm while the coiled-coil domain is predicted to be ~24 nm with no unstructured regions. It follows then that the length of the Myo2p lever arm and coiled-coil are exquisitely tuned against one another, as there is minimal unstructured regions predicted at the end of the head or beginning of the tail that could increase its flexibility. This fact was unknown when I performed experiments presented in the Chapter 2 with the Myo2-4IQ-3xGFP allele, which was utilized simply because it slowed the motors down to allow for two-color imaging. However, all experiments performed with the *myo2-4IQ* allele were in molecule counting experiments in the diffusing and transport steps and not in recycling analysis. Misregulation of Myo2p could complicate the number of motors I observed bound to a vesicle, but it seems clear from the puncta fluorescence that similar numbers of either wildtype or 4IQ motors bind. Nevertheless, this finding should be taken into consideration in future counting experiments.

REFERENCES

Chernyakov, I., Santiago-Tirado, F., and Bretscher, A. (2013). Active segregation of yeast mitochondria by Myo2 is essential and mediated by Mmr1 and Ypt11. Curr. Biol. *23*, 1818–1824.

Gietz, R.D., Schiestl, R.H., Willems, A.R., and Woods, R.A. (1995). Studies on the transformation of intact yeast cells by the LiAc/SS-DNA/PEG procedure. Yeast *11*, 355–360.

Hammer, J.A., and Sellers, J.R. (2011). Walking to work: roles for class V myosins as cargo transporters. Nat. Rev. Mol. Cell Biol. *13*, 13–26.

Jin, Y., Sultana, A., Gandhi, P., Franklin, E., Hamamoto, S., Khan, A.R., Munson, M., Schekman, R., and Weisman, L.S. (2011). Myosin V Transports Secretory Vesicles via a Rab GTPase Cascade and Interaction with the Exocyst Complex. Dev. Cell *21*, 1156–1170.

Karcher, R.L. (2001). Cell Cycle Regulation of Myosin-V by Calcium/Calmodulin-Dependent Protein Kinase II. Science *293*, 1317–1320.

Legesse-Miller, A., Zhang, S., Santiago-Tirado, F.H., Van Pelt, C.K., and Bretscher, A. (2006). Regulated phosphorylation of budding yeast's essential myosin V heavy chain, Myo2p. Mol. Biol. Cell *17*, 1812–1821.

Li, X.-D., Jung, H.S., Wang, Q., Ikebe, R., Craig, R., and Ikebe, M. (2008). The globular tail domain puts on the brake to stop the ATPase cycle of myosin Va. Proc. Natl. Acad. Sci. USA *105*, 1140–1145.

Nascimento, A.F.Z., Trindade, D.M., Tonoli, C.C.C., de Giuseppe, P.O., Assis, L.H.P., Honorato, R.V., de Oliveira, P.S.L., Mahajan, P., Burgess-Brown, N.A., Delft, von, F., et al. (2013). Structural insights into functional overlapping and differentiation among myosin V motors. J. Biol. Chem. *288*, 34131–34145.

Santiago-Tirado, F.H., Legesse-Miller, A., Schott, D., and Bretscher, A. (2011). PI4P and Rab inputs collaborate in myosin-V-dependent transport of secretory compartments in yeast. Dev. Cell *20,* 47-59.

Schott, D., Ho, J., Pruyne, D., and Bretscher, A. (1999). The COOH-terminal domain of Myo2p, a yeast myosin V, has a direct role in secretory vesicle targeting. Journal of Cell Biology *147*, 791–808.

Velvarska, H., and Niessing, D. (2013). Structural Insights into the Globular Tails of the Human Type V Myosins Myo5a, Myo5b, and Myo5c. PLoS ONE *8*, e82065.

Yin, H., Pruyne, D., Huffaker, T.C., and Bretscher, A. (2000). Myosin V orientates the mitotic spindle in yeast. Nature *406*, 1013–1015.

CHAPTER 4

TRACKING INDIVIDUAL SECRETORY VESICLES REVEALS A TIMELINE OF EVENTS IN EXOCYTOSIS

OVERVIEW

Work presented in the previous chapters detailed the delivery cycle of the entire population of Myo2p motors. That is, my dynamic studies on the motor have in general followed the bulk population either entering or leaving the bud. Since this work was largely published in 2012, upgrades to the available microscope have allowed for finer photobleaching control while a new laser system has allowed for slightly better signal-to-noise ratios. Due to these changes, I wondered if it might be possible to track individual secretory vesicles as they enter the bud and fuse with the cortex. Tracking vesicles in specific mutants and colocalizing two proteins over time would aid in the creation of a timeline of events in yeast exocytosis, which despite years of study is still underdeveloped.

By analogy, a mechanistic understanding of endocytosis was only possible from pioneering imaging work from the Drubin Lab, when Marco Kaksonen tracked six individual endocytosis proteins and determined how the dynamics of each is related to the others (Kaksonen et al., 2003). For the first time, the precise order in which different proteins arrive at sites of endocytosis could be visualized, which when coupled to previous biochemical data revealed a timeline for a single endocytosis event. In the intervening decade, more than 60 proteins have been localized to the pathway, leading to a comprehensive understanding of the order of events in yeast endocytosis (Weinberg and Drubin, 2012). However, many of these proteins are present in hundreds or even thousands of copies per endocytic site, which are readily observed by

microscopy. Further, sites of endocytosis are spatially separate from one another, allowing for relatively easy analysis of individual patches.

In contrast, yeast exocytosis can take place at any location on the bud, and as I showed in the Chapter 2 the numbers of molecules per vesicle are few. Perhaps the most challenging aspect is related to the polarization of most proteins in the post-Golgi secretory pathway; fluorescently tagged proteins on vesicles that enter the bud can easily get "lost in the noise." In this chapter, I will highlight my attempts to track individual secretory vesicles docking and fusing, examine the effects various mutants have on key steps in exocytosis, and begin to build a framework for the order of events using two-color live cell imaging.

MATERIALS AND METHODS

Yeast Strains and Molecular Biology Techniques

Cells were grown and selected for using standard molecular biology techniques (Sherman, 2002). Yeast transformations were performed using lithium acetate-based methods (Gietz et al., 1995).

Vesicle Tethering Assay

"Vesicles" in this assay are defined as GFP-Sec4 -positive puncta. Strains were tagged with chromosomally integrated GFP-Sec4 under the endogenous promoter, as described in Chapter 2. All assays were done in strains grown to early-mid log phase in appropriate synthetic media containing dextrose. The imaging surface, a 35mm MatTek dish, was prepared by spotting 0.05 mg/mL Concanavalin A (EY Laboratories Inc., San Mateo, CA) onto the glass for 10

minutes. Following removal of the waste, the strain to be imaged was spotted onto the glass dish for an additional 10 minutes before washing 2X in synthetic media.

Imaging was performed on a CSU-X spinning disc confocal microscope system (Intelligent Imaging Innovations, Denver, CO, USA) using a DMI600B microscope (Leica, Wetzlar, Germany) and CoolSnap HQ2 camera (Photometrics, Tuscon, AZ, USA). Micrographs were captured using the 100X objective with 2X binning, for an effective pixel resolution of ~14 nm^2. Movies were taken in a z-stack of 5 planes (covering 2.5 μm), each with 150 ms exposure times from a 473 nm laser, for a time resolution of ~1.32 seconds. About half of the bud of late-G2 cells were captured using this method. Photobleaching of the entire bud was performed using a vector system with 1 ms dwell time and a raster block size of '10' (Intelligent Imaging Innovations).

Vesicles entering the bud after FRAP were tracked in 3 dimensions in Slidebook 5.0 using the "Mean Adjusted Center of Intensity" manual particle tracking tool. This finds the coordinates of the center of the object (weighted by intensity values that are above the mean intensity) for accurate tracking of the center of fluorescence. Vesicles were tracked by eye until one clearly touched the membrane ("first contact"). The manual particle tracker tool was then used to measure the particles location in 3D space of the multi-planed image until it disappeared. Only those vesicles that I saw touch the membrane from the cytoplasm, were unambiguous throughout their time there (that is, no other vesicle appeared next to it or overlapped with it) and quickly vanished in the middle three planes of the five plane image were used. This last criterion was included to prevent sampling vesicles that might drift out of the field of view in the z direction. Statistics related to the path of the vesicle were then obtained from Slidebook 5.0 and exported for work in Microsoft Excel and GraphPad Prism. Failed tethering events for different

strains were scored as the vesicles that dissociated from the cortex after being tethered for at least five consecutive frames (~6.5 sec) in the first 60 timepoints of 20 separate movies.

Colocalization experiments were performed with either 3xGFP or 3xmCherry fused to the C-terminus of the protein of interest. All PCR amplified fragments were sequenced following ligation to ensure fidelity. Myo2-3xmCherry was created by removing a 3xGFP module from pRS306-cctail-3xGFP (described in Chapter 2) and ligating a 3xmCherry module between the BamHI and NotI restriction sites. The vector was then cut with a unique HindIII site for integration at the 3' end of the endogenous *MYO2* gene. Strains containing Sec15-3xmCherry were created by ligating a PCR amplified fragment of the 3' end of *SEC15* (1008 nt) between restriction sites HindIII and BamHI in the pRS306 vector. A 681 nt fragment of the *SEC15* 3' untranslated region was ligated upstream, between XhoI and HindIII while the 200 nt fragment of the *SEC15* terminator was amplified and ligated between the SacI and NotI sites. Following ligation of the 3xmCherry module between BamHI and NotI, the construct was linearized with the unique HindIII site to integrate 3xmCherry immediately 3' of the *SEC15* gene. Sec3p and Sec5p were tagged with 3xGFP by amplifying the 3' 1000 nt of each gene sequence and ligating into to a previously created pRS303-3xGFP-tADH1 construct (made by Felipe Santiago) between BamHI and SalI restriction sites. Each gene fragment has a unique ClaI restriction site; when linearized, each construct integrated at the 3' end of the gene in question.

Colocalization microscopy of Sec4p ,Myo2p, Sec15p, Sec3p, and Sec5p was performed by imaging a single bottom plane of the cell. This was done to increase time resolution to <1 sec and because it was found that docked vesicles in wildtype cells do not move around much once tethered (Figure 4.2d). Channel and time information can be found in figure legends. The times of disappearance for proteins analyzed was calculated by simply observing movie frames and

comparing to timestamps. FLIP experiments were performed similarly to experiments presented Chapter 2, though using the 3I Vector control system with 1 ms dwell time and '20' raster block size. Each exocyst component used in this study was tagged with GFP by amplifying PCR cassettes from pFA6a-GFP vectors and selected for using the appropriate media.

RESULTS

Vesicles tether to the membrane for about 18 seconds in wildtype cells

As detailed in Chapter 2, a yeast cell with chromosomally tagged GFP-Sec4 contains ~7000 copies per cell, with ~4000 copies present in the bud. This presented a challenge to tracking individual secretory vesicles marked by GFP-Sec4p, with only ~75 copies per actively transported vesicle, since they quickly become part of the background in the daughter cell. Two solutions to the problem of tracking individual secretory vesicles were developed. First, cells used in the analysis were in late-G2, just before the intrinsic switch to neck-directed growth. This ensured maximal cortex surface area and spatial separation of vesicles. Secondly, the background signal of GFP-Sec4 was completely photobleached, allowing only newly transported vesicles to be localized. Using this process, I was able to image individual secretory vesicles docking and fusing with the cortex in wildtype and mutant cells.

Control experiments showed that photobleaching the entire mother cell in late-G2 phase with a 473 nm laser did not affect the growth rate compared to wildtype cells, suggesting that photobleaching was not disturbing essential processes in exocytosis (data not shown). Wildtype GFP-Sec4 containing cells were then subjected to vesicle tracking as detailed in the methods. In brief, 5 planes (covering 2.5 μm in the z-dimension) were imaged rapidly, with ~1.3 seconds per frame time resolution. This setup captures about half of the bud cortex. After the bleach event,

GFP-Sec4 vesicles entering the bud were tracked from tethering to fusion. Vesicles used in the analysis had to meet three criteria: (1) their docking event to the plasma membrane had to be captured, (2) at no point in their time on the cortex could they wander out of the viewing area or be spatially indistinct from another vesicle, and (3) their fusion event must occur in the middle three planes; this ensures that their disappearance is not due to the vesicle wandering out of the captured area. I am likely capturing individual secretory vesicles in this analysis as the number of vesicles entering the bud per unit time matches expected rates of exocytosis (about 1 per three seconds, as detailed in Chapter 2).

Since photobleaching the bud leaves no trace of the cortex outline, I needed to be sure that the puncta I am visualizing are actually docked to the cortex. However, for maximal time resolution only one channel could be imaged in the experiment. As a pilot control experiment, I co-imaged GFP-Sec4 and a plasma membrane marker, a tandem fragment of the cortical ER tether Ist2p fused to mCherry (mCherry-2xIst2$^{928\text{-}948}$). Following the bleach event, line scan analysis of newly transported GFP-Sec4p puncta showed a high degree of colocalization with the cortex (Figure 4.1a). This shows that GFP-Sec4 puncta can be visualized when docked to the plasma membrane.

As described in point (3) above, the vesicle's fusion event is critical for determining the time spent on the membrane. For this analysis, vesicle fusion was defined as a rapid, frame-to-frame disappearance of the GFP-Sec4 puncta already docked to the membrane. As the vesicle fuses, the GFP-Sec4 molecules would be expected to diffuse from a relatively small vesicle membrane to the much larger plasma membrane. To determine if the dynamics of diffusing GFP-Sec4 would show a rapid disappearance, I took advantage of the *msb3Δ msb4Δ* GAP-null strain. In this strain, I noticed that GFP-Sec4 is not immediately extracted by Gdi1p and is instead

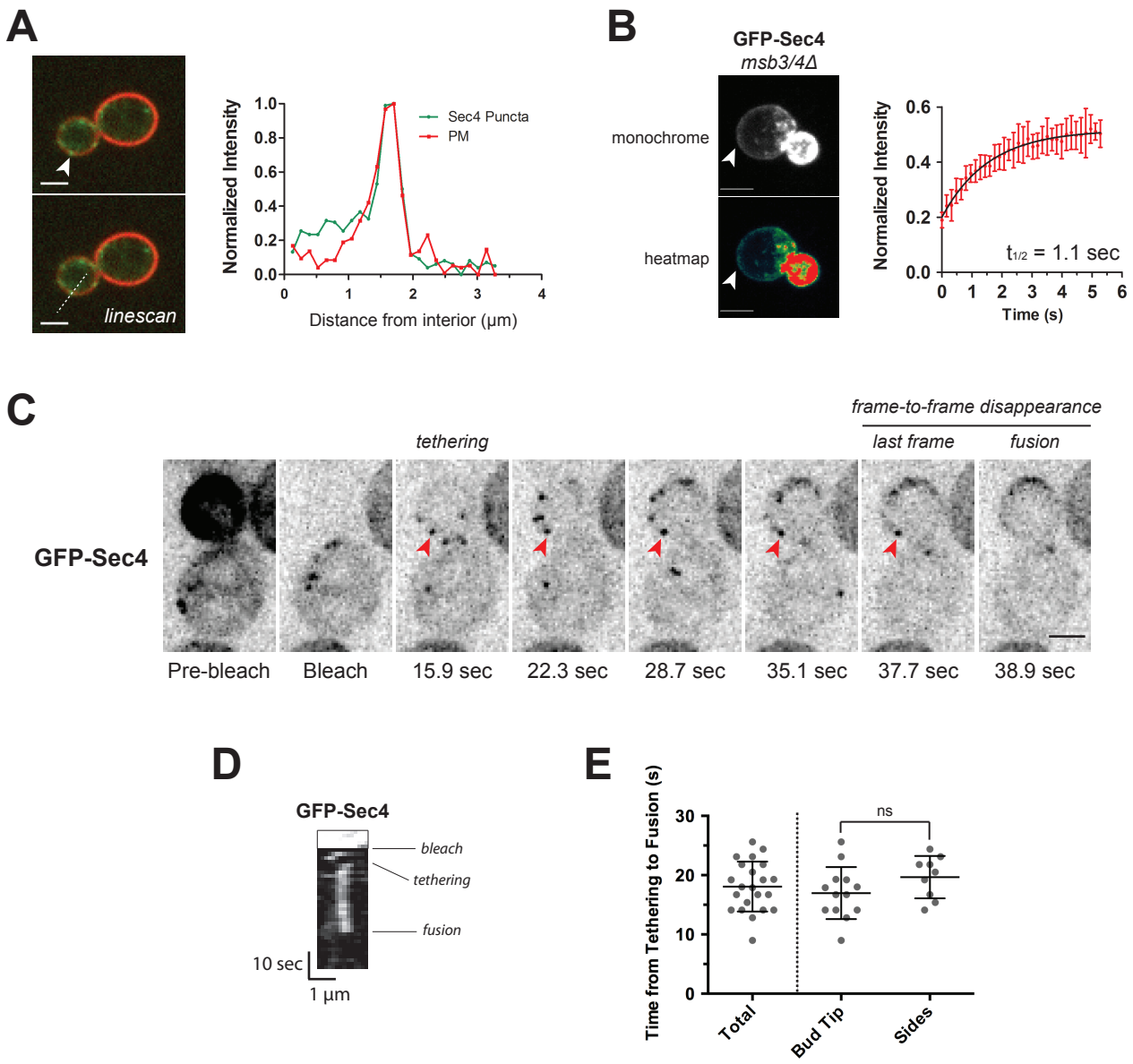

Figure 4.1. Vesicles tether to the membrane for about 18 seconds in wildtype cells.

(A) Linescan analysis of GFP-Sec4 puncta (arrow) and plasma membrane (PM) marker mCherry-2xIst2$^{928\text{-}948}$ show vesicles on the cortex following a bleach event. X-axis is the distance from the interior side of the line. Scale = 2 μm.

(B) FRAP analysis of cortex-localized GFP-Sec4 in GAP-null *msb3/4Δ* cells suggest GFP-Sec4 diffuses quickly in the membrane. Arrows point to cortex-localized GFP-Sec4 pool. Scale = 2 μm. Error bars are standard deviation.

(C) Still-frames of a typical GFP-Sec4 vesicle tracking experiment in a wildtype cell, in inverted monochrome for clarity. Arrows point to GFP-Sec4 puncta tethered to the membrane. Note that this is a maximum projection of a z-series, so z-axis information is compressed. Scale = 2 μm.

(D) Kymograph of GFP-Sec4 vesicle puncta shown by arrow in (C). The x-axis represents distance in a line drawn through the cortex while the y-axis represents time. Note that this is a maximum projection of a z-series, so z-axis information is compressed. Commentary shows key events in the experiment. Scale as shown.

(E) Column scatter plot of the time from tethering to fusion (seconds) in wildtype cells for the whole population (n=22), bud tip (n=13), and bud sides (n=9). ns, not significant. Lines show mean and 95% confidence intervals.

found all over the plasma membrane in limited quantities. Photobleaching a small patch of membrane-localized GFP-Sec4p in this strain showed a $t_{1/2}$ of 1.1 ± 0.1 sec (n= 12; Figure 4.1b). This shows that GFP-Sec4 diffuses relatively quickly in the membrane and so the very rapid disappearance seen in my vesicle tracking studies is most likely the Rab moving from vesicle to cortex during the fusion event.

Vesicles were tracked entering the bud, tethering, and fusing with the cortex after the bleach event. Their location was tracked in three dimensions for statistical purposes; for presentation in this thesis, all images are maximum projections of individual movie frames (Figure 4.1c) or kymographs (Figure 4.1d). The duration vesicles in wildtype cells reside on the membrane, from tethering to fusion, is remarkably consistent, with an average of 18.1 ± 4.2 sec (n=22; Figure 4.1e). This consistency suggests a carefully timed set of ordered events regulates tethering and fusion. Some vesicles tracked in this analysis were near the sides of the bud, which may have fusion dynamics different from vesicles docked towards the bud tip. To determine if the vesicles used in my analysis represent the true mean of the time from docking to fusion, I compared vesicles that docked at the bud tip (n=13) to those that docked along the sides of the bud (n=9). There was no difference in their times from tethering to fusion (Figure 4.1e), suggesting that fusion times do not depend on location in the bud.

Vesicles take 2.5x longer to fuse in a constitutively active Sec4p mutant

I next wanted to determine how the time from tethering to fusion would change in a mutant where GTP hydrolysis is impaired. The Sec4-Q79L protein, which contains a point mutation in the phosphoryl-binding site that reduces GTP hydrolysis to 30% of wildtype levels *in vitro*, was fused to GFP and subjected to the same analysis (Walworth et al., 1992). Incredibly,

the duration spent on the membrane increased 2.5-fold, to 45.6 ± 11.7 seconds (n=15; Figures 4.2a-b), and was far more variable, suggesting that the timing of GTP hydrolysis after tethering directly affects the time to fusion and interferes with the order of exocytic events. Further analysis showed that the vesicles did not appear to "wander" on the plasma membrane any more than in wildtype cells. This was analyzed in two ways. First, a simple FRAP experiment was performed where the entire cell *except* for a small section on the cortex was bleached; GFP-Sec4-Q79L vesicles in this bleach region did not wander into an adjacent bleached section of cortex at rates different than wildtype GFP-Sec4 vesicles (Figure 4.2c). Secondly, position data for vesicles observed to tether and fuse with the membrane was extracted and the mean adjusted center of intensity in three dimensions was tracked over time; this allowed for relatively precise localization of the vesicle on the membrane. Vesicles in wildtype cells and GFP-Sec4-Q79L cells both wandered at a rate of 130 nm/s, suggesting that they are both fixed to the membrane even though their time from tethering to fusion differs (Figure 4.2d). This slow velocity could be due to low diffusion rates of Rho proteins in the membrane (which are bound to the exocyst complex). However, even though they do not appear to wander, there was a significant increase in the number of "failed fusion events" observed per second for GFP-Sec4-Q79L. That is, docked vesicles can be seen in movies dissociating from the cortex and diffusing again around the bud cytosol. Note that the observation area is only about half of a late-G2 budded cell or less. Wildtype GFP-Sec4 cells were remarkably good at completing fusion, with only 0.0021 observed failed tethering events/sec (Figure 4.2e). This was increased nearly 8-fold for GFP-Sec4-Q79L vesicles, at 0.016 observed failed tethering events/sec (several instances observed per cell during the bleaching experiment). This implies that the timing of GTP hydrolysis is important, and when delayed can cause the fusion machinery to become defective.

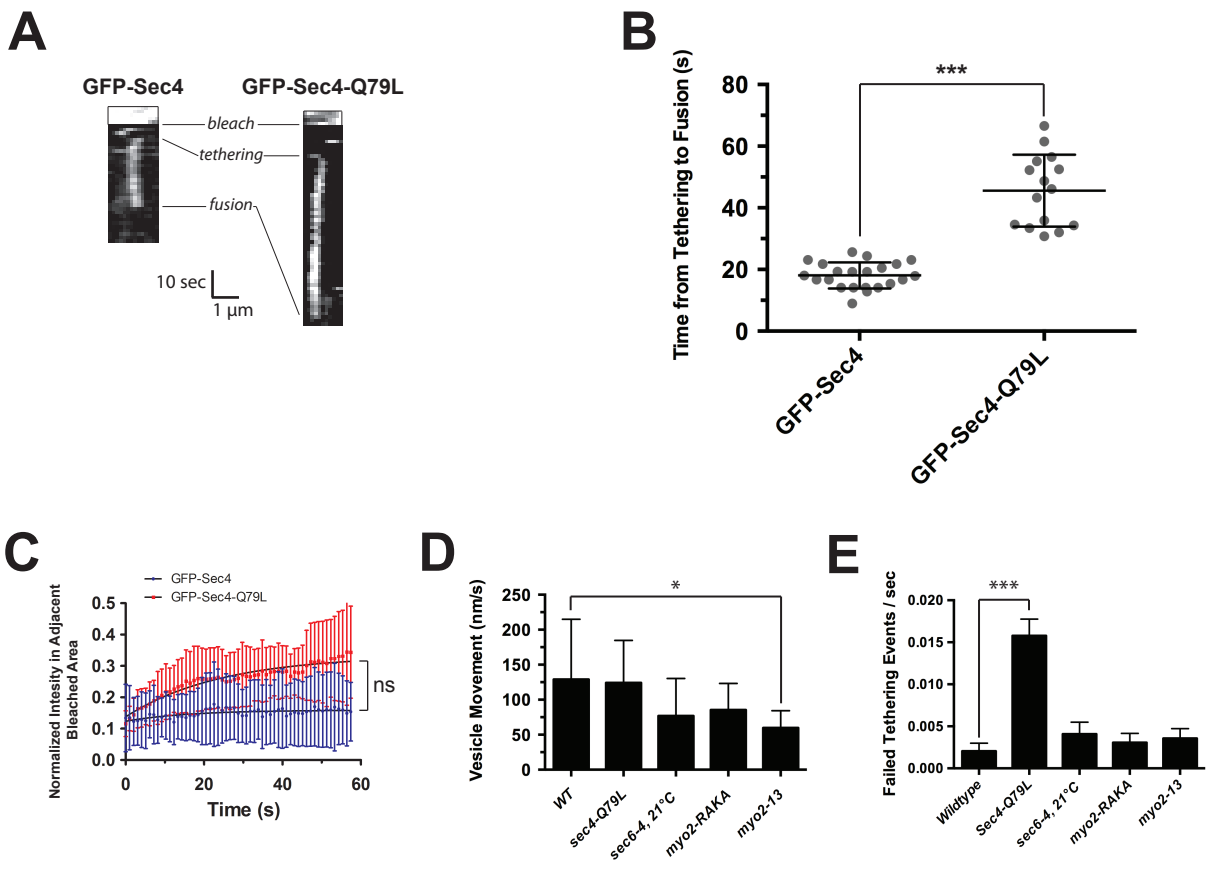

Figure 4.2. Vesicles take 2.5x longer to fuse in a constitutively active mutant, but vesicle dynamics on the cortex are unchanged.

(A) Kymographs of vesicle puncta of wildtype GFP-Sec4 and GFP-Sec4-Q79L cells. The x-axis represents distance in a line drawn through the cortex while the y-axis represents time. Note that this is a maximum projection of a z-series, so z-axis information is compressed. n=22, wildtype GFP-Sec4; n=15, GFP-Sec4-Q79L.

(B) Column scatter plot of the time from vesicle tethering to fusion (seconds) in the indicated strains. ***, $p<0.0001$. Lines show mean and 95% confidence intervals.

(C) Normalized intensity of GFP-Sec4 and GFP-Sec4-Q79L on the cortex in vesicle movement FRAP experiment. There is no significant difference in the recovery rates between the two strains. Error bars are standard deviation.

(D) Movement (nm/s) of puncta on the cortex for the strains indicated at 21 °C. n=22, wildtype; n=15, GFP-Sec4-Q79L; n=16, *sec6-4*; n=16, *myo2-RAKA*; n=15, *myo2-13*. *, $p<0.05$. Error bars are standard deviation.

(E) Observed failed tethering events per second for vesicle puncta in different strains. Note that the observation area does not include the entire bud. n=20 movies for each strain. ***, $p<0.0001$. Error bars are standard deviation.

Vesicle tethering does not occur at the restrictive temperature in sec6-4 cells while vesicles are unable to fuse in sec1-1 cells

Additional tracking of vesicles was done in a select few late-acting conditional secretory mutants. Analysis at the restrictive temperature was complicated by the fact that vesicles are still transported in these mutants, so it was important to take data quickly after the shift before the fusion machinery became saturated. Further, fusion never occurs at the restrictive temperature, so observation was limited to events before fusion. I first performed tethering experiments in a mutant of Sec6p, which at the restrictive temperature causes the exocyst complex to break apart and depolarizes individual components (Donovan and Bretscher, 2012; Lamping et al., 2005; TerBush and Novick, 1995). At the permissive temperature, GFP-Sec4 vesicles in *sec6-4* cells showed significantly longer tethering times than in wildtype cells, at 23.1 ± 5.6 seconds (n=16; Figures 4.3a,c). However, these cells showed no difference in vesicle wandering or in failed fusion events compared to wildtype (Figure 4.2d-e), so this minor timing delay may be caused by a defect in its role in regulating downstream fusion events (such as through t-SNARE Sec9p or fusion stimulator Sec1p). After a five-minute shift to the restrictive temperature, vesicles were observed moving around the bud cytosol but almost never tethered to the membrane. Kymographs of the entire bud cortex 'stretched out' confirmed that vesicle fusion events occur at the permissive temperature, but any association with the cortex was transient at the restrictive temperature (Figure 4.3d). Despite nearly 20 years of research on the exocyst complex, this might be the first direct *in vivo* evidence that it functions as a tether.

In contrast, vesicle tethering proceeded normally in a mutant to the SM-like protein Sec1p, which has been proposed to stimulate assembled SNARE complexes to complete fusion. The time from tethering to fusion at the permissive temperature of GFP-Sec4 vesicles was 19.8 ± 5.5 sec (n=15; Figures 4.3b-c), which was not significantly different from wildtype. Short shifts

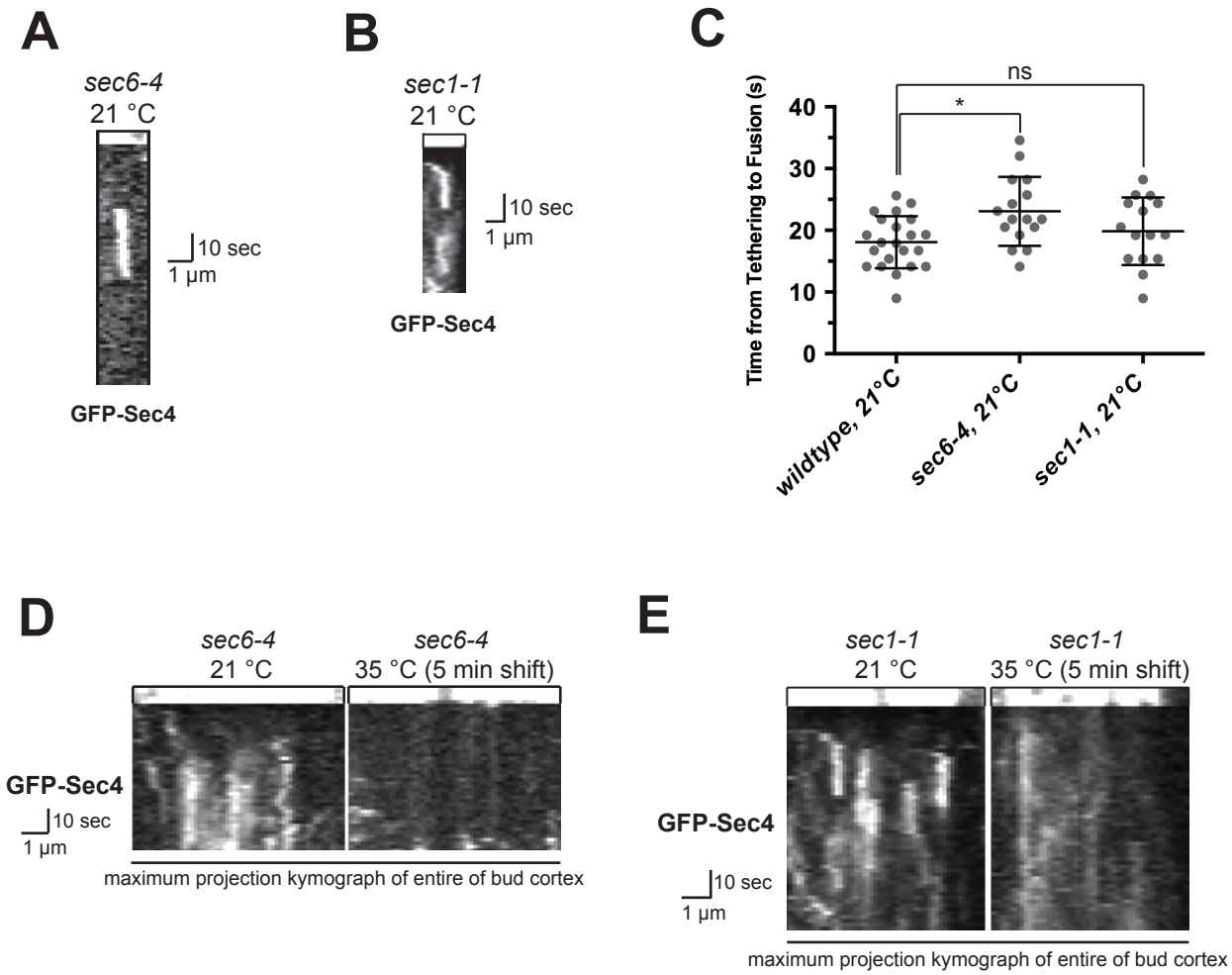

Figure 4.3. Vesicle tethering does not occur at the restrictive temperature in *sec6-4* cells while vesicles are unable to fuse in *sec1-1* cells.

(A) Kymograph of GFP-Sec4 vesicle puncta shown in *sec6-4* strain at the permissive temperature. The x-axis represents distance in a line drawn through the cortex while the y-axis represents time. Note that this is a maximum projection of a z-series, so z-axis information is compressed. Scale as shown.

(B) Kymograph of GFP-Sec4 vesicle puncta shown in *sec1-1* strain at the permissive temperature. The x-axis represents distance in a line drawn through the cortex while the y-axis represents time. Note that this is a maximum projection of a z-series, so z-axis information is compressed. Scale as shown.

(C) Column scatter plot of the time from tethering to fusion (seconds) in wildtype (n=22), *sec6-4* (n=16) and *sec1-1* (n=15) cells at 21 °C. *, $p<0.05$; ns, not significant. Lines show mean and 95% confidence intervals.

(D) Kymograph of GFP-Sec4 along the entire bud cortex in *sec6-4* strain at the permissive and restrictive temperatures. The x-axis represents the 'stretched out' cortex while the y-axis represents time. Note that this is a maximum projection of a z-series, so z-axis information is compressed. Scale as shown.

(E) Kymograph of GFP-Sec4 along the entire bud cortex in *sec1-1* strain at the permissive and restrictive temperatures. The x-axis represents the 'stretched out' cortex while the y-axis represents time. Note that this is a maximum projection of a z-series, so z-axis information is compressed. Scale as shown.

to the restrictive temperature revealed vesicles tethering to the membrane but no clear fusion events were detected. This was confirmed by kymograph analysis; at the restrictive temperature, long traces of tethered vesicles were observed without a clear fusion event occurring (Figure 4.3e). This experiment supports previous studies postulating a role for Sec1p downstream of vesicle tethering.

Vesicle tethering is not delayed in a point mutant implicated in Sec15p binding and motor inactivation

I showed in Chapter 3 that the Myo2p-tail residues R1402/K1473 are involved in the regulation of the motor. Mutating these residues results in hyperpolarized, autoactivated motors that are defective in recycling, leading to secretion and general cargo-transport defects. The Weisman Lab has also shown that these residues are important for Sec15p binding (Jin et al., 2011). To determine if this basic patch (with its varying roles) helps dictate the time from tethering to fusion, I performed my vesicle-tethering assay in a mutant where these residues were changed to alanine (*myo2-RAKA*).

The time GFP-Sec4 vesicles spent tethered in *myo2-RAKA* cells was 16.1 ± 4.9 sec (n= 16; Figure 4.4a), which is not significantly different than wildtype cells. There was also no significant difference in vesicle motility on the membrane or in observed failed tethering events (Figures 4.2d-e). First, this suggests that the Myo2p-Sec15p interaction is not important for the actual vesicle tethering and fusion event. Second, it shows that when the Myo2p inactivation mechanism is disrupted, vesicles can still fuse normally. It is likely that hyperactive motors can still be released from vesicles normally, but remain polarized at sites of growth for a long time due to the motor's inability to turn off. However, I previously showed that a different allele, Myo2-13-GFP, is also hyperpolarized and auto-activated. This observation led to the conclusion

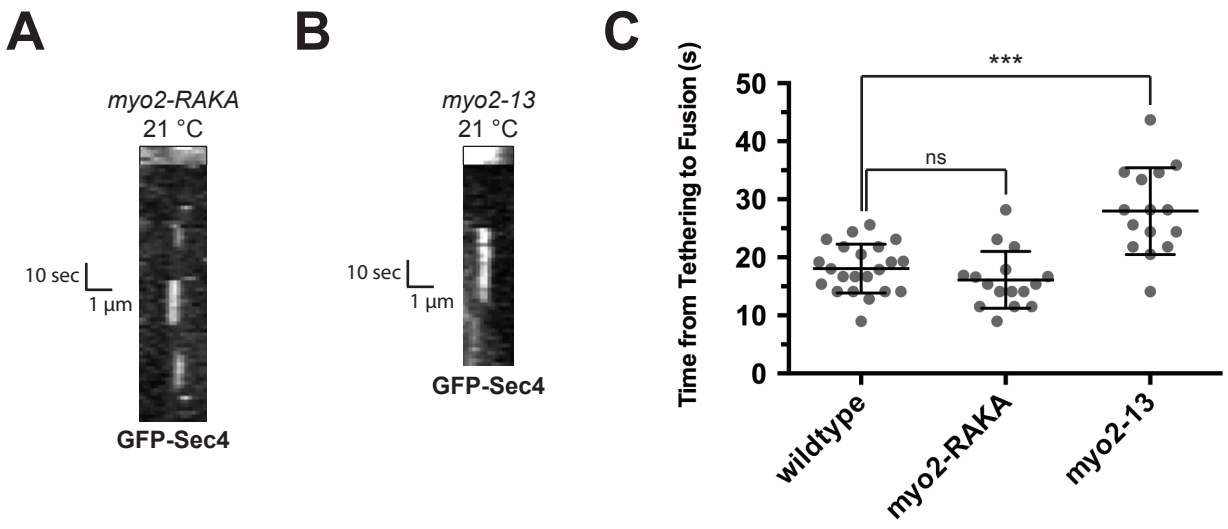

Figure 4.4. Vesicle tethering is not delayed in a point mutant also implicated in Sec15p binding and motor inactivation.

(A) Kymograph of GFP-Sec4 vesicle puncta shown in *myo2-RAKA* strain. The x-axis represents distance in a line drawn through the cortex while the y-axis represents time. Note that this is a maximum projection of a z-series, so z-axis information is compressed. Scale as shown.

(B) Kymograph of GFP-Sec4 vesicle puncta shown in *myo2-13* strain at the permissive temperature. The x-axis represents distance in a line drawn through the cortex while the y-axis represents time. Note that this is a maximum projection of a z-series, so z-axis information is compressed. Scale as shown.

(C) Column scatter plot of the time from tethering to fusion (seconds) in wildtype (n=22), *myo2-RAKA* (n=16) and *myo2-13* (n=15) cells at 21 °C. ***, $p<0.0001$; ns, not significant. Lines show mean and 95% confidence intervals.

that the motor must be turned off in order to recycle efficiently. Since vesicles are not transported at the restrictive temperature, vesicle tracking assays were performed at the permissive temperature, which still show a significant defect in motor recycling and minimal polarization of secretory vesicles (Donovan and Bretscher, 2012; unpublished observations). Surprisingly, the time from tethering to fusion of GFP-Sec4 vesicles in *myo2-13* cells is 50% longer than wildtype, at 28.0 ± 7.5 sec (n=15; Figures 4.4b-c), and shows significantly less mobile vesicles tethered to the membrane (Figure 4.2e). This doesn't appear to agree with the results presented above with the *myo2-RAKA* allele. An answer to this is likely related to the gross structural changes to the tail induced by these mutations, and will be touched on later in the discussion.

Myo2p dissociates from the vesicle ~4 seconds prior to fusion while Sec15p dissociates at the fusion event.

In Chapter 2, I used photobleaching experiments and specific temperature sensitive mutants to show that Myo2p recycling is dependent on exocyst complex tethering and the hydrolysis of Sec4-GTP, but is independent of SNARE action. To further develop a timeline of how motor release is integrated with events at the bud tip, I used two-color timelapse imaging of single vesicles as they dock and fuse with the cortex. I first wanted to determine at which point Myo2p is released from vesicles. Since my previous data suggested that Myo2p is still present on vesicles after they tether to the cortex, it follows that they are released at some point in the next 18 seconds before fusion.

To image Myo2p on vesicles, Myo2-3xmCherry was generated and integrated into a wildtype cell with no ill effects. To identify vesicles, GFP-Sec4 was also integrated into this strain. Because previous results showed that docked vesicles do not move much once tethered

(<150 nm per second; Figure 4.2d), only one plane was used in imaging to allow for faster acquisition. Analysis of tethering and fusion events showed that Myo2p leaves vesicles 3.9 ± 2.0 seconds before the Sec4p fusion event (n=22; Figure 4.5a, c). This piece of data is in line with work presented in Chapter 2, as Myo2p was shown to leave after tethering but before fusion, with a $t_{1/2}$ recycling time of the vesicle associated fraction of 32.5 ± 13.7 seconds. With the time needed to dock and tether, this seems reasonable. Further, most puncta of Myo2p disappeared slowly over the course of a few frames, as evident by the 'gradient' of loss presented in the kymograph (Figure 4.5a).

I next co-imaged integrated Sec15-3xmCherry and GFP-Sec4 to determine when the exocyst complex dissociates from the vesicle. As the eight-member, ~750 kDa exocyst complex is attached to the vesicle only through Sec15p, this seemed like the logical component of the exocyst to track. Co-imaging Sec15-3xmCherry and GFP-Sec4 showed no difference in the time that Sec15p and Sec4p disappear (n=30; Figure 4.5b-c), implying that release of the exocyst complex from the vesicle is concurrent with vesicle fusion.

Individual exocyst components disappear at the fusion event and recycle from the bud as a single complex

The exocyst complex is rather large, with its longest dimension of about 25 nm (Hsu et al., 1998). Thus, it seems likely that some rearrangement would need to occur during the process of vesicle fusion to allow an 80 nm vesicle to contact the cortex. Further, the existence of sub-complexes and the finding that two portions of the exocyst (vesicle associated and plasma membrane associated) have different dynamics going into the bud makes it likely that the exocyst complex splits up at some point in its cycle (Boyd et al., 2004). To further understand

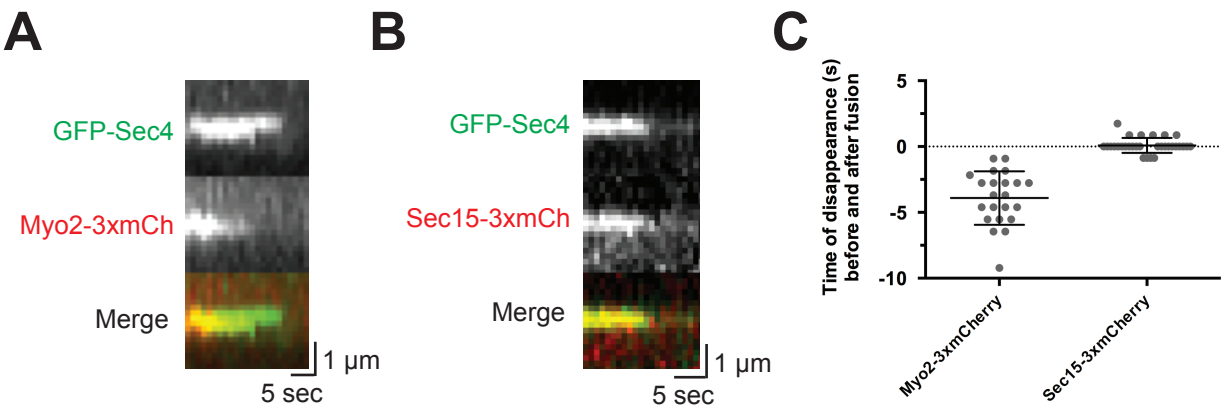

Figure 4.5. Myo2p dissociates from the vesicle ~4 seconds prior to fusion while Sec15p dissociates at the fusion event.

(A) Kymographs of GFP-Sec4 and Myo2-3xmCherry puncta during the fusion event. Note the gradual decrease in intensity of Myo2-3xmCherry prior to its complete disappearance. Each frame captured GFP-Sec4 for 120 ms and Myo2-3xmCherry for 750 ms. The y-axis represents distance while the x-axis represents time. Scale as shown.

(B) Kymographs of GFP-Sec4 and Sec15-3xmCherry puncta during the fusion event. Each frame captured GFP-Sec4 for 120 ms and Sec15-3xmCherry for 650 ms. The y-axis represents distance while the x-axis represents time. Scale as shown.

(C) Column scatter plot of the time of disappearance (s) for the protein in question prior to the fusion event (GFP-Sec4 disappearance). Myo2-3xmCherry, n=22; Sec15-3xmCherry, n=30. Lines show mean and 95% confidence intervals.

the dynamics of the exocyst complex in polarized secretion, I tagged individual components of the complex and performed timelapse colocalization experiments.

I tagged three components and captured pairwise timelapse movies of vesicles docked to the plasma membrane. Sec15-3xmCherry was colocalized with either Sec5-3xGFP or Sec3-3xGFP. I chose to tag Sec5p because it is a core member of the vesicle-associated complex but does not interact with Sec15p. Sec3p was chosen because it localizes to the plasma membrane independent of vesicle trafficking. Surprisingly, Sec15-3xmCherry was always colocalized on punctate structures with either Sec5-3xGFP or Sec3-3xGFP, and when one showed rapid disappearance the other did as well; no component left the complex before the other (Figure 4.6a-c). This suggests that once the exocyst complex forms, it recycles as a single unit and does not dissociate at the plasma membrane prior to fusion.

To determine if the exocyst complex recycles as one unit, the recycling dynamics of individual exocyst complex members was determined via FLIP experiments. Sec3p, Sec5p, and Sec15p were chromosomally tagged with GFP. Consistent with the colocalization studies presented above, FLIP experiments showed that all three members of the exocyst complex tagged had recycling dynamics that were not significantly different from one another (Figure 4.6d). Half-times of loss were calculated from single-exponential decay curves and showed rather long times to recycle, varying from 58.1 ± 9.4 sec (Sec5p; n=13) to 78.2 ± 17.1 sec (Sec15p; n=10). This further implies that the exocyst complex does not dissociate at sites of growth and instead recycles back into the mother cell as one complex.

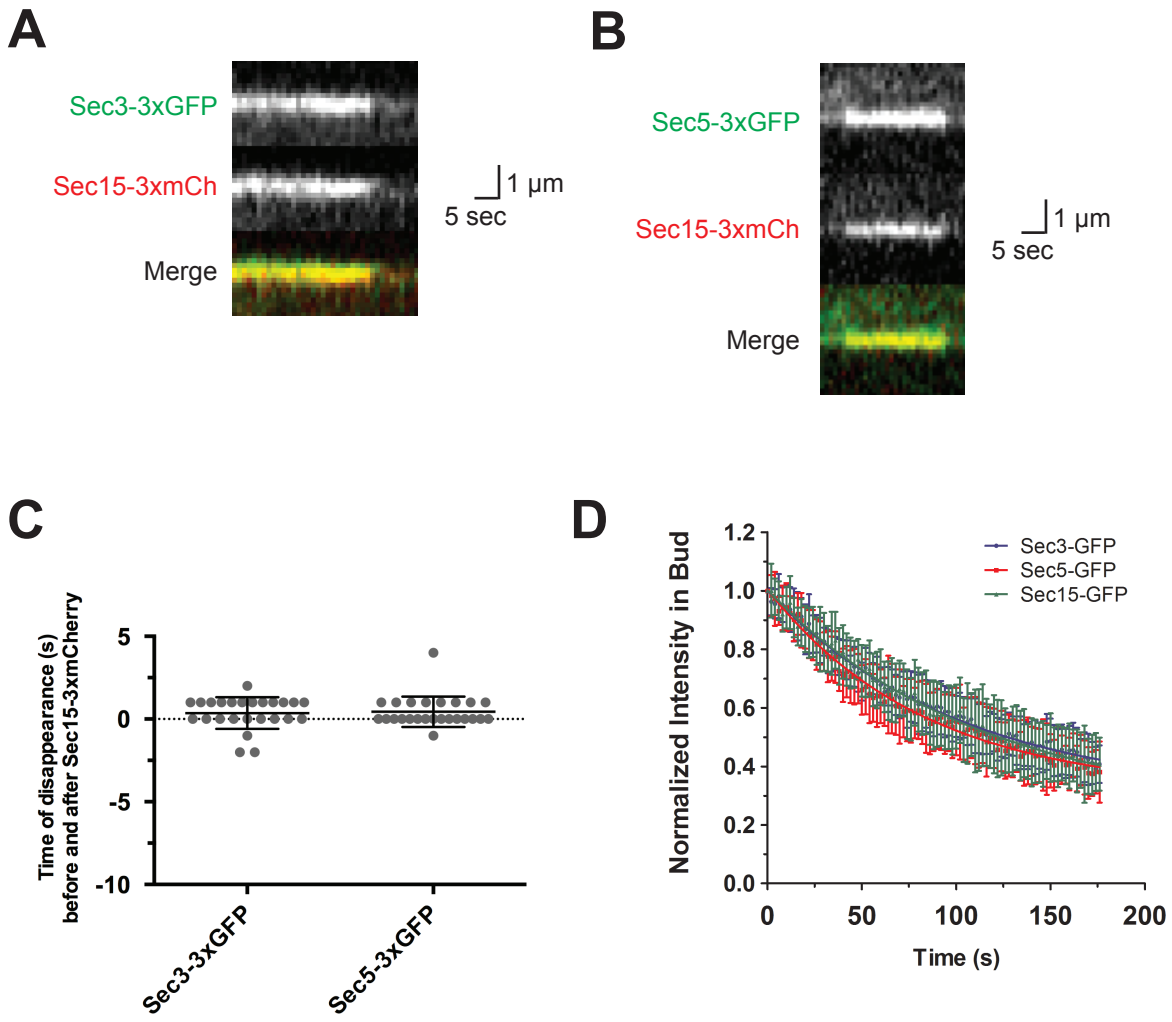

Figure 4.6. Individual exocyst components disappear at the fusion event and recycle back as a single complex.

(A) Kymographs of Sec3-3xGFP and Sec15-3xmCherry puncta during the fusion event. Each frame captured Sec3-3xGFP for 400 ms and Sec15-3xmCherry for 500 ms. The y-axis represents distance while the x-axis represents time. Scale as shown.

(B) Kymographs of Sec5-3xGFP and Sec15-3xmCherry puncta during the fusion event. Each frame captured Sec5-3xGFP for 400 ms and Sec15-3xmCherry for 500 ms. The y-axis represents distance while the x-axis represents time. Scale as shown.

(C) Column scatter plot of the time of disappearance (s) for the protein in question prior to the fusion event (Sec15p disappearance). n=25 for both datasets. Lines show mean and 95% confidence intervals.

(D) FLIP experiment showing the normalized intensity in the bud for tagged exocyst components. Best fit curves were single-exponential decay with one rate of loss. Halftimes of loss from the bud were 71.0 ± 9.4 sec (Sec3-GFP, n=15), 58.1 ± 9.4 sec (Sec5-GFP; n=13), and 78.2 ± 17.1 sec (Sec15-GFP; n=10).

DISCUSSION

Despite more than thirty years of work dissecting post-Golgi secretion, a full timeline of the order of events at the cell cortex has been elusive. This is likely due to the well-integrated signaling and interaction networks at sites of exocytosis (as shown in Figure 1.6). For instance, the Rab Sec4p binds to no fewer than seven proteins at the bud tip, and many of those binding partners also interact with one another. While much research has beautifully characterized this protein interaction network (Figure 1.6), the "order of operations" necessary for a vesicle to fuse with the plasma membrane is still murky. My goal with this line of research was to clarify the effects different proteins have on the tethering and fusion of a vesicle, as well as how the dynamics of a particular protein is integrated with others.

Before discussing these findings, I would like to explain one potential caveat of this chapter: the definition of the fusion event. Early in this work, I defined the fusion event as the frame-to-frame disappearance of GFP-Sec4. Due to the rapidity of its disappearance, and the fast rate of diffusion of plasma membrane localized GFP-Sec4, it is likely that I am imaging the diffusion of Sec4p from a relatively confined 100 nm vesicle to the entire cortex. Various approaches to confirm this was the fusion event were tried and unfortunately did not work. These included (1) the expression of a luminal-expressed pH-sensitive GFP variant that would fluoresce at the fusion event, (2) the co-localization with a v-SNARE marker (too dim) and (3) observing a decrease in fluorescence from a plasma membrane marker (mCherry-2xIst2$^{928\text{-}948}$) when the vesicle fused. Complicating the generation of fusion reporters is the fast rate of secretion in yeast, ranging from 8-30 minutes from translation to export (Novick and Schekman, 1983). The half-time for folding the common S65T GFP variant is 27 minutes (Heim et al., 1995), so any GFP molecule used with a probe would likely not have enough time to fold

correctly. Perhaps work with 'super-folding' variants of fluorescent proteins could aid in the creation of a fusion reporter.

It should also be noted that the GFP-Sec4 I used might have either GTP or GDP bound, so the timing of the hydrolysis event is unknown. To address this issue, I also tried to create a Sec4-GTP reporter (analogous to the Cdc42p CRIB probe) using known effectors. These included minimal fragments of Sro7p and Sec15p; they showed promise in yeast two-hybrid experiments but were cytosolic when fused to GFP, even when also fused to general membrane-targeting C2 domains. Despite all of this, the rapid frame-to-frame disappearance in 1.3 seconds of ~75 molecules of GFP-Sec4 is most likely due to the fusion event. If it were another biologically relevant event, such as GDI extraction of Sec4p, I would expect to see a more gradual extinction of the puncta fluorescence. Further work is clearly needed, but it is more than likely that the fusion event is really being captured.

The core finding of this chapter is a basic timeline of events (presented in Figure 4.7) that extends results presented in Chapter 2. Vesicles dock with the plasma membrane in an exocyst-mediated fashion, as expected. The total time from tethering to fusion in wildtype cells is ~18 seconds, while this is extended 2.5-fold in a mutant where GTP hydrolysis is delayed. In most wildtype vesicles analyzed, there was a gradual tapering of Myo2p from the vesicle until they completely disappear about 4 seconds before the fusion event. Vesicle fusion also appears to cause the release of the exocyst complex from the membrane, which then recycles back as one complex.

One intriguing possibility shown indirectly in this timeline is the Sec4-GTP hydrolysis event, which has not been pinpointed even though it is critical for efficient fusion to occur. Previous work has shown that Myo2p-secretory vesicle interaction is dependent on Sec4-GTP

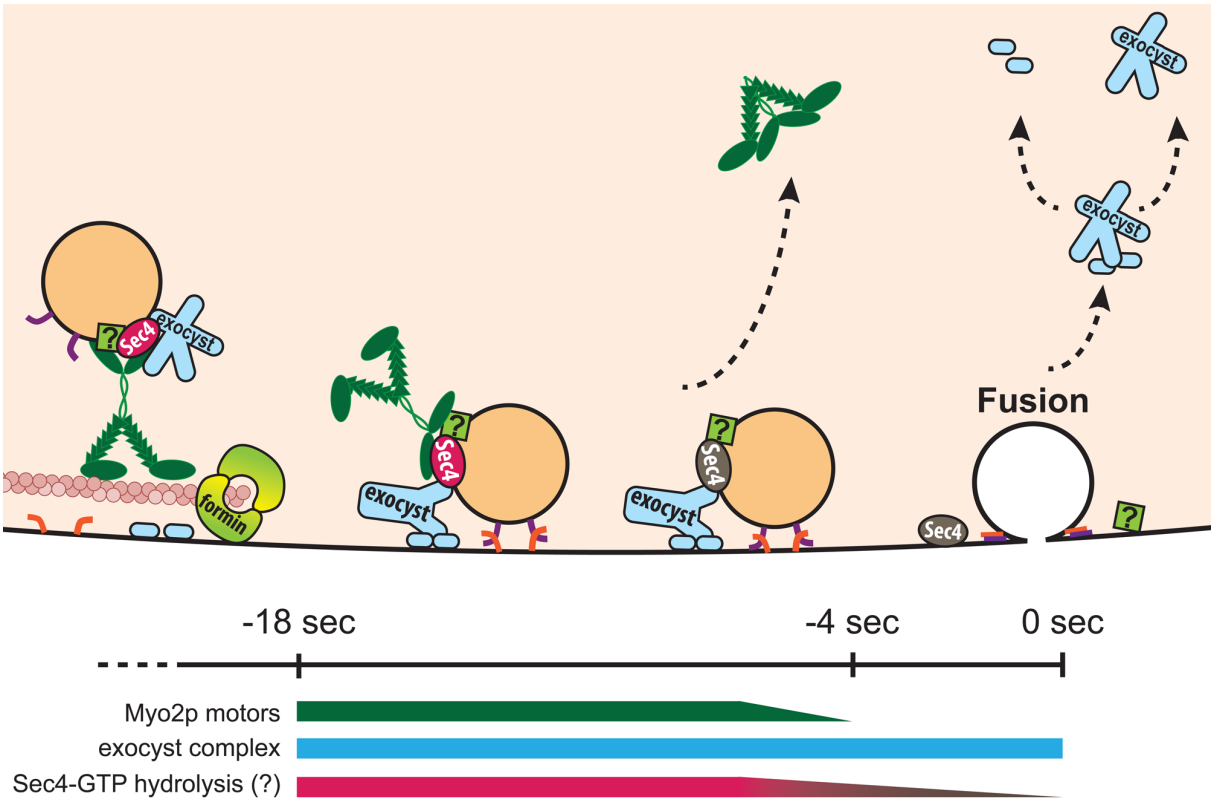

Figure 4.7. A timeline of events for exocytosis.

Several Myo2p motors (one is shown for simplicity) transport a vesicle to the bud tip through its interactions with Sec4p, the exocyst (through Sec15p) and an unknown component interacting with PI4P (shown as '?'). Vesicle tethering via the exocyst complex physically attaches the vesicle to the cortex, which lasts for 18 seconds in wildtype cells. Myo2p motors are released gradually, with all dissociated about 4 seconds prior to fusion. This may indicate that Sec4-GTP is also hydrolyzed on a continuum. Finally, the exocyst complex is released at the moment of vesicle fusion, which then likely breaks into vesicle-associated and plasma-membrane associated components for another round of tethering. Not shown is the recycling event of the SNARE proteins, Sec4p by GDI or the recycling of the unknown component of the receptor complex.

(Jin et al., 2011; Santiago-Tirado et al., 2011); in Chapter 2, I presented data showing that the hydrolysis event is required for efficient Myo2p recycling. Since there appears to be a gradual tapering of Myo2p present on vesicles up to about 4 seconds before the fusion event, an attractive hypothesis is that Sec4-GTP hydrolysis stimulated by Msb3/4p happens in a small window of time *before* the actual fusion event occurs. This would fit with known data provided the SNARE complex has already formed, as mutants with defective Sec4p show reduced SNARE complex formation (Grote and Novick, 1999). Since the vesicle has already been tethered for ~14 seconds before Myo2p is gone, this seems plausible. In addition, the finding that constitutively active Sec4-Q79Lp directly increases tethering time makes sense given previous results. Mutants where the event is defective show a build up of vesicles in the bud (Walworth et al., 1992).

Does data from this chapter square with data presented in Chapter 2? In the first chapter, I showed that there are two populations of Myo2p motors in the bud: a faster diffusive component (those that are inactive or have already dissociated and in the process of recycling) and a slower component made up of motors that are present on secretory vesicles and need to be released. This faster population has a half-time of loss of ~10 seconds while the slower population on docked vesicles takes ~30 seconds to recycle. Since Myo2p is present on these vesicles for ~14 seconds after tethering, it is remarkable how well the numbers fit together for Myo2p; if given a few seconds for transport of the vesicle to the docking site and ~10 seconds to recycle after release, the two methods presented in this thesis converge on similar answers. Less well-fitting is the recycling data for Sec4p, which I showed had a half-time of loss from the bud of ~90 seconds in one-phase decay. If the vesicle spends a few seconds being transported to the docking site, and ~18 seconds docked, the rest of that time (more than a minute) needs to be

made up for post-fusion. The only explanation for this is if its GDI extraction and recycling takes some time. It has been shown *in vitro* that Cdc42 extraction by GDI takes less than 10 seconds (Nomanbhoy et al., 1999), but since most of the GFP-Sec4 fluorescence is in the bud it seems like the only explanation.

The finding that GFP-Sec4 tethering times in *myo2-RAKA* cells show no significant difference from wildtype is interesting, as results presented in Chapters 2 and 3 suggest that a constitutively active motor takes a long time to recycle. This result also implies that the Myo2p-Sec15p interaction, also occurring at the R1402/K1473 site, is not required for efficient vesicle tethering and fusion. What is likely happening is that the ability of Myo2p to become disconnected from the vesicle is not affected in this mutant. Instead, once disconnected, the motor remains trapped at sites of growth and is unable to recycle efficiently. However, a different allele (*myo2-13*) that is also constitutively active showed contradictory results. In spite of this, the *myo2-13* allele contains mutated residues that are buried within it; it is likely that these mutations in particular distort the tail structure, as evidenced by the fact that this allele cannot easily bind to Sec4p even at the permissive temperature (Figure 2.1f) Thus, the 50% increase in the time vesicles spend tethered to the membrane in this allele is likely to be indirect, possibly through a defect in regulating downstream effectors. Since Myo2p binds to known fusion regulators, including Sro7/77p, Mso1p, and Sec4p, this possibility seems plausible.

Perhaps the most interesting finding from this timeline study relates to how exocyst complex dynamics is integrated into the fusion event. My initial hypothesis was that there must be some rearrangement of the exocyst prior to fusion, as it seemed unlikely that a large 5 x 5 x 25 nm complex could exist between the cortex and vesicle during the fusion event; I thought that the ‘v-exocyst’ would recycle back separately from the ‘t-exocyst,’ which could be detected by

two-color imaging. However, this does not appear to be the case and instead the exocyst complex recycles as a single unit as shown by FLIP experiments. In retrospect, this is in line with previous biochemical work showing that most of the individual proteins run in a large complex when separated by affinity chromatography. Nevertheless, it is interesting that Myo2p, which is Sec4-GTP dependent, recycles earlier than Sec15p, which is also Sec4-GTP dependent. There are a few explanations for this, which are not mutually exclusive. First, as pointed out before, the hydrolysis of about 75 molecules of Sec4-GTP likely occurs on a continuum; perhaps different Sec4-GTP binding partners modulate the rates of hydrolysis by GAPs Msb3/4p though their ability to access the Rab. Secondly, even if hydrolysis occurs and the vesicle-exocyst interaction is disrupted (leaving only SNARE interactions), the entire complex is still physically tethered to the cortex through its Rho/PI(4,5)P_2 linkages. Somehow, the fusion event would release the complex for recycling as a single unit. How this would occur is unknown and is complicated by the fact that Sec3p/Exo70p interactions with Rho proteins occur GTP-independently (Roumanie et al., 2005). Perhaps the influx of lipids from a 100nm vesicle during the fusion event momentarily dilutes the pool of PI(4,5)P_2 present in the cortex, leading to the disruption of Exo70p/Sec3p (and thus the entire complex) from the membrane. The localization of these proteins has been shown to be very sensitive to PI(4,5)P_2 levels, but this is just speculation.

Interestingly, a mammalian study on exocyst dynamics was published the same week I performed these experiments on exocyst dynamics (Rivera-Molina and Toomre, 2013). Sec8-tagRFP was localized to vesicles, was found at the membrane for only ~8 seconds, and recycles ~2 seconds *after* the fusion event. These mammalian results give confidence to my findings that tethering times are short and the exocyst remains cortex-localized until the moment of fusion. What is happening after fusion and what releases the exocyst is still a mystery though.

The recycling of the exocyst brings up another complication. My data show that three exocyst components all disappear from the vesicle at the fusion event (if one uses the transitive principle, since Sec4p/Sec15p disappeared together while each Sec3p/Sec15p and Sec5p/Sec15p disappear together). These components have a halftime of loss from the bud of ~70 seconds, which doesn't seem consistent with the recycling time following an 18 second tethering event. One explanation is that the diffusion rates of a nearly mega-Dalton complex is drastically reduced from normal proteins, though this seems unlikely as a single ~550 kDa Myo2p motor (with light chains) recycles relatively quickly. An alternate explanation may simply be binding to a different site on the membrane following fusion, or even binding to another vesicle about to engage in the tethering step. After disappearance from the fusion event, it is possible that the exocyst may diffuse to a different site on the cortex. Anecdotal evidence may support this, as in a few instances I saw Sec15p puncta on the cortex that did not appear to colocalize with any Sec4p puncta. More work would be needed to show this conclusively though. Also a mystery is when (and how) Sec3p/Exo70p dissociate from the rest of the complex, as they are the only two components that localize independently of vesicle trafficking (Boyd et al., 2004). Most likely, a rearrangement of the exocyst occurs in the cytoplasm after recycling that separates Sec3p/Exo70p and allows them to function on the cortex for another round of tethering.

Results presented here show a basic timeline of events in exocytosis. Future work will need to address the dynamics of additional proteins in the pathway, as well as how their dynamics change in different mutants. However, a few problems complicate going in this direction. First, most proteins involved in vesicle secretion after the tethering step (Sec1p, Sec9p, Sso1p, etc.) are diffusely polarized on the cortex and not restricted to punctuate structures. This makes observing their individual dynamics almost impossible. Additional work will likely need

to be done using super-resolution microscopy to understand the single molecule dynamics of these proteins. Secondly, performing additional tethering experiments in post-tethering mutants (such as in *sec9-4* and *sec1-1*) is challenging due to their defects in secretion. Even at the permissive temperature, the vast majority of GFP-Sec4 is present in the bud; new vesicles entering the bud following bleaching seem to be dimmer and harder to track. Secondly, the secretion machinery is likely saturated even at the permissive temperature given the number of vesicles in the bud. Tracking newly arriving vesicles and waiting until a few of them tether to the membrane would require *a lot* of movies and analysis. Nevertheless, this may be an area that could be explored in the future.

REFERENCES

Boyd, C., Hughes, T., Pypaert, M., and Novick, P. (2004). Vesicles carry most exocyst subunits to exocytic sites marked by the remaining two subunits, Sec3p and Exo70p. J. Cell Biol. *167*, 889–901.

Donovan, K.W., and Bretscher, A. (2012). Myosin-V Is Activated by Binding Secretory Cargo and Released in Coordination with Rab/Exocyst Function. Dev. Cell *23*, 769–781.

Gietz, R.D., Schiestl, R.H., Willems, A.R., and Woods, R.A. (1995). Studies on the transformation of intact yeast cells by the LiAc/SS-DNA/PEG procedure. Yeast *11*, 355–360.

Grote, E., and Novick, P. (1999). Promiscuity in Rab-SNARE interactions. Mol. Biol. Cell *10*, 4149.

Heim, R., Cubitt, A.B., and Tsien, R.Y. (1995). Improved green fluorescence. Nature *373*, 663–664.

Hsu, S.-C., Hazuka, C.D., Roth, R., Foletti, D.L., Heuser, J., and Scheller, R.H. (1998). Subunit Composition, Protein Interactions, and Structures of the Mammalian Brain sec6/8 Complex and Septin Filaments. Neuron *20*, 1111–1122.

Jin, Y., Sultana, A., Gandhi, P., Franklin, E., Hamamoto, S., Khan, A.R., Munson, M., Schekman, R., and Weisman, L.S. (2011). Myosin V Transports Secretory Vesicles via a Rab GTPase Cascade and Interaction with the Exocyst Complex. Dev. Cell *21*, 1156–1170.

Kaksonen, M., Sun, Y., and Drubin, D.G. (2003). A pathway for association of receptors, adaptors, and actin during endocytic internalization. Cell *115*, 475–487.

Lamping, E., Tanabe, K., Niimi, M., Uehara, Y., Monk, B.C., and Cannon, R.D. (2005). Characterization of the Saccharomyces cerevisiae sec6-4 mutation and tools to create S. cerevisiae strains containing the sec6-4 allele. Gene *361*, 57–66.

Nomanbhoy, T.K., Erickson, J.W., and Cerione, R.A. (1999). Kinetics of Cdc42 membrane extraction by Rho-GDI monitored by real-time fluorescence resonance energy transfer. Biochem. *38*, 1744–1750.

Novick, P., and Schekman, R. (1983). Export of major cell surface proteins is blocked in yeast secretory mutants. J. Cell Biol. *96*, 541–547.

Rivera-Molina, F., and Toomre, D. (2013). Live-cell imaging of exocyst links its spatiotemporal dynamics to various stages of vesicle fusion. J. Cell Biol. *201*, 673–680.

Roumanie, O., Wu, H., Molk, J.N., Rossi, G., Bloom, K., and Brennwald, P. (2005). Rho GTPase regulation of exocytosis in yeast is independent of GTP hydrolysis and polarization of the exocyst complex. J. Cell Biol. *170*, 583–594.

Santiago-Tirado, F.H., Legesse-Miller, A., Schott, D., and Bretscher, A. (2011). PI4P and Rab

inputs collaborate in myosin-V-dependent transport of secretory compartments in yeast. Dev. Cell *20*, 47–59.

Sherman, F. (2002). Getting started with yeast. Met. Enzymol. *350*, 3–41.

TerBush, D.R., and Novick, P. (1995). Sec6, Sec8, and Sec15 are components of a multisubunit complex which localizes to small bud tips in Saccharomyces cerevisiae. J. Cell Biol. *130*, 299–312.

Walworth, N.C., Brennwald, P., Kabcenell, A.K., Garrett, M., and Novick, P. (1992). Hydrolysis of GTP by Sec4 protein plays an important role in vesicular transport and is stimulated by a GTPase-activating protein in Saccharomyces cerevisiae. Mol. Cell Biol. *12*, 2017–2028.

Weinberg, J., and Drubin, D.G. (2012). Clathrin-mediated endocytosis in budding yeast. Trends Cell Biol. *22*, 1–13.

CHAPTER 5

SUMMARY AND FUTURE DIRECTIONS

Most studies of class-V myosin motors have focused on how they interact with various cargoes and effector proteins. Missing from such analyses is the dynamic properties of the motors and how their dynamics is regulated at the molecular level. In this thesis, I have attempted to clarify and characterize how one canonical myosin-V motor, Myo2p, coordinates its actions with those of its essential cargo of secretory vesicles. Using several imaging techniques coupled to genetic and biochemical work, I have described the transport cycle of Myo2p at four distinct stages: (1) binding and activation, (2) transport, (3) release from cargo, and (4) recycling. Since most of the proteins relevant to this transport cycle are conserved in higher organisms, these results are likely widely applicable.

I will first take a moment to summarize the key findings of this work at the four different stages of the Myo2p transport cycle. One of the major results is that Myo2p is activated from an inactive state by binding to a competent secretory vesicle. This contradicted a previous study that suggested the polarization state of Myo2p is unaffected by its cargo. The previous analysis comes from a series of conditional Myo2p tail mutants, which at the restrictive temperature leave secretory vesicles behind in the mother cell but can still move to sites of growth. While this conclusion was supported by the available data, I show in Chapter 2 that a wildtype Myo2p motor requires competent secretory cargo in order to polarize. Without an active secretory system, such as in *sec4-8* and *sec23-1* cells, Myo2p motors are found depolarized throughout the cytoplasm. Further, it seems likely that direct binding to Sec4p activates Myo2p as opposed to other components of the receptor complex. The most direct experiment testing this is the finding

that Myo2-Y1415R-GFP, which cannot bind Rab proteins, is significantly more depolarized than wildtype motors.

Using sensitive *in vivo* quantification techniques, I showed that approximately 10 Myo2p motors bind to secretory vesicles before being transported to sites of growth. The fact that there are so many suggests that the rate-limiting step to transport is finding and engaging an actin cable. Once motors have transported their cargo into the bud, motors stay bound until they reach the cortex. This was deduced by comparing quantitative immunoblots with whole-cell projections of fluorescently tagged proteins in different regions of the bud. The fact that there was an equal number of "vesicle complements" of Myo2p and Sec4p at the bud tip suggested the two proteins do not dissociate until they arrive at the cortex.

Experiments with conditional exocyst complex members and SNARE proteins strongly argue that Myo2p is released at a point after vesicle tethering but before vesicle fusion. This was later confirmed through single-vesicle tracking experiments, where Myo2p was found to leave vesicles about 4 seconds prior to fusion. The signal to release Myo2p from vesicles appears to be the Sec4-GTP hydrolysis event, as motors were defective in recycling when Sec4p GAP proteins Msb3/4p were deleted or experiments in cells containing constitutively active Sec4-Q79Lp. Work with hyperactive Myo2p mutants showed that Myo2p must become deactivated, likely through head-to-tail autoinhibition, in order to recycle efficiently from sites of growth. When this regulation is perturbed, Myo2p remains polarized and essential cargo transport functions of the motor are severely compromised.

Other experiments using single-vesicle tracking techniques showed that vesicles are only tethered for about 18 seconds, and the time from tethering to fusion is modulated by the ability of Sec4-GTP to be hydrolyzed. Further, the timeline of exocytic events was built out by studying

exocyst complex dynamics. The exocyst complex appears to recycle back as a single complex and is released from vesicles at the moment of fusion, as determined by two-color live cell imaging and FLIP experiments.

The most obvious direction to take for future work is to develop a more complete model of events occurring at the bud tip using the single-vesicle tracking technique presented in Chapter 4. Unfortunately, I have likely pinpointed the dynamics of most of the low-hanging fruit. The major problem with observing other proteins is that many of them are distributed along the cortex in a polarized manner and not clustered together (such as on a vesicle or endocytic patch). Additional work may need to be done with super-resolution techniques to visualize the dynamics of these proteins. Important players that could be added to the model include the SM-like protein Sec1p, the GEF Sec2p, the kinesin-like Smy1p, and the Rab Sec4p. While the dynamics of the Rab Sec4p were quite clearly shown in this thesis, the model would be greatly enhanced by knowing when the Sec4-GTP hydrolysis event is actually occurring. To this end, I tried on two separate occasions to design fluorescent reporters with known Sec4-GTP effector domains (analogous to the CRIB-probe for Cdc42-GTP), but these were unsuccessful. The dynamics of Myo2p leaving vesicles suggests that the hydrolysis event occurs well before fusion, but a targeted reporter might show this more clearly.

One fruitful area to take single-vesicle tracking experiments is not at the cortex, but observing vesicles mature from the trans-Golgi network. Our lab has movies of Ypt32p-positive structures breaking up into smaller puncta, and work presented at meetings suggests that Sec4p and Ypt32p can coexist on the same membrane. Observing the dynamics of a maturing vesicle, as Ypt31/32p, Sec4p, Sec2p, Myo2p, and the exocyst complex are added and lost, would be quite informative. For instance, does the loading of Myo2p happen rapidly? This could suggest some

cooperative binding effect for the motor. Performing this experiment in different mutants might reveal key regulatory steps similar to those I showed at the cortex. I performed pilot experiments attempting just this; the problem is that secretory vesicles diffuse around the cytoplasm very quickly (TGN membranes are slow by comparison) and capturing several imaging planes in two or three colors makes it unfeasible. Using more sensitive cameras (or those that capture two colors simultaneously) might help mitigate this effect.

Another avenue for future research is determining how individual Myo2p effectors influence the motor's dynamics. Some of this work is presented in the appendix following this chapter, and I show how overproduction of Smy1p, Sec4p, and PI4P affect motor transport and recycling. A more complete picture of how these (and other) accessory proteins affect Myo2p might be achieved through reconstitution studies of Myo2p, though this might prove very difficult. Our lab has had some success purifying the tail of Myo2p and seeing how known components of the receptor complex affect its binding to liposomes; purifying the entire motor and performing similar studies to probe events like cargo activation would be immensely challenging.

Going along with this idea, it would be interesting to see how competition between different receptors affects the dynamics of Myo2p. Competition has been observed *in vivo* in work from the Weisman lab, as motors defective in vacuole binding have a greater volume of mitochondria inherited and vice versa. I would suspect that the dynamics of the motor would change as well, which could be probed by the photobleaching techniques presented in this paper. For instance, overexpression of the receptor Mmr1p has been shown in our lab to hyperpolarize Myo2p to very punctate structures at the bud tip. This would likely lead to motors that are unable

to recycle efficiently. Probing this in targeted *myo2*, *ypt11* and *mmr1* mutants may yield important insights into how the transport cycle of Myo2p can be modulated.

The past decade of Myo2p research has been very exciting. Nearly all receptors for known cargoes have been found and we now have a very complete picture of receptor-mediated transport. Future work will need to extend these results and explain how these cargoes, receptors, and their accessory proteins can modulate the transport cycle of Myo2p. As I have shown for the essential cargo of secretory vesicles, Sec4-GTP receptor binding and accessory factors such as the exocyst can have an enormous impact on this transport cycle. Taking a dynamics-based approach, using some of the techniques outlined in this paper, will very likely lead to further insights. Understanding their influence in budding yeast could lead to additional breakthroughs of myosin-V function affecting human health and disease.

APPENDIX

MODULATING MYO2 DYNAMICS BY DISTURBING ASSOCIATED PROTEINS AND LIPIDS

OVERVIEW

Part of this thesis used selected conditional secretory mutants to modulate the dynamics of Myo2p. I took advantage of this to propose a model for how Myo2p is released and recycled from secretory vesicles. In particular, I showed that when the exocyst complex or the ability of Sec4-GTP to hydrolyze is disturbed, Myo2p remains in the bud for 2-3 fold longer and thus cannot recycle efficiently. While these secretory mutants gave great insight into the transport cycle of Myo2p, I wondered if deleting or overexpressing known binding partners could modulate Myo2p dynamics as well. I will present some of the findings from these experiments and suggest reasons for why the motor's dynamics change. These are areas that could be pursued in the future.

MATERIALS AND METHODS

Deletion of genes was carried out by either PCR cassette methods or using the yeast deletion consortium collection and checking by PCR to ensure the correct gene is deleted. Overexpression of Rab proteins was accomplished by cloning full length *SEC4*, *YPT31*, or *YPT51* with their own terminators behind the $Gal_{1/10}$ promoter on a pRS315 vector. Overexpression was induced in SRaff-Leu media with 2% galactose for the indicated times. Overexpression of full length *SMY1* was similarly done through a 1 hour Gal overexpression. Overexpression of *PIK1* was performed using a pRS425 2-micron plasmid and compared to a vector only control. FRAP and FLIP experiments with Myo2-GFP were performed as described

in Chapter 2. Molecule counting experiments were performed using methods described in Chapter 2.

For experiments with the actin treadmilling mutant, experiments were performed using the Drubin lab wildtype strain (ABY105) and the *act1-V159N* allele from their lab (ABY3110). Actin was visualized using a pRS316-pADH1-Lifeact-GFP plasmid created in our lab by MJ Shin. Growth assays were carried out using a 1:10 serial dilution assay as described in previous chapters. FLIP experiments with Myo2-3xGFP were performed as described.

RESULTS AND DISCUSSION

Overexpression of SEC4 leads to increased motor recruitment on vesicles, but doesn't change the transport dynamics of Myo2p

The Myo2p-Sec4p and Myo2-Ypt31/32p interactions are essential for viability (Lipatova et al., 2008; Santiago-Tirado et al., 2011). To determine if the absolute number of either of these Rabs altered the dynamics of Myo2p in the cell, I first overexpressed them for one or three hours and observed their phenotype (Figure A.1a). Overexpression was driven by the $Gal_{1/10}$ promoter, and done in media containing 2% galactose. There was no change in the phenotype of Myo2-GFP when either *YPT31* or the control endocytic Rab *YPT51* were overexpressed. However, I did notice an increase in brightness of Myo2-GFP-positive punctate structures in the cell when *SEC4* was overexpressed, which could indicate increased recruitment of Myo2p to secretory vesicles.

In Chapter 2, I showed that ~10 motors bind to secretory vesicles and transport them to sites of growth. They do this by binding to the Rab Sec4p and an unknown component dependent on PI4P. To determine if the numbers of receptors on the vesicle might be important for the number of Myo2-3xGFP motors recruited, I overexpressed Sec4p from the Gal promoter and

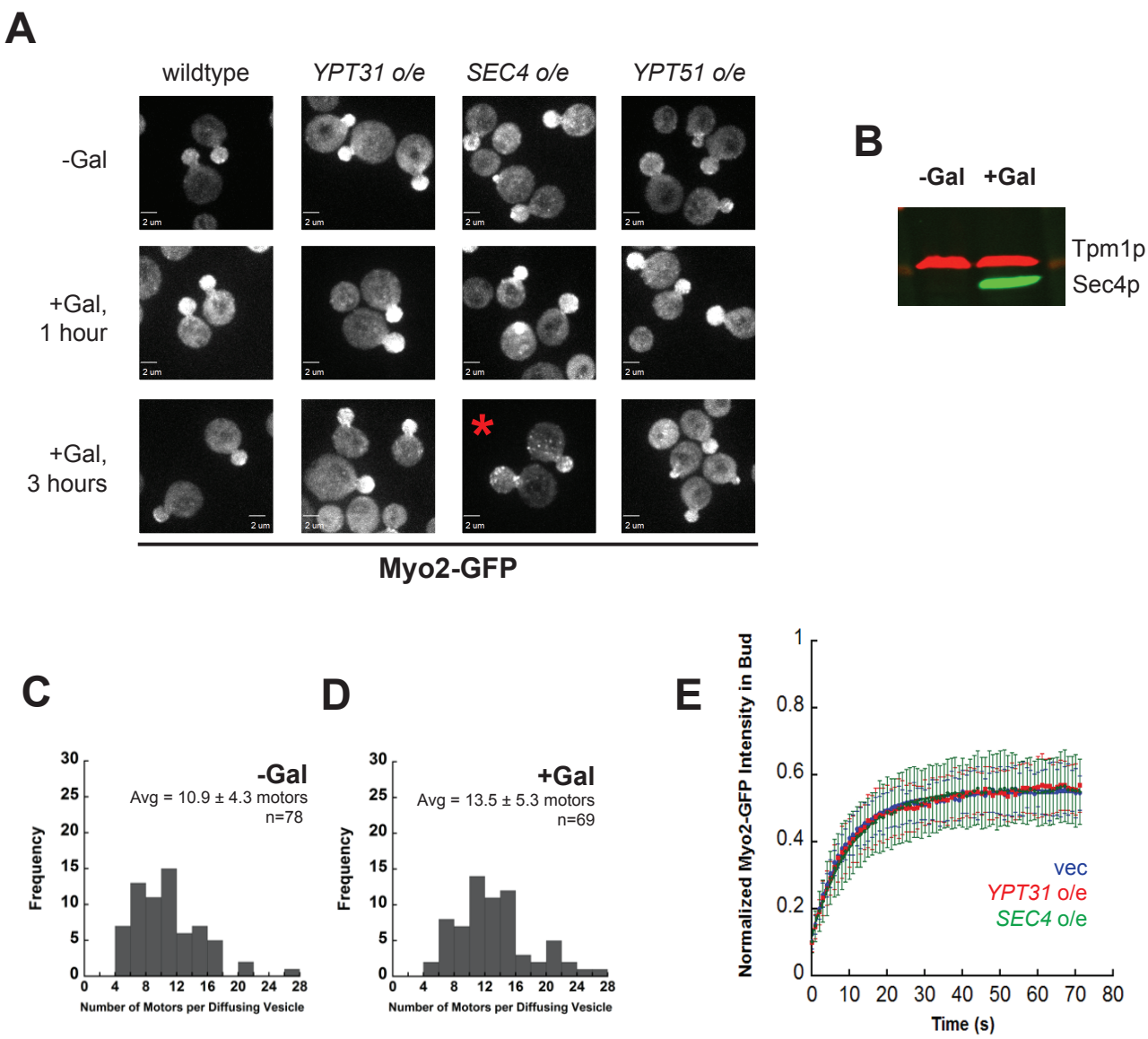

Figure A.1. Overexpression of Rab proteins increases the number of motors on vesicles, but doesn't change the transport dynamics of Myo2p.

(A) Myo2-GFP phenotypes when Rabs *YPT31*, *SEC4*, and *YPT51* are overexpressed with 2% galactose for 1 or 3 hours. Note the increase in cytoplasmic Myo2-GFP puncta during 3 hour *SEC4* induction (*). Scale bars are 2 μm.

(B) Induction of *SEC4* is robust during 3 hour +Gal induction. Tpm1p used as a loading control. Note that the Sec4p antibody does not detect endogenous levels of Sec4p well.

(C) Number of Myo2-3xGFP motors per diffusing vesicle without induction of Sec4p. Average is 10.9 ± 4.3 motors (n=78).

(D) Number of Myo2-3xGFP motors per diffusing vesicle with 3 hour induction of Sec4p. Average is 13.5 ± 5.3 motors (n=69).

(E) Normalized Myo2-GFP inensity in bud during 3 hour Rab overexpression in FRAP experiment. All curves show a half-time to recovery of about 7.5 ± 2.5 sec (n=13-14).

performed quantitative motor counting experiments as described in Chapter 2. Sec4p was clearly overexpressed over the 3 hour induction time as characterized by the increase in Sec4p levels (Figure A.1b). Note that the antibody used is not very sensitive toward endogenous levels of Sec4p, but judging from the blot the number of Sec4p molecules in the lysate goes up significantly when overexpressed. Also, I have no way of knowing if all of these Sec4p molecules are bound to a vesicle and activated by Sec2p (more than likely they are not). However, when molecule-counting experiments were performed with vesicles diffusing in the cytoplasm, there was a significant increase in the number of Myo2-3xGFP motors per vesicle, from 10.9 ± 4.3 (n= 78; Figure A.1c) to 13.5 ± 5.3 (n=69; Figure A.1d). This suggests that the absolute number of Sec4p receptors is responsible for recruiting Myo2p motors.

I find this quite surprising though, as the number of Sec4p molecules on vesicles is already 3-fold greater than the number of Myo2p motors (if both tails are binding to Sec4p as might be expected). This result does make sense though in light of other work from our lab by post-doctoral associate Li Xu. When she reduced the levels of Sec4p in the cell ~4-fold (by changing the promoter), the number of Myo2p motors on vesicles was significantly reduced (unpublished data). This suggests that the absolute number of Myo2p motors binding secretory vesicles is influenced by the amount of available receptors.

Since the number of motors that are recruited to the vesicle appears to increase when *SEC4* is overexpressed, I next wanted to determine if the transport dynamics of Myo2p changes. I overexpressed either *SEC4* or *YPT31* for 3 hours from the Gal promoter and performed standard FRAP photobleaching experiments as described in Chapter 2 (Figure A.1e). There was no difference in the recovery rates when either Rab was overexpressed compared with the vector control, suggesting that the numbers of motors doesn't change the forward transport dynamics of

Myo2p. Half-times of recovery were all approximately 7.5 ± 2.5 sec (n=13-14). Note that the half-time of recovery for Myo2-GFP in this system is slightly less than those shown in Chapter 2; this was the first experiment I performed on a new photobleaching system and that may be the cause of it. This result is not that surprising, since increased numbers of motors would probably not change the velocity of vesicle transport.

SMY1 deletion causes no effect on the dynamics of Myo2p, but its overexpression results in motors that are significantly delayed in recycling.

As briefly mentioned in the introduction, Smy1p is a nonessential binding partner of Myo2p. It is a non-functional kinesin homolog that binds the tail of Myo2p at an unknown site, though some evidence from our lab indicates that it binds to subdomain II at the very C-terminus of the tail (Kyaw Myo Lwin, unpublished data). Interestingly, it has been implicated in a number of diverse functions, including modulating formin Bnr1p activity (Chesarone-Cataldo et al., 2011) and serving as an electrostatic tether to increase Myo2p processivity (Hodges et al., 2009). To determine the effects this interesting non-essential protein has on the dynamics of Myo2p, I did several photobleaching experiments in strains that were either overexpressing *SMY1* or in cells where *SMY1* was deleted.

Deletion of *SMY1* resulted in cells that grew no different than wildtype at several temperatures. I first observed the phenotype of Myo2-GFP in wildtype and *smy1Δ* cells; there were no obvious phenotypic differences between the two strains (Figure A.2a). When subjected to both FRAP and FLIP experiments, I also saw no difference in the transport or recycling rates of Myo2-GFP between wildtype and *smy1Δ* cells (Figures A.2b-c). This implies that the loss of Smy1p is not critical for the transport or recycling of Myo2p. If Myo2p were indeed aided by

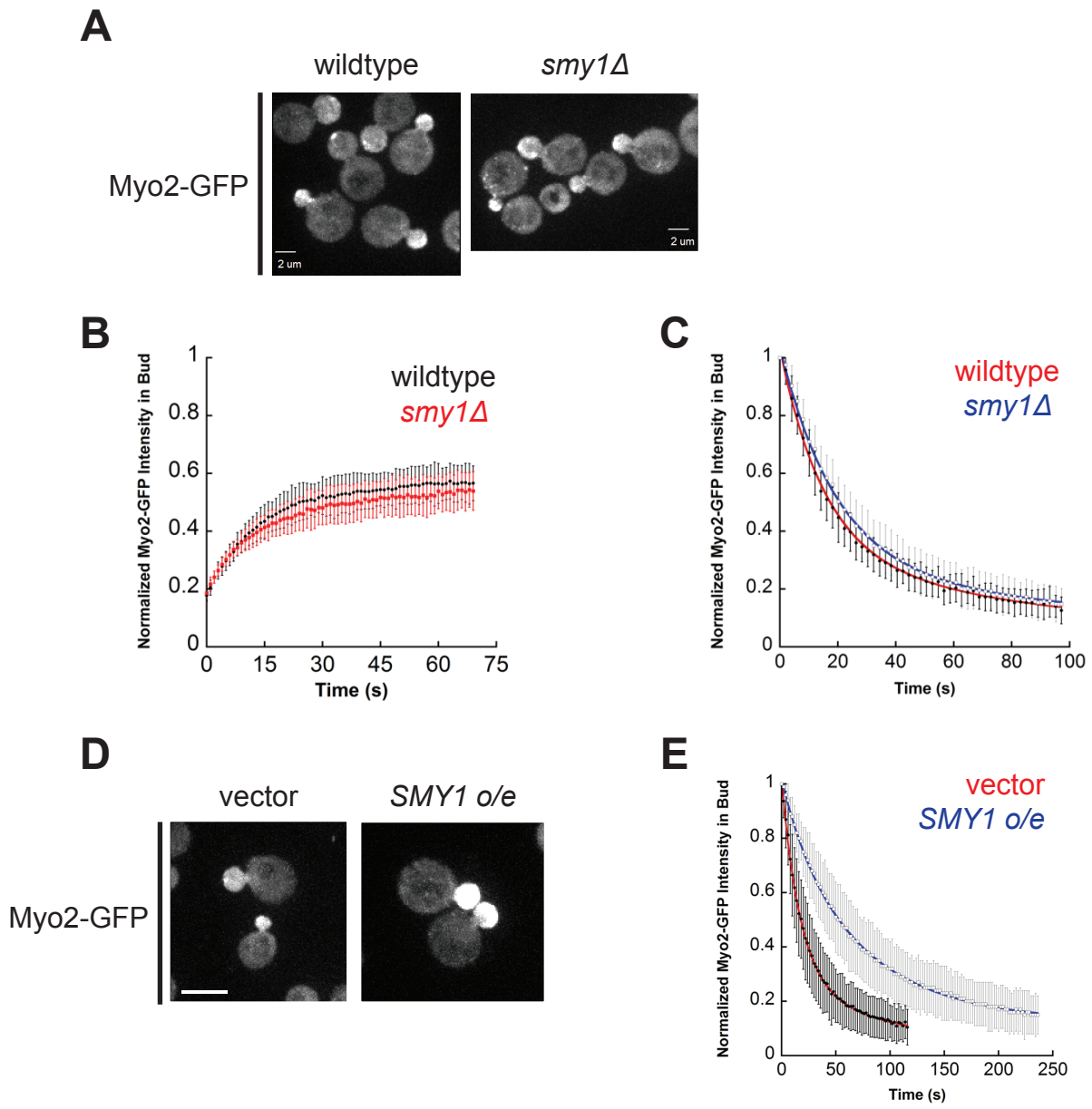

Figure A.2 *SMY1* deletion causes no effect on the dynamics of Myo2p, but its overexpression results in motors that are significantly delayed in recycling.

(A) Myo2-GFP phenotype in wildtype and *smy1Δ* strains. Scale bars are 2 µm.

(B) Normalized Myo2-GFP intensity in the bud for wildtype and *smy1Δ* cells in FRAP experiment. There is no significant difference in the rates of recovery (n=12 each).

(C) Normalized Myo2-GFP intensity in the bud for wildtype and *smy1Δ* cells in FLIP experiment. There is no significant difference in the rates of loss from the bud (n=12 each).

(D) Myo2-GFP phenotype in vector control cells and cells overexpressing *SMY1* for 1 hour with 2% Gal. Note the hyperpolarization of Myo2-GFP. Scale bar is 5 µm.

(E) Normalized Myo2-GFP intensity in the bud of vector and *SMY1* overexpressing cells in FLIP experiment. There was a significant 2-fold increase in the half-times of loss for the vesicle associated fraction when *SMY1* was overexpressed. n=12 each.

Smy1p as an electrostatic tether, I might have expected to see some difference in the recovery rates between the two strains. This difference may be undetectable though.

However, when Smy1p was overexpressed by the Gal promoter for only one hour, there appeared to be an increase in the amount of Myo2p motors present in the bud compared to the vector control (Figure A.2d). That is, overexpression of Smy1p hyperpolarizes Myo2p. To determine if the recycling dynamics of Myo2p change, I performed FLIP experiments between induced and uninduced strains. When Smy1p was overexpressed for 1 hour, recycling of Myo2p was significantly delayed (Figure A.2e). We have some evidence that Smy1p may be acting as a non-essential "bridge" protein between Sec4p and Myo2p (Kyaw Myo Lwin, unpublished data). While this model is still underdeveloped, perhaps overexpression of Smy1p maintains the Sec4p-Myo2p interaction for longer at the bud tip, resulting in motors that are unable to recycle. This is an interesting hypothesis and definitely one that should be pursued further.

Increasing PI4P levels affects the ability of Myo2p to recycle, but does not change motor transport dynamics

Work done in our lab has shown a role for PI4P in linking Myo2p to secretory membranes. However, this interaction does not appear to be direct, leading us to suggest that an unidentified factor exists to link the motor to PI4P. We also have some evidence that GEF Sec2p may bind to Myo2p, which could be the identity of the receptor since Sec2p also binds to PI4P directly (Felipe Santiago, unpublished data; Mizuno-Yamasaki et al., 2010). However, Sec2p is depolarized in the conditional *pik1-101* kinase mutant after 1 hour at the restrictive temperature while Sec6p was still polarized, indicating vesicles are still transported (Mizuno-Yamasaki et al., 2010). This makes it likely that another protein may serve as the receptor protein.

Regardless, I reasoned that the dynamics of Myo2p might change if I modulate this unidentified receptor's interaction with Myo2p. To this end, I started disturbing PI4P levels. PI4P is synthesized at the Golgi by the Pik1p kinase (Flanagan et al., 1993; Walch-Solimena and Novick, 1999). Overexpression of has been shown to increase PI4P levels modestly, no more than 1.5-2 fold (Garcia-Bustos et al., 1994; Santiago-Tirado et al., 2011). However, when subjected to FRAP experiments, there was no significant change in Myo2p's transport dynamics compared to the vector control (Figure A.3a).

I also wanted to determine if modulating the cortex pool of PI4P could affect Myo2p transport and recycling dynamics. PI4P is dephosphorylated by Sac1p, acting in *trans* from the ER to influence the cortex pool of PI4P. Deletion of Sac1p has been shown to boost cortex-localized pools of PI4P about 8-fold (Foti et al., 2001). As expected, there was no significant change in the transport dynamics of Myo2p as deduced from a FRAP experiment (Figure A.3b). The decrease in the mobile population of motors is likely due a slight hyperpolarization of the motor; when bleached, there are fewer motors in the mother cell observed to take their place.

Strikingly, there was a small but significant increase in the half-times of loss of vesicle-associated motors from the buds of *sac1Δ* cells compared to wildtype (Figure A.3d), Half-times of loss for this population increased from 23.2 ± 9.4 sec (n=15) to 43.6 ± 20.7 sec (n=16). This indicates that when PI4P levels are increased at the cortex, the ability of Myo2p to recycle is slightly reduced. The most likely explanation of this is related to the coincidence detection model we have proposed, as both PI4P and Sec4p together are important for recruitment of Myo2p to secretory vesicle. In *sac1Δ* cells, boosting PI4P levels 8x at the plasma membrane may tilt the scales enough such that the PI4P-Sec4p-Myo2p interaction persists longer, thereby delaying

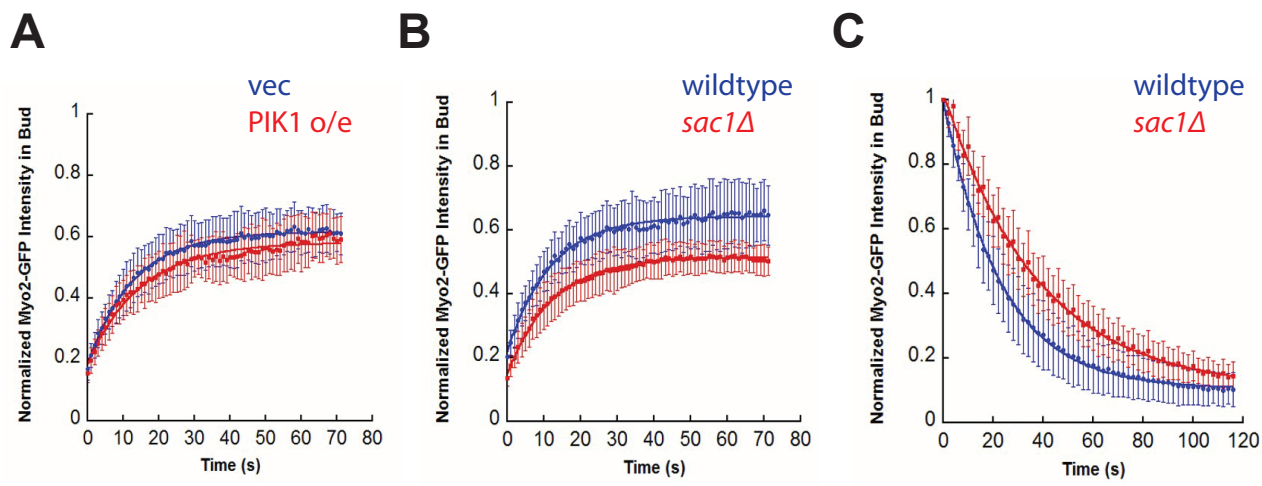

Figure A.3. Increasing PI4P levels affects the ability of Myo2p to recycle, but does not change transport dynamics.

(A) FRAP experiment of Myo2-GFP with vector control and *PIK1* overexpression strains. There was no significant difference in the rates of recovery into the bud (n=11,14).
(B) FRAP experiment of Myo2-GFP in wildtype and *sac1Δ* strains. There was no significant difference in the rates of recovery into the bud (n=12,14). The mobile fraction of *sac1Δ* likely decreased because of a slight hyperpolarization phenotype, which would reduce the number of observable motors in the cell when bleached
(C) FLIP experiment of Myo2-GFP in wildtype and *sac1Δ* strains. There was a significant increase in the half-time of loss for vesicle-associated population of motors, going from 23.2 ± 9.4 (n= 15) for wildtype to 43.6 ± 20.7 with *SAC1* deleted (n= 16).

recycling. Alternatively, unrelated vesicle fusion defects could delay timing of the release of the motor, which could be detected by vesicle-tracking assays.

Myo2p likely recycles back by diffusion, and not actin treadmilling as some models suggest

Since myosin-V motors adopt an inactive closed form that I showed can have wide-ranging effects on their ability to transport cargo, I wanted to test two models for Myo2p recycling. As previously discussed in the introduction, two contrasting models exist for the f-actin binding state of Myo2p when inactive. One model suggests myosin-V is in a post-power stroke conformation indicative of tight f-actin binding while another suggests the motor is in a post-rigor conformation predicted to have weak f-actin affinity. Since the primary difference is related to filamentous actin binding, it has been proposed that tight binding would allow the motor to recycle out of f-actin rich areas through actin treadmilling (Liu et al., 2006). In yeast, this occurs at 300 nm/s (Yang and Pon, 2002). An analysis of rates of recycling presented in Chapter 2 was inconclusive as to whether actin treadmilling plays a role, and is complicated by the second-order fit of motor populations leaving the bud. If the faster rate is free motors in the bud as discussed, a ~10 second recycling half-time of loss could be accomplished by actin treadmilling or diffusion given the size of the buds used. However, what is needed is a more direct test.

To discern if Myo2p recycles back on actin cables, I performed FLIP experiments in wildtype cells and an actin mutant, *act1-V159N*. This mutant has been shown *in vitro* to have 1/3 slower filament assembly and depolymerization (Belmont and Drubin, 1998; Belmont et al., 1999). Effectively, this creates a mutant that has 1/3 slower rates of treadmilling. Cells containing this mutation grow about half as fast as wildtype cells and feature a relatively

organized actin cytoskeleton with slightly longer cables (Figures A.4a-b). Despite my best efforts, I was unable to determine if the *in vitro* rates of polymerization are similar to those found *in vivo* with formins. Methods to check filament extension using actin binding proteins Lifeact-GFP and Apb140-GFP, as well as observing Bni1-3xGFP speckles in retrograde flow, were all inconclusive. When FLIP experiments with Myo2-GFP were performed between *ACT1* and *act1-V159N* cells, there was no difference in the ability of Myo2p to recycle (Figures A.4c-d). If this mutant performs as it does *in vitro*, this would indicate that Myo2p does not recycle back on actin cables; instead, it is more likely the diffusion-based method supported by Hammer and Sellers. I have never observed Myo2p stuck on actin structures in the bud under normal conditions, so this result seems correct.

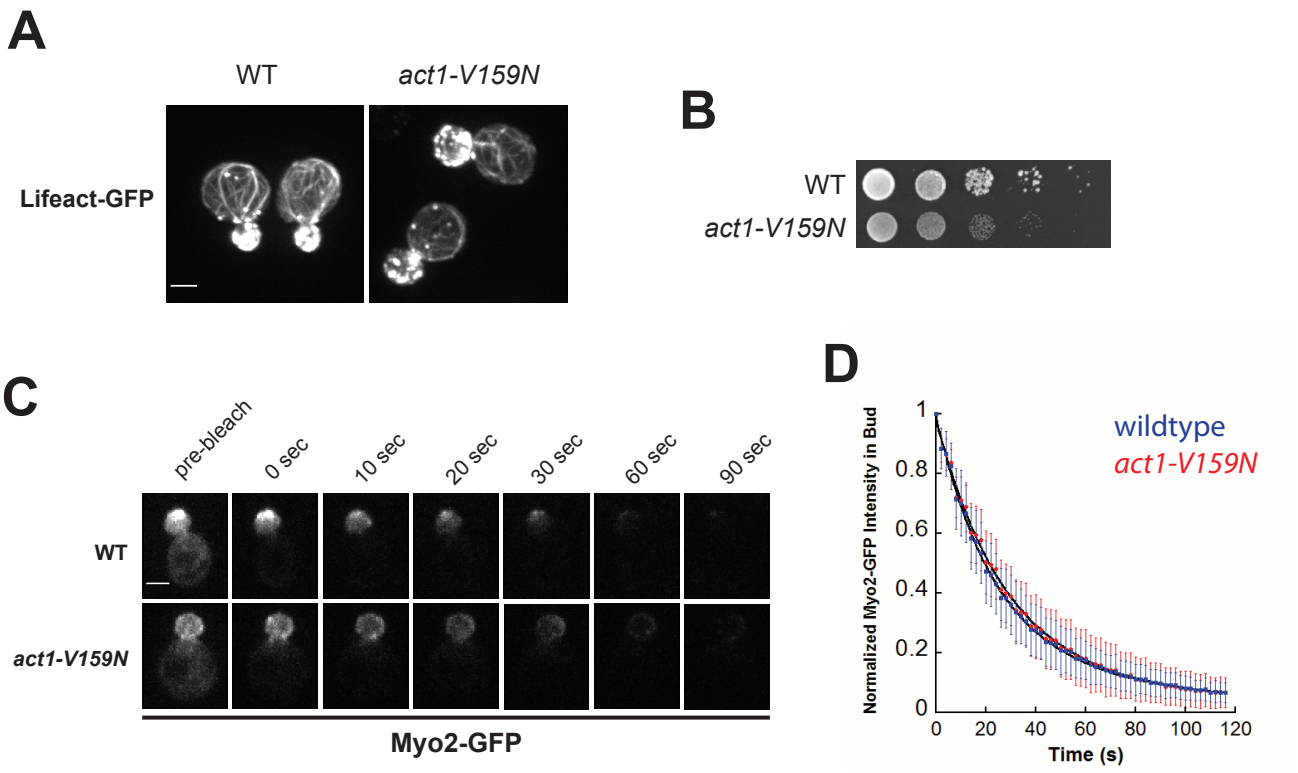

Figure A.4. Myo2p likely recycles back by diffusion, and not actin treadmilling as some models suggest.

(A) Actin cables for wildtype and *act1-V159N* cells as visualized by Lifeact-GFP. Staining by phalloidin gave a similar result (data not shown). Scale bar is 2 μm.
(B) Growth rates for wildtype and *act1-V159N* cells on YPD at 26 °C. Note that this mutant is temperature sensitive above this, with death occurring by 37 °C.
(C) Still frame images of Myo2-GFP FLIP experiment in wildtype and *act1-V159N* cells.
(D) Normalized intensity of Myo2-GFP in the bud of wildtype and *act1-V159N* cells. There was no significant difference in the recycling rates of motors (n= 10,13)

REFERENCES

Belmont, L.D., and Drubin, D.G. (1998). The yeast V159N actin mutant reveals roles for actin dynamics in vivo. J. Cell Biol. *142*, 1289–1299.

Belmont, L.D., Orlova, A., Drubin, D.G., and Egelman, E.H. (1999). A change in actin conformation associated with filament instability after Pi release. Proc. Natl. Acad. Sci. USA *96*, 29–34.

Chesarone-Cataldo, M., Guérin, C., Yu, J.H., Wedlich-Soldner, R., Blanchoin, L., and Goode, B.L. (2011). The Myosin Passenger Protein Smy1 Controls Actin Cable Structure and Dynamics by Acting as a Formin Damper. Dev. Cell *21*, 217–230.

Flanagan, C.A., Schnieders, E.A., Emerick, A.W., Kunisawa, R., Admon, A., and Thorner, J. (1993). Phosphatidylinositol 4-kinase: gene structure and requirement for yeast cell viability. Science *262*, 1444–1448.

Foti, M., Audhya, A., and Emr, S.D. (2001). Sac1 lipid phosphatase and Stt4 phosphatidylinositol 4-kinase regulate a pool of phosphatidylinositol 4-phosphate that functions in the control of the actin cytoskeleton and vacuole morphology. Mol. Biol. Cell *12*, 2396–2411.

Garcia-Bustos, J.F., Marini, F., Stevenson, I., Frei, C., and Hall, M.N. (1994). PIK1, an essential phosphatidylinositol 4-kinase associated with the yeast nucleus. EMBO J. *13*, 2352–2361.

Hodges, A.R., Bookwalter, C.S., Krementsova, E.B., and Trybus, K.M. (2009). A nonprocessive class V myosin drives cargo processively when a kinesin- related protein is a passenger. Curr. Biol. *19*, 2121–2125.

Lipatova, Z., Tokarev, A.A., Jin, Y., Mulholland, J., Weisman, L.S., and Segev, N. (2008). Direct interaction between a myosin V motor and the Rab GTPases Ypt31/32 is required for polarized secretion. Mol. Biol. Cell *19*, 4177–4187.

Liu, J., Taylor, D.W., Krementsova, E.B., Trybus, K.M., and Taylor, K.A. (2006). Three-dimensional structure of the myosin V inhibited state by cryoelectron tomography. Nature *442*, 208–211.

Mizuno-Yamasaki, E., Medkova, M., Coleman, J., and Novick, P. (2010). Phosphatidylinositol 4-Phosphate Controls Both Membrane Recruitment and a Regulatory Switch of the Rab GEF Sec2p. Dev. Cell *18*, 828–840.

Santiago-Tirado, F.H., Legesse-Miller, A., Schott, D., and Bretscher, A. (2011). PI4P and Rab inputs collaborate in myosin-V-dependent transport of secretory compartments in yeast. Dev. Cell *20*, 47–59.

Walch-Solimena, C., and Novick, P. (1999). The yeast phosphatidylinositol-4-OH kinase pik1 regulates secretion at the Golgi. Nat. Cell Biol. *1*, 523–525.

Yang, H.-C., and Pon, L.A. (2002). Actin cable dynamics in budding yeast. Proc. Natl. Acad. Sci. USA *99*, 751–756.